Alma Mater Studiorum – Università di Bologna

DOTTORATO DI RICERCA IN

CHIMICA

Ciclo XXIX

Settore Concorsuale di afferenza: 03/C2

Settore Scientifico disciplinare: CHIM/04

GAS PHASE TRANSFORMATION OF (BIO)-POLYOLS INTO CARBOXYLIC ACIDS BY MEANS OF MULTIFUNCTIONAL CATALYSIS

Presentata da: Claudia Bandinelli

Coordinatore Dottorato — **Prof. Aldo Roda**

Relatore — **Prof. Fabrizio Cavani**

Esame finale anno 2017

Ai brav'uomini.

Preface

The research activity carried out during the Ph.D. focused on the employment of bio-based building blocks for the production of higher added-value chemicals and the development of more sustainable processes. In particular, it aimed at the development of new synthetic routes for the production of acrylic and methacrylic acid using bio-alcohols as raw materials, respectively glycerol and propylene glycol.

The first chapter of the thesis concerns the one-pot transformation of glycerol into acrylic acid, performed by using multifunctional catalysts. The overall process formally consists in two reaction steps: i) glycerol dehydration to acrolein, promoted by acid catalysis, and ii) acrolein oxidation to acrylic acid, promoted by redox catalysis. The design of suitable multifunctional catalysts is a complex matter and, so far, fundamental understanding behind the catalytic phenomenon remains unclear. In this context, the research work here reported aimed to shed light on the molecular-level relations that lie behind the catalytic results shown by several types of V-containing catalysts.

The second chapter of the thesis concerns the study of a new synthetic route for the production of methacrylic acid starting from bio-propylene glycol. The overall process formally consists in three reaction steps: i) propylene glycol dehydration to propanal, ii) propanal oxidation to propionic acid, and iii) propionic acid condensation with formaldehyde, generated in-situ from methanol.
In particular, referring to reactions i) and ii), the research activity focussed on the possibility to perform the single-step gas-phase transformation of propylene glycol into propionic acid, by means of multifunctional catalysis (as previously done for glycerol one-pot transformation to acrylic acid). Therefore, the catalytic activity of different acid and redox materials was investigated, with the aim to understand which are the main critical points of the transformation of propylene glycol to propionic acid, and to determine how the peculiar features of each material influence the various stages of the oxidehydration process.

Finally, the study of the latter stage of the overall process to produce methacrylic acid was started, that is the condensation reaction between propionic acid and formaldehyde, generated in-situ from methanol. In particular, the catalytic activity of aluminium phosphate was fully investigated, so as to define the reactions that may occur when feeding propionic acid and methanol on pure acid catalysts.

1. Structure-Reactivity Correlations in Vanadium-Containing Catalysts for One-Pot Glycerol Oxidehydration to Acrylic Acid

This chapter was previously published as: "Structure–Reactivity Correlations in Vanadium-Containing Catalysts for One-Pot Glycerol Oxidehydration to Acrylic Acid", Chieregato A., Bandinelli C., Concepciòn P., Soriano M.D., Puzzo F., Basile F., Cavani F., Lòpez Nieto J.M., (2017) ChemSusChem, 10 (1), 234-244.

1.1 Introduction

Acrylic acid (AA) is the fundamental building block for the production of polyacrylates, that is the chemical backbone of many kinds of plastics, rubbers, synthetic fibers, and so on.[1] Nowadays, the world production of AA is estimated to be approximately 5-6 million tons per year, and its demand is foreseen to increase steadily, mainly owing to the growing needs of emerging economies, particularly China.[2] Most of the current AA productions use propylene as the raw material, in turn synthesized from naphtha steam cracking or, in minor amounts, by the dehydrogenation of propane.[3] The price of propylene is constantly increasing as a result of a shift in the feed of crackers from naphtha to natural gas, mainly ethane, and the increasing demand for polypropylene.[4] Provided with these market trends and the environmental concerns linked to the utilization of fossil feedstocks, alternative "green" routes have been explored in the last decade to produce AA from renewable resources.[2,5–7] Amongst the various options, one of the most explored paths has been the utilization of bio-glycerol as a starting material, produced as a coproduct of biodiesel synthesis.[5,8–10] Particularly, great attention has been focused on substituting the first step of conventional AA production, that is, partial oxidation of propylene to acrolein, with glycerol acid catalyzed dehydration to the same aldehyde. Indeed, this would be a drop-in technology that could be implemented in the existing two-step processes to produce AA from propylene. Nonetheless, if the AA demand keeps increasing, the construction of new plants would be required to avoid running existing facilities above their optimal capacities.

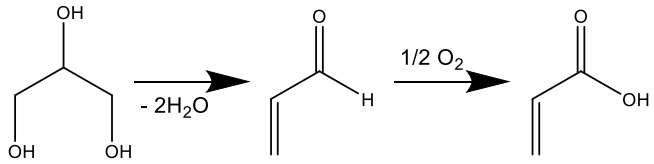

Scheme 1. The two reaction steps required for glycerol transformation into acrylic acid.

In the latter scenario, the ideal option would be to synthesize acrylic acid from glycerol (Scheme 1) with as little economic and engineering effort as possible.[2,5] From this viewpoint, the ideal solution would be to perform the transformation of glycerol into acrylic acid as a single-step (i.e., one-pot) reaction by using a multifunctional catalyst. However, the design of multifunctional acid and redox catalysts for the dehydration of glycerol and the partial oxidation of acrolein is a major challenge. The first attempts to perform the one-pot reaction were reported both in patents and in the open literature;[11–13] however, the AA yields on single catalysts were always low (<15^%). After these first studies, catalysts related to the family of perovskites greatly improved the AA yields, up to 28^%;[14–16] nevertheless, both the productivities and the overall catalytic performance remained unsatisfactory. In the last few years, many efforts have been made to improve the performance of catalysts for the one-pot oxidehydration of glycerol to AA. Overall, catalysts related to metal-oxide bronzes seem to be the best-performing materials, and they are capable of efficiently transforming glycerol into acrylic acid with yields >50^% and productivities of industrial relevance.[14,17–19] Nonetheless, other systems have shown promising results, such as V-doped zeolites[20,21] and V-P oxides.[22,23]

Interestingly, the common point of all these catalytic systems is the presence of vanadium as one of the main (or only) redox elements; however, despite this leitmotif, the catalytic behavior of these mixed oxides is fairly different. As it was recently reviewed,[24] the impressive versatility of vanadium as a catalyst for different gas-phase reactions is a remarkable feature of this element, probably unique in the entire periodic table. The environment that characterizes the vanadium contour in the different catalytic systems makes it possible to forge its properties, weakening some of them in favor of others. Taking into account the lack of molecular-level information on the one-

pot oxidehydration reaction of glycerol, that only recently started to be fulfilled,[25] it is presented herein an in-depth study that aimed to link the results obtained by reactivity tests performed in a flow reactor with those obtained by in-situ FTIR spectroscopy studies by using the reaction intermediate (i.e., acrolein), as well as X-ray diffraction (XRD), X-ray photoelectron spectroscopy (XPS), Raman spectroscopy, temperature-programmed reduction and temperature-programmed desorption of ammonia mass spectrometry (NH_3-TPD-MS).

Representative multifunctional V-containing catalysts were considered: one, hexagonal tungsten bronzes (HTBs) with in-framework or extra-framework vanadium species; two, zeotype materials, that is, modified-$AlPO_4$-5 catalysts[26] with in-framework and extra-framework vanadium species; three, a commercial vanadyl pyrophosphate (VPP) catalyst.[27] Remarkable structure-reactivity correlations were revealed for the one-pot oxidehydration of glycerol that shed light on the different behaviors of vanadium as a function of the physical and chemical features of the oxide in which it was present. V-free parent materials were also studied as reference materials for both characterization and catalytic tests purposes.

1.2 Experimental Section

1.2.1 Catalyst preparation

Hydrothermal synthesis of HTBs

Pure hexagonal tungsten oxide (sample WO_x) and a hexagonal-tungsten/vanadium oxide (sample WV) were prepared through the hydrothermal method, following a previously reported procedure.[15] The initial solutions were prepared from the salts of selected metals, i.e. ammonium metatungstate hydrate (≥ 85 wt% WO_3 basis, Sigma-Aldrich) and vanadium (IV) oxide sulfate hydrate (≥ 99.99%, Sigma-Aldrich). For the synthesis of WO_x, ammonium metatungstate is dissolved in water and oxalic acid is used as the reducing agent. For the synthesis of WV, the same procedure is followed, but vanadium sulfate is added to the clear solution of tungsten. The solution is transferred to a teflon-lined stainless steel autoclave, fitted with two valves that allow purging the autoclave with a flow of nitrogen, so as to create an inert atmosphere. An over pressure of nitrogen (1

bar) is finally set. The autoclaves are heated at 175°C for 48 h. The solid obtained is filtered off with distilled water and dried at 100°C for 16 h. Finally, the solid (precursor) is heat-treated at 600°C during 3 h under N_2.

Ion-exchange

VO-WO_x was synthesized through an ion-exchange process. WO_x-precursor (i.e. the un-treated materials containing ammonium ions in the channels) was exchanged with V-ions (precisely, VO^{2+} ions). Indeed, it is known that the ions present in the hexagonal channels (e.g., NH_4^+) of tungsten bronzes can be exchanged with other cations.[28] To do so, WO_x-precursor was immersed in an aqueous solution containing $VOSO_4$; the amount of ion to exchange was set to obtain a theoretical atomic ratio V/W = 0,3. This is approximately the maximum theoretical amount of cation that can be host in the hexagonal channels of an HTB. The catalyst was left stirring for 4 hours at room temperature and the solid was finally filtered and washed (ca. 200 mL of water per gram of catalyst) to remove the excess of ions that might have been adsorbed on the surface of the catalyst rather than incorporated within the channels of the material. Once dried, VO-WO_x was heat-treated at 450°C.

Hydrothermal synthesis of modified AlPO4-5 and incipient wetness impregnation

Zeotype $AlPO_4$-5 catalysts were prepared hydrothermally by following conventional procedures.[29] Cobalt was also introduced during the synthesis to improve the acid properties (sample CoAPO). Vanadium was added either during the synthesis, so as to obtain in-framework vanadium species (sample VCoAPO) or by using postsynthetic incipient impregnation to create extra-framework vanadium species (VO_x/VCoAPO); particularly, VCoAPO was impregnated with an additional amount of V to obtain a catalyst with both in-framework and extra-framework V species.

Sample VCoAPO was synthesized by hydrothermal method using triethylamine as a template. Aluminum hydroxide (Catapal A, Sasol) was added to an 85% solution of phosphoric acid (Aldrich) in water, and the mixture was stirred until a homogeneous solution was obtained. Triethylamine was added to this mixture under continuous stirring. Then an aqueous solution of cobalt (II) acetate was incorporated along with a

V_2O_5/triethylamine solution. The final reaction mixture was stirred until achieving a homogeneous gel. The gel was introduced in Teflon-lined stainless steel autoclaves and heated at 200°C for 16 hours. After crystallization, the sample was centrifuged at 10,000 rpm, washed with distilled water and dried overnight at 100°C. Sample CoAPO was prepared using the same procedure, except for the addition of vanadium pentoxide during the synthesis.

Vanadium oxide supported on VCoAPO (sample name VOx/V-CoAPO) was prepared by wetness impregnation of the sample V-CoAlPO with an aqueous solution of ammonium metavanadate. After the impregnation, water was removed by rotavapor and the oxide was dried overnight at 100°C. Dried materials were calcined in air for 6 hours at 550°C.

Commercial VPP catalyst

The commercial VPP catalyst used for this study was the industrial catalyst used by DuPont to produce maleic anhydride from *n*-butane; this catalyst was studied in depth by various authors.[27] Particularly, we used its calcined form.

1.2.2 Catalyst characterization

IR spectroscopy studies were performed with a Bruker Vertex 70 FTIR spectrometer by using a MCT detector and acquiring at 4 cm^{-1} resolution. An IR cell allowing in situ studies under controlled atmospheres and temperatures from 25 to 600°C was connected to a vacuum system with gas dosing facility. For IR spectroscopy studies, the samples were pressed into self-supported wafers and treated at 300°C in air flow (20 $mLmin^{-1}$) for 2 h followed by evacuation at 10 mPa at 350°C for 1 h. After activation, the samples were cooled down to 25°C under dynamic vacuum conditions followed by adsorption of the different reactants, that is, acrolein, O_2, and/or H_2O in a molar ratio of 1:7:20. Spectra were recorded at increasing temperatures from 25 to 400°C. At each temperature, one spectrum was recorded at the working temperature and another one after cooling down the pellet to 25°C to favor re-adsorption of products desorbed to the gas phase. X-ray photoelectron spectra were collected by using a SPECS spectrometer equipped with a Phibos 150 MCD-9 detector and by using a monochromatic AlK_α (1486,6 eV) X-ray source and charge compensation by means of additional electron flow. Spectra were recorded

by using an analyzer pass energy of 50 eV, an X-ray power of 100 W under an operating pressure of 10^{-4} mPa. During data processing of the XPS spectra, the binding energy (BE) values were referenced to O 1s (peak settled at BE = 530,5 eV) or P 2p (in zeotypes, peak settled at BE = 133,5 eV). Spectra treatment was performed by using CASA software. Raman spectra were recorded at ambient temperature with a λ=514 nm laser excitation with a Renishaw Raman spectrometer ("in via") equipped with an Olympus microscope and a CCD detector. The laser power on the sample was 15 mW and a total of 20 acquisitions were taken for each spectra. Powder X-ray diffraction was used to identify the crystalline phases present in the catalysts. An Enraf Nonius FR590 sealed tube diffractometer, with a monochromatic $CuK_{\alpha 1}$ source operating at 40 kV and 30 mA was used. Temperature-programmed reduction (TPR) was performed in a Micromeritics Autochem 2910 equipped with a TCD detector by using 10% H_2 in Ar as the reducing gas (total flow rate of 50 $mLmin^{-1}$). The temperature was varied from room temperature to 800°C. The heating rate was maintained at 10°$Cmin^{-1}$. Temperature programmed desorption of ammonia mass spectrometry (NH_3-TPD-MS) experiments were performed with a TPD/2900 apparatus from Micromeritics. The sample (0,30 g) was pretreated in a He stream at 450°C for 1 h. Ammonia was chemisorbed by pulses at 100°C until equilibrium was reached. Then, the sample was fluxed with He stream for 15 min prior to increasing the temperature up to 500°C in a helium stream of 100 $mLmin^{-1}$ and by using a heating rate of 10°$Cmin^{-1}$. The NH_3 desorption was monitored with a thermal conductivity detector (TCD) and a mass spectrometer following the characteristic mass of ammonia at 15 amu.

1.2.3 Gas-phase catalytic tests

Gas-phase reactivity experiments were performed by using a continuous flow reactor made of glass, operating at atmospheric pressure. For each condition, all the reaction parameters are listed in each figure. A catalyst amount ranging from 0,1 to 0,5 g was loaded in powder form. Residence time is calculated as the ratio between catalyst volume (mL) and total gas flow (mL/s), the latter being measured at room temperature. The residence time was varied by keeping constant the total gas flow and changing the

catalyst amount. Inlet feed composition was also changed according to the desired compositions. If not differently specified, the catalytic results were obtained after a reaction time of 60 min.

The effluent stream was bubbled through two/three in-series abatement devices filled with water, and put into a cool bath at the temperature of 0-2°C. After the abatement step, where the condensable organic molecules were collected, the gaseous stream still containing oxygen and carbon oxides, was fed into an automatic sampling system for on-line gas chromatography (GC-TCD) analysis. The aqueous solution was analyzed off-line by GC-FID analysis, using a reference standard (valeric acid). Both the gas chromatographic analyses were performed with a Hewlett–Packard 5890 instrument, equipped with either FI and TC detectors. A semi-capillary ZB-FFAP (nitroterephthalic acid modified polyethylene glycol) column was used for the separation of condensed compounds, whereas two wide-bore columns were used for the separation of non-condensable products: a Mol Sieve 5A Plot for O_2 and CO, and a Silica Plot for CO_2. Compounds were identified by means of both GC–MS analysis and the injection of pure reference standards for the comparison of retention times in the GC associated to the plant. Conversion, yields and selectivities were calculated by the following formulas: $X_R = [(\text{mol } C_R^{in} - \text{mol } C_R^{out})/\text{mol } C_R^{in}]*100$; $Y_i = (\text{mol } C_i^{out}/ \text{mol } C_R^{in})*100$; $S_i = (Y_i/ X_R)*100$.

In particular, mol C_R^{in} and mol C_R^{out} represent the moles of carbon atoms of the reagent R, and mol C_i^{out} the moles of carbon atoms of the *i*th reaction product.

A few unknown compounds, always consisting into minor compounds, were also eluted in the GC column; we attributed them the same response factor of the corresponding known compound with the closest retention time. In figures, all minor compounds are grouped together under the heading “Others”. Heaviest compounds not eluted from the GC column (left as residues on both the catalyst surface and reactor walls) were quantified as the remainder of the total carbon balance and labeled as “Heavy compounds”. Carbon balance was calculated by the formula: Carbon balance = $[(\sum_1^n Y_i)/X_R]*100$.

1.3 Results and Discussion

1.3.1 Physicochemical properties of the oxides

All the samples studied were analyzed by X-ray diffraction (XRD) (Figure 1). The tungsten-based oxides (Figure 1, patterns a-c) present the typical pattern of the hexagonal phase (JCPDS: 33-1387). The V-exchanged HTB, that is, VO-WO_x (Figure 1, trace b), presents a structure basically identical to that of the parent material, WO_x (Figure 1, trace a). However, the diffraction peaks of these two samples are slightly broader than those of hexagonal tungsten/vanadium oxide, WV (Figure 1, trace c). This might be due to small differences in morphology (different growth along the crystalline planes) and/or incomplete crystallization of the hexagonal phase. A role might also be played by the lower heat-treatment temperature used for WO_x and VO-WO_x relative to that used for WV (i.e., 450 vs. 600°C); indeed, if heated at temperatures >450°C, the former two structures evolve into monoclinic forms (i.e., WO_3 and V-doped WO_3). As previously demonstrated by high-resolution transmission electron microscopy (HRTEM) with selected area electron diffraction (SAED), as well as morphological and spectroscopic analyses,[17,30,31] there is remarkable evidence that proves that the majority of vanadium in VO-WO_x is incorporated as extra-framework species. Only if another transition element (e.g., V, Nb, Mo, Ti) enters the hexagonal tungsten oxide framework is the HTB structure stable at temperatures significantly higher than those bearable by the material built up by only W atoms (WO_x). Hence, it can be concluded that vanadium is mainly present in VO-WO_x as extra-framework species, eithe deposited on the external surface or inside the hexagonal channels. Taking into account the washing of the catalyst after the ion-exchange process (see the Experimental Section), and the Raman spectra (see below), the latter option is more likely. The modified $AlPO_4$-5 systems (Figure 1, patterns d-f) present the characteristic pattern of zeotype materials with AFI structure (JCPDS: 41-0044), which confirms the correct preparation of the $AlPO_4$-5 catalysts. For both CoAPO and VCoAPO catalysts, no changes are observed in the diffraction patterns, which confirms the insertion of cobalt and vanadium in the oxide framework as tetrahedral units.[32] However, if an additional amount of vanadium is added to the VCoAPO catalyst

by wet impregnation (sample VO_x/VCoAPO; Figure 1, pattern f), extra-framework vanadium species are formed as V_2O_5, which are responsible for the additional diffraction peaks observed for the latter sample. The XRD pattern of the VPP catalyst (Figure 1, pattern g) shows the presence of the characteristic phase $(VO)_2P_2O_7$; the lack of additional peaks confirms that no other V-P-O phases constitute the bulk phase of the catalyst.[27]

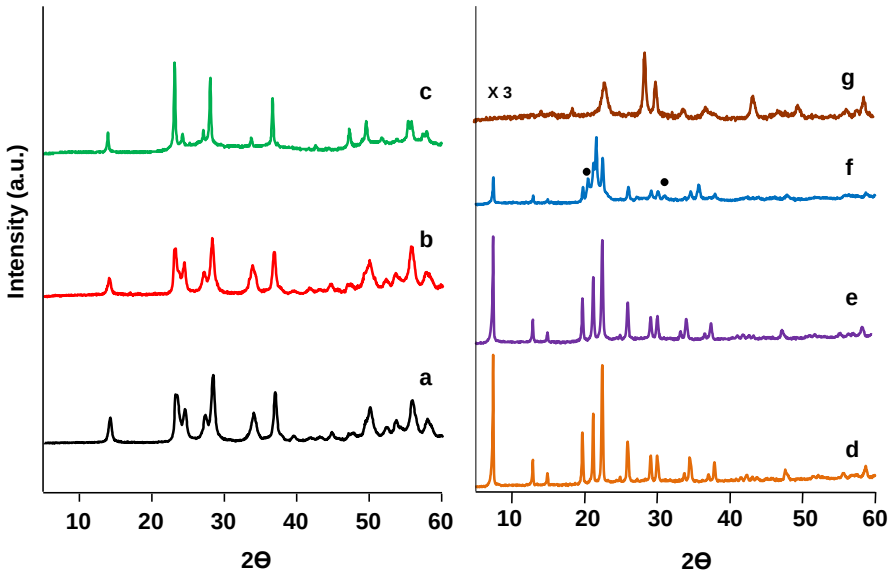

Figure 1. XRD patterns of catalysts: a) WO_x; b) VO-WO_x; c) WV; d) CoAPO; e) VCoAPO; f) VOx/VCoAPO, g) VPP. (•) indicates V_2O_5 diffraction peaks.

Raman spectroscopy was used to improve the understanding on the structure of the various catalytic systems prepared, particularly to shed light on the nature of the vanadium species in the HTB-like materials.[33–35] If vanadium enters the HTB framework, a new band at $\bar{\nu}$ = 970 cm^{-1} appears in the Raman spectrum (sample WV, Figure 2-A). This can be related to the greater number of W-O bonds generated by a structural defect as a result of vanadium incorporation and/or V-O bonds associated to polymeric V-O-W chains.[15,30] In the VO-WO_x sample, this band is very weak but is not completely absent; moreover, the main bands located at $\bar{\nu}$ = 694 and 819 cm^{-1} are shifted to lower frequencies relative to the main bands of the pristine WO_x sample, as in the case of substituted-HTBs.[30] Hence, although the majority of vanadium occupies extra-

framework positions, as previously discussed, it can be inferred that a minor portion of it might replace the in-framework W atoms, most likely during heat treatment through a solid-solid reaction. Overall, the absence of a band at $\bar{\nu}$ = 1035 cm^{-1} excludes the presence of V-O stretching assigned to 2D vanadium species; moreover, the absence of a sharp signal at $\bar{\nu}$ = 995 cm^{-1}, as well as more broad features at $\bar{\nu}$ = 700, 530, 500, 400, and 300 cm^{-1}, exclude the presence of V_2O_5 nanoparticles.[34–36] Considering these results, it is possible to conclude that the majority of vanadium is present in VO-WO_x as extra-framework species, precisely as V ions located inside or, most likely, in the mouth of the hexagonal channels.

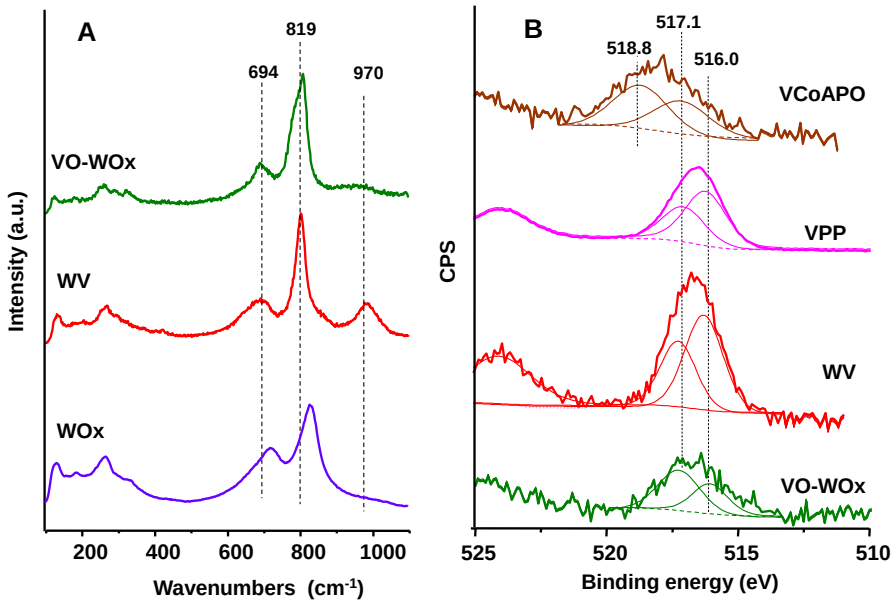

Figure 2. Raman (A) and V2p3/2 XPS spectra (B) of selected catalysts.

XPS measurements were performed to shed light on the oxidation state of V on the surface of catalysts (see Figure 2-B and Table 1). Different states of V ions can be evidenced; both V^{5+} (binding energy (BE): 517,1 eV) and V^{4+} (BE: 516,1 eV) ions can be detected on the WV sample, whereas a higher V^{5+}/V^{4+} surface ratio is shown for the extra-framework V species in the ion-exchanged sample, VO-WO_x. Considering that the ion exchange was performed by using vanadyl ions (VO^{2+}), the XPS results point out a partial oxidation process during catalyst preparation, consistently more severe in the

case of the extra-framework V species. Moreover , the VPP catalyst presents V^{4+} as the predominant species, but the presence of V^{5+} is also significant, despite the fact that the XRD pattern only shows the presence of $(VO)_2P_2O_7$; this observation agrees with previous reports by other authors,[37–39] who attribute the presence of V^{5+} species to the coexistence of $VOPO_4$ domains in addition to $(VO)_2P_2O_7$ on the surface of the catalyst. Finally, the VCoAPO sample shows both V^{5+}/V^{4+} ions, whereas V^{5+} is mainly observed on the VO_x/VCoAPO sample. The high BE of V^{5+} in both zeolite-type samples (518,8 eV) is due to high dispersion of the V ions in the lattice framework.[29]

Table 1. Physicochemical properties of the reported catalysts.

	BET SSA	NH_3-TPD		XPS results		
	$m^2\ g^{-1}$	$\mu mol_{NH3}\ g^{-1}$	$\mu mol_{NH3}\ m^{-2}$	V^{5+} (BE)	V^{4+} (BE)	V^{5+}/V^{4+}
WO_x	31	135	4.4	-	-	-
WV	21	76	3.7	517.1	516.1	0.64
VO-WOx	25	113	4.5	517.2	516.0	1.68
CoAPO	263	241	0.9	-	-	-
VCoAPO	298	331	1.1	518.7	516.7	3.9
VO_x/VCoAPO	192	249	1.3	518.7	-	1
VPP	41	90	2.2	517.1	516.2	0.70

The redox and acid properties of the prepared materials were assessed by temperature-programmed reduction (H_2-TPR) and NH_3-TPD-MS experiments, respectively (Figure 3). As previously reported,[15] HTB-like materials present two main reduction peaks: one between 450 and 500°C and another at temperatures >550°C.

Relative to WV, the ion-exchanged sample (VO-WO_x) is reduced at higher temperatures, in accordance with the presence of extra-framework V ions. In-framework V species in the VCoAPO sample are reduced at temperatures < 500°C,[29] whereas the extra-framework V_2O_5 particles in the VO_x/VCoAPO sample are reduced only at higher temperatures. Finally, VPP presents a small and broad reduction peak between 350 and 500°C and a major reduction peak at a high temperature.[22] The NH_3-TPD-MS

experiments highlight that ion exchange with V ions has a minor impact on acidity if the acidity of VO-WO_x is compared to that of its parent material WO_x. Indeed, the NH_3-TPD profiles (and therefore their total acidity, see Table 1) are quite similar. VCoAPO and VO_x/VCoAPO also have similar profiles; however, the extra-framework V species considerably affect the overall acidity (≈ -25%). Despite the fact that the acidity on the mass bases of the zeotype materials is higher than that on the modified-HTBs, the acid density (acid sites per m^2 of surface area) is actually consistently lower for the former materials. The TPD results also suggest that the VPP catalyst has acidic character (in terms of the strength of the acid sites) similar to that of WV, but approximately half its density of acid sites.

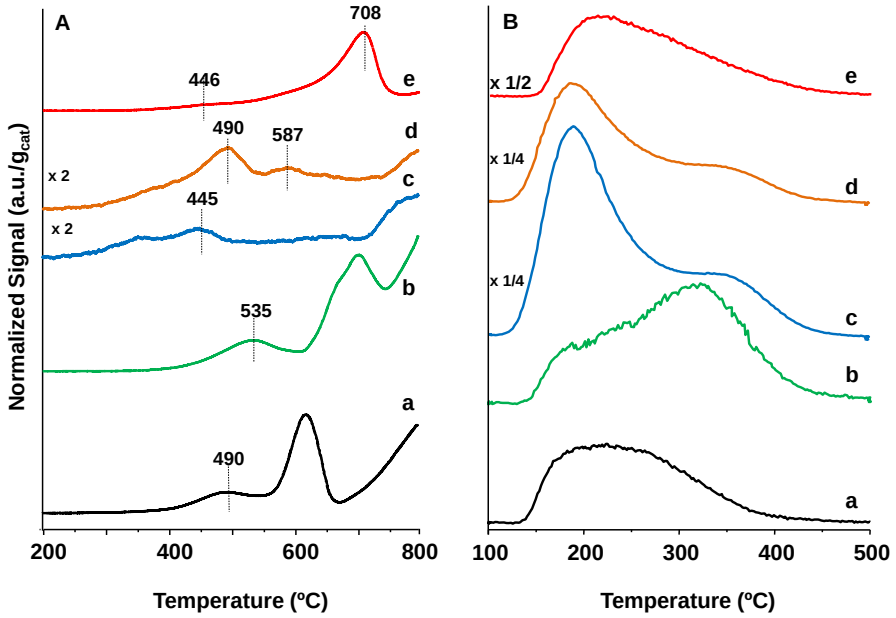

Figure 3. H_2-TPR (A) and NH_3-TPD-MS (m/z=15) patterns (B) of catalysts: a) WV; b) VO-WO_X; c) VCoAPO; d) VO_X/VCoAPO; e) VPP.

1.3.2 Catalytic tests

The studied materials were used as catalysts for the transformation of glycerol in the gas phase. As an explorative test, the contact time optimal for WV (≈ 0,4 s, see Ref. [18]) was also used for the other oxides. Preliminary studies were performed by using the CoAPO catalyst, without vanadium (Figure 4); despite the acid properties of this material,

glycerol conversion was complete only at temperatures ≥ 360°C and no acrylic acid was formed. Moreover, significant amounts of heavy compounds were produced (selectivity between 40 and 50%).

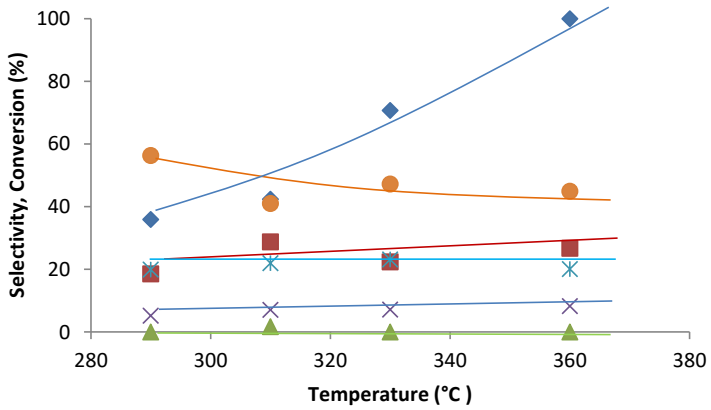

Figure 4. Catalytic behavior of CoAPO catalyst for the glycerol oxidehydration as a function of temperature (contact time 0,4s). Symbols: Glycerol conversion (◆), acrolein (■), acrylic acid (▲), CO_x (X), heavy compounds (●) and others (*). Among the others are listed acetaldehyde, acetic acid and unknown compounds.

However, the addition of V species consistently improved the activity of the catalyst, as in all cases and for all temperatures, glycerol conversion was always complete for both VCoAPO and VO_x/VCoAPO (Figure 5). This is in line with an increase in both the acid (Table 1) and redox sites favoring an increase in activity owing to the formation of oxidation products. Furthermore, VPP and WV both always showed complete conversion of glycerol. The glycerol dehydration step to acrolein has been the focal point of a vast number of reports in the literature,[17,40–44] and there is a general consensus on the pivotal role played by Brønsted acid sites to dehydrate glycerol selectively to acrolein. The significant presence of these sites is known for all the catalytic systems reported herein, that is, HTB-like materials,[17] $CoAlPO_4$-5,[45] and VPP,[46] and this explains the high conversions and selectivities to acrolein (and, in turn, acrylic acid) obtained for WV, VCoAPO, and VPP.

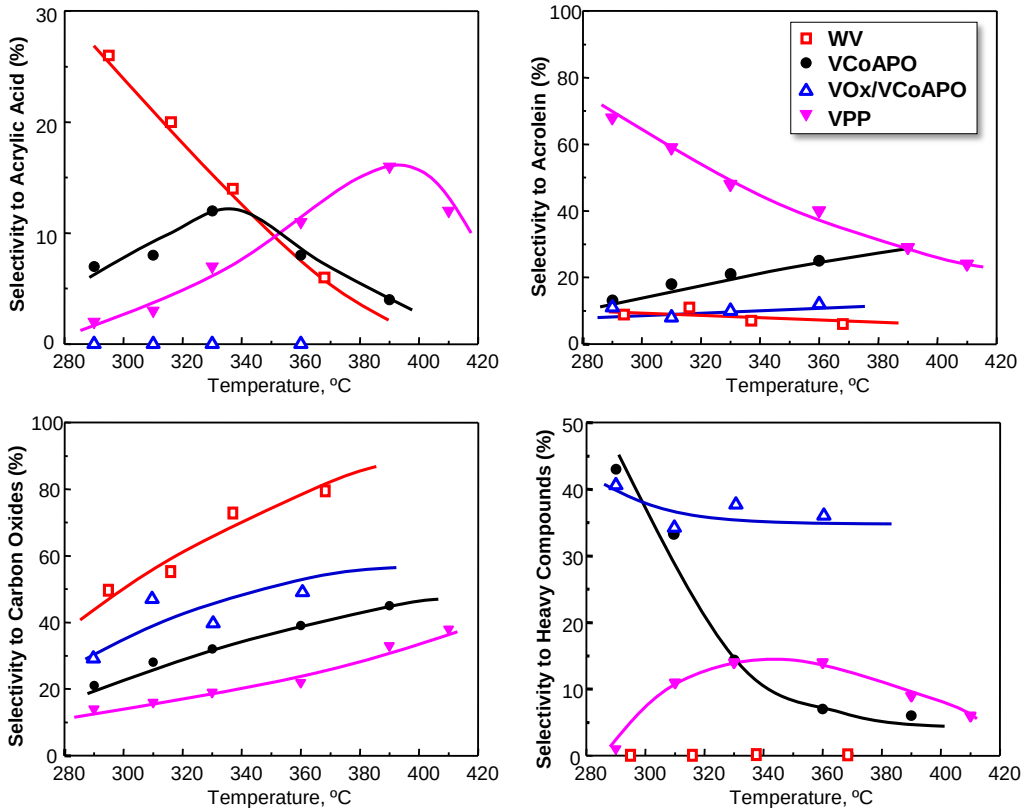

Figure 5. Variation of the selectivity to the main reaction products (acrylic acid, acrolein, carbon oxides and heavy-compounds) with reaction temperature over WV, VCoAPO, VOx/VCoAPO and VPP catalysts. Glycerol conversion always complete. Feed composition (mol%): glycerol/oxygen/water/nitrogen = 2/4/40/54. Contact time 0,4 s. Acetaldehyde, acetic acid and other compounds formed with the following selectivities on each catalyst: VCoAPO 15-25%, VPP and VOx/VCoAPO 11-18%, WV 8-12%. Among the "other compounds", hydroxyacetone was also present. However, numerous unknown species also formed.

Taking into consideration the product distribution observed for VO_x/VCoAPO and comparing it to those observed for VCoAPO, the extra-framework vanadium species seem to: one, block the more active in-framework V sites; two, enhance total oxidation to carbon oxides; three, be completely inactive towards the selective oxidation of acrolein to acrylic acid. It is of interest to compare our results to those obtained by others using V-impregnated zeolites.[20,21] Indeed, although extra-framework vanadium species were also present in the latter materials, acrylic acid selectivities up to 25% (5%V-impregnated zeolite beta)[21] and 17% (V_2O_5/MFI)[20] were obtained. Despite the fact that

V_2O_5 particles were clearly present in those catalysts, the higher production of AA can be attributed to better dispersion of V, as pointed out by XPS analyses.[21]

The industrial VPP catalyst displayed very peculiar catalytic behavior, as some aspects were similar to those of the VCoAPO catalyst but others were completely opposite to those of the WV catalyst. The CO_x selectivity, at all the temperatures investigated, was the lowest among all the catalysts; however, what is mainly remarkable is the increase in the selectivity to acrylic acid at high temperatures (maximum 16% at 390°C), that is, at which all the HTB-like catalysts showed minimum values. As a consequence, the acrolein yield decreased, as it was partially and totally oxidized to acrylic acid and CO_x.

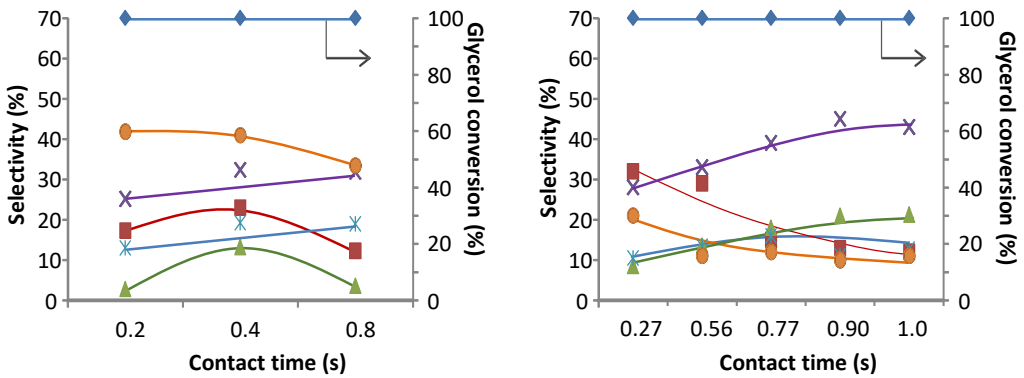

Figure 6. Influence of contact time on the catalytic performance of VCoAPO (left) and VPP (right) catalysts. Feed composition: 2 mol% glycerol, 4 mol% oxygen, 40 mol% water, and 54 mol% nitrogen. Symbols: Glycerol conversion (◆), acrolein (■), acrylic acid (▲), CO_x (X), heavy compounds (●) and others (*). Among the others are listed acetaldehyde, acetic acid and unknown compounds.

To deepen the knowledge of the catalytic behavior of the most active catalysts, that is, WV, VCoAPO, and VPP, catalytic tests as a function of feed molar ratios were performed, as previously reported for other kinds of substituted-HTBs.[17,18] However, to better evaluate the catalytic performance of each oxide, preliminary studies on the influence of contact time were undertaken (Figure 6), which proved that VCoAPO had its optimal contact time at approximately 0,4s (as WV), whereas that of VPP was located at higher values, approximately 1s.

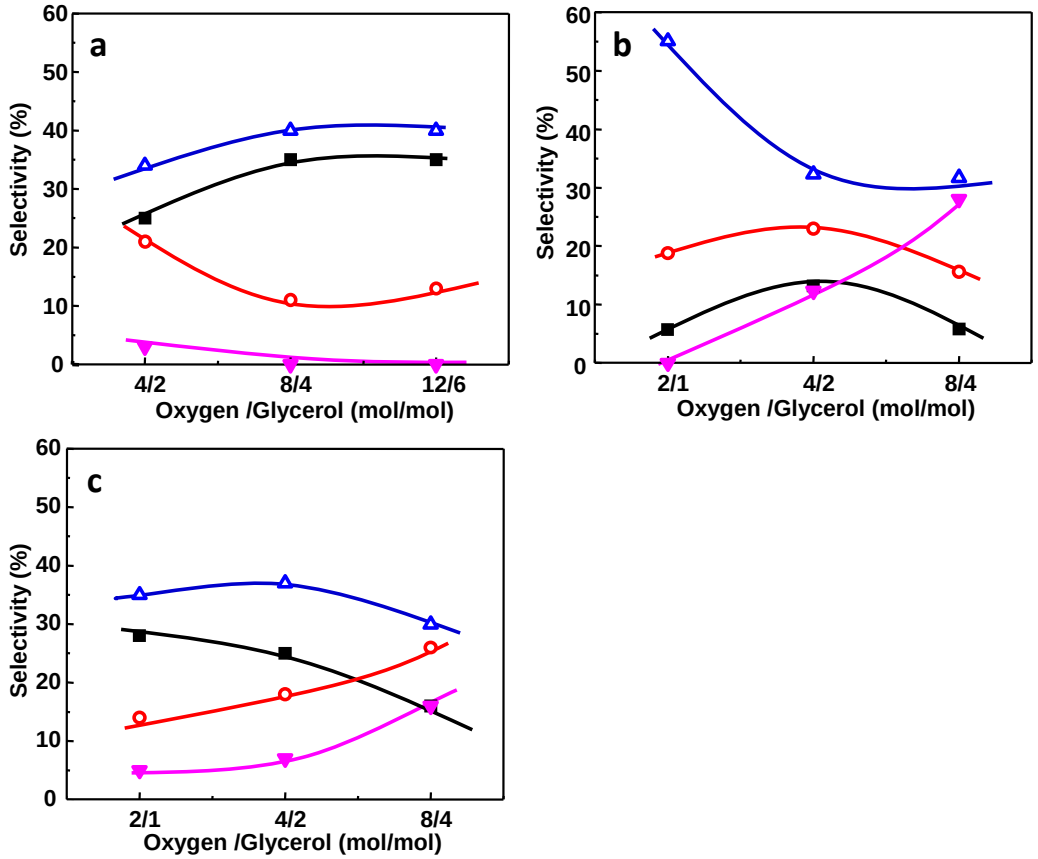

Figure 7. Glycerol oxidehydration as a function of feed oxygen/glycerol molar ratio on WV (a), VCoAPO (b) and VPP (c). Glycerol conversion always complete. Symbols: Acrylic Acid (■), Acrolein (○), COx (Δ), Heavy compounds (▲). Further compounds detected but not reported in the plot: (i) WV: acetic acid + acetaldehyde 2-3%, unknown compounds 2-3%; (ii) VCoAPO: acetaldehyde + acetic acid 8-17%, unknown compounds 3-7%; (iii) VPP: acetic acid ca. 10%, unknown compounds 2%. Reaction conditions: **a**) T (temperature) = 290°C, Tau (contact time) = 0,4s; **b**) T= 330°C, Tau= 0,4s; **c**) T= 390°C, Tau= 1s. Water concentration in feed 40 mol%.

Figure 7 reports the product distribution for each mixed oxide as a function of feed composition (the glycerol-to-oxygen molar ratio and water concentration in the feed were kept constant) by using the optimal temperature and contact time for each catalyst (see details in the figure caption). WV showed its maximum acrylic acid selectivity (35%) under glycerol-rich conditions (feed composition glycerol/oxygen/water/ nitrogen = 6/12/40/42 mol%), as previously observed for all the other HTB-like catalysts.[17,18] VCoAPO did not improve its performance by varying the feed composition, as the acrylic acid maximum (12%) was found to lie under the previously explored conditions, that is,

glycerol/oxygen molar ratio of 0,5 (2:4 mol%). Also in this case, VPP showed behavior that was opposite to that of the HTB-like catalysts, and it presented the maximum acrylic acid yield (28%) at low glycerol concentrations (feed composition glycerol/oxygen/water/nitrogen= 1/2/40/57 mol%).

At higher pressures of the reactants, both partial and total oxidation were hampered, which provoked an increase in the intermediate product (acrolein) and finally the formation of heavy compounds.

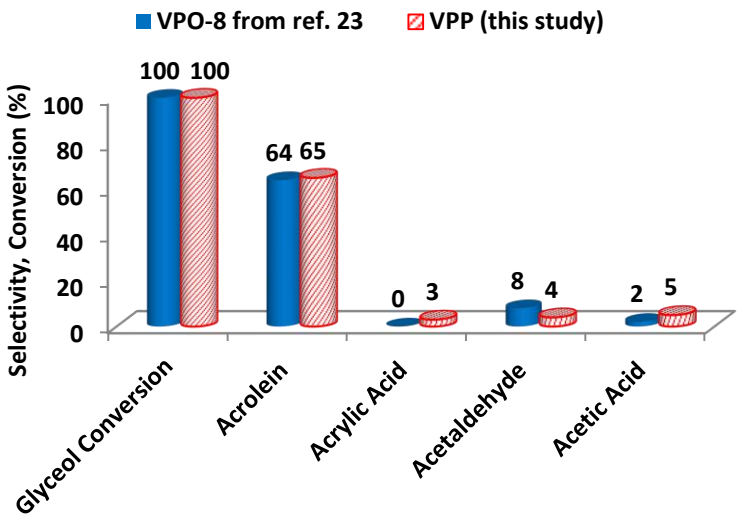

Figure 8. Comparison of the catalytic performance of VPP (this study) under the same reaction conditions reported in ref. 23. Reaction conditions: temperature 300°C, inlet feed composition: Gly/Ox/H_2O: 1,4/12,7/30,3. Time factor: 0,006 g min mL^{-1}.

At this stage, it is worth mentioning that V-P oxides were previously studied by others for this reaction.[23] Among the V-P-O materials prepared, it was found that the one treated at 800°C was the best performing phase, with acrolein selectivity up to 64% but only trace amounts of acrylic acid. Moreover, regardless of the catalyst thermal treatment, acrylic acid was always produced in trace amounts. Although the different results obtained in this work upon using the industrial VPP catalyst could be explained by taking into account the fact that the physicochemical properties (e.g., surface area, heat treatments, preparation method, etc.)[22] of the latter catalyst are different than those of the previously reported V-P oxides, it is safe to say that the major role is actually

played by the reaction conditions. Indeed, upon testing the industrial catalyst under the same reaction conditions as those reported in Ref. [23], the catalytic performance was almost identical for both catalysts (Figure 8).

To further explore the structure-reactivity correlations of multifunctional catalysts for the oxidehydration of glycerol, the catalytic behavior of the WV sample was compared to that of the ion-exchanged catalyst, VO-WO_x (Figure 9). Despite the formation of acrolein on VO-WO_x, acrylic acid was formed in just minor amounts (3%), whereas CO_x was formed in remarkable amounts. This may be related to the lower redox behavior of the V ions, which decreases the oxidation rate of the acrolein intermediate and favors secondary reactions (finally leading to heavy compounds). Despite the fact that the content of vanadium in the ion-exchanged sample was lower than that in WV (VO-WO_x 0,15 vs 0,21, see Table 2), the distinct catalytic behavior cannot be attributed merely to the different compositions; indeed, previously reported V-containing HTBs with in-framework V species and a similar V/W ratio to that in VO-WO_x showed acrylic acid selectivity > 20% under identical reaction conditions (see Ref. [15] and Figure 9-A).

Moreover, differently from WV, VO-WO_x did not show any significant change in catalytic performance upon exposure to higher partial pressures of the reactants (see Figure 9-B). These results seem to point out that the presence of V species in the framework positions enhances the oxidation properties of the transition element. However, as discussed in the in situ FTIR spectroscopy studies (see below), the picture at the molecular level is actually opposite, in which the strong acid sites in VO-WO_x play a major role in the formation of consecutive products owing to strong adsorption of the reaction intermediates. Overall, although the absolute values of the product selectivities might also depend on the real accessibility of the V sites on the different samples (e.g., acrolein and other C_3 molecules can enter the micropores of zeolites,[43] whereas HTBs have only external surface area available for catalysis),[31] the remarkable differences displayed by the catalysts reported herein as a function of temperature and feed molar ratios open important questions. Despite the fact that all of the studied materials efficiently dehydrated glycerol into acrolein and that they all had V as the only active element to perform the partial oxidation, their catalytic behavior is sometimes opposite. This

highlights that close proximity of acid and redox sites (i.e., V ions) at the atomic level is mandatory to efficiently perform the oxidehydration reaction of glycerol on a single catalyst.

Table 2. Atomic ratios of elements in the studied catalysts.

Sample	Atomic ratios[a]					
	W	**V**	**K**	**Al or (Si)**	**P**	**Co**
WOx	1	-	-	-	-	-
VO-WOx	1	0.15	-	-	-	-
WV	1	0.21	-	-	-	-
CoAPO	-	-	-	0.46	0.52	0.022
V-CoAPO	-	0.0046	-	0.46	0.53	0.031
V/V-CoAPO	-	0.0079	-	0.49	0.51	0.019
VPP	-	0.37	-	(0.19)	0.44	-
a) Results obtained by EDX analyses.						

In the pursuit of the intimate relations that link the catalyst structure and the catalytic results, in situ FTIR spectroscopy analyses were performed by studying the oxidation of the intermediate product, that is, acrolein, on the different multifunctional catalysts. Attempts were also made to adsorb glycerol on the surfaces of the catalysts, but its high boiling point prevented it from being transferred into the IR cell in a controllable fashion, as previously reported.[47] This made it impossible to control the stoichiometry of the two reactants, glycerol and oxygen, inside the IR cell. In 2014, C. Sievers and co-workers reported an ex situ method that could be used to overcome this issue with some catalysts.[44] Indeed, the catalyst could be slurred for 24h in an aqueous solution of glycerol, and water was finally removed. However, V-based systems are known to leach vanadium species if dispersed in aqueous solutions, which unfortunately made the application of this ex situ method unreliable, if not impossible, in the case of the bifunctional catalytic systems reported herein.

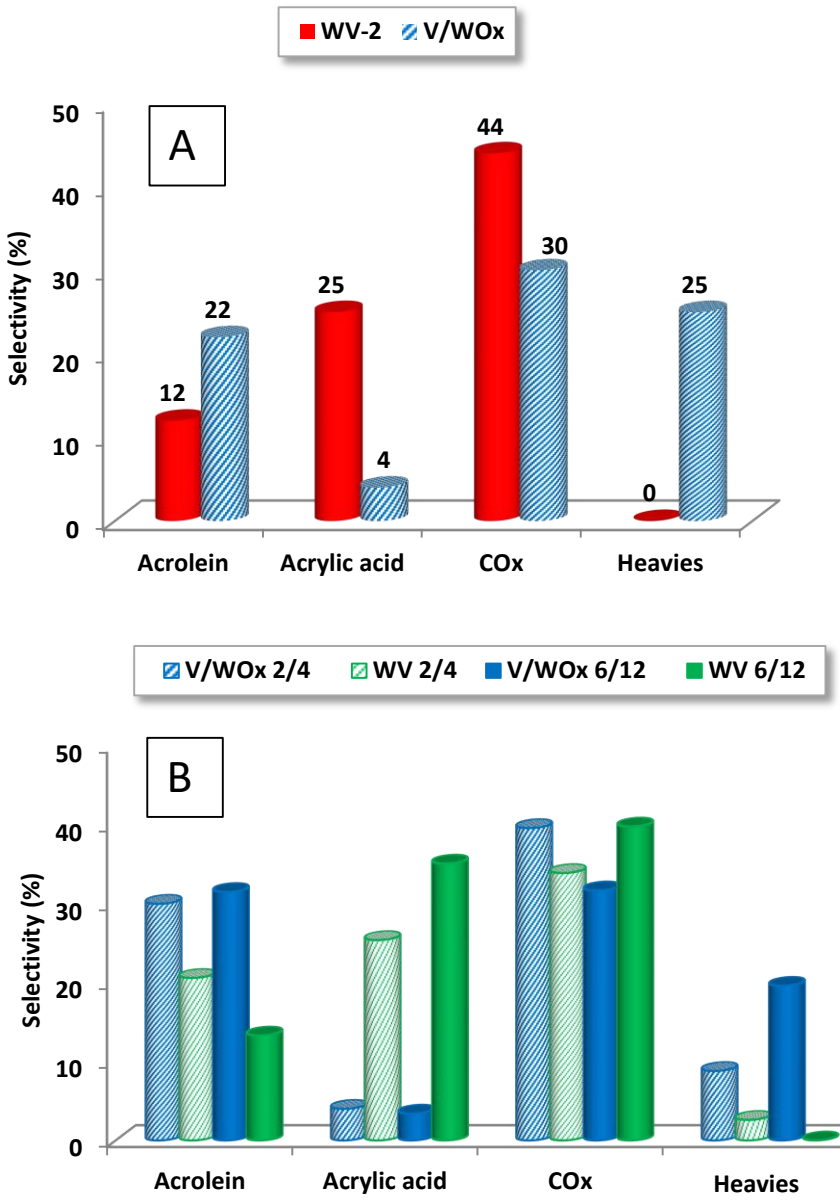

Figure 9. A) Comparison of the catalytic performance of sample WV-2 (atomic ratio V/W: 0,12) in ref. 14 to VO-WO_x, contact time 0,4s. **B)** Comparison of the catalytic performance of sample WV to VO-WO_x, contact time 0,4s. Feed composition: 2 mol% glycerol, 4 mol% oxygen, 40 mol% water, and 54 mol% nitrogen, **or**, 6 mol% glycerol, 12 mol% oxygen, 40 mol% water, and 42 mol% nitrogen.

1.3.3 In situ FTIR spectroscopy study with acrolein

In the first step of the one-pot oxidehydration of glycerol, that is, dehydration of glycerol to acrolein, acid sites of specific acid strength and type are required to favor the desired dehydration reaction to acrolein.[43] The presence of Lewis acid sites and, particularly, Brønsted acid sites is fundamental to direct the dehydration of the secondary hydroxy group selectively to form acrolein.[44] In the second step, that is, the oxidation of acrolein to acrylic acid, both Lewis acid and redox sites are involved.[48] Depending on the surface properties of the catalyst (acid--base character, nature of oxygen species, and V surface sites), the adsorbed intermediate species evolve into different products such as acrylic acid, acetaldehyde, acetic acid, and CO_x.[49]

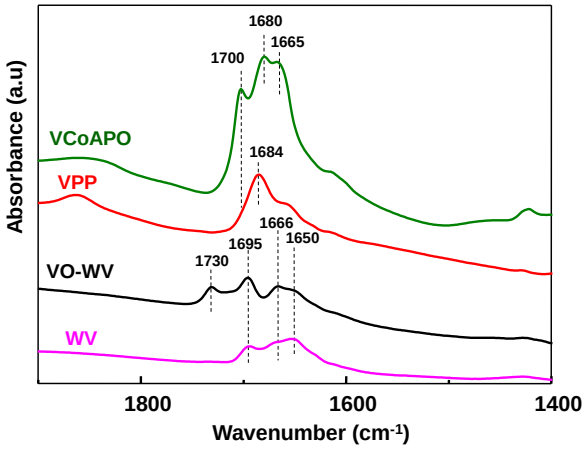

Figure 10. IR spectra of acrolein adsorbed at 25°C on selected samples.

Preliminary evaluation of the interaction of acrolein with the surfaces of the catalysts was performed under anaerobic conditions at room temperature (Figure 10). For the WV, VO-WO_x, VCoAPO, and VPP catalysts, rather complex IR spectra can be observed after acrolein adsorption. The band at approximately $\bar{\nu}$ = 1695 cm^{-1} can be assigned to the stretching vibration of the C=O moiety interacting with the OH groups (i.e., Brønsted acid sites) on the catalyst surface,[50] whereas bands at approximately $\bar{\nu}$ = 1680, 1666, and 1650cm^{-1} are associated to the same carbonyl group interacting with the Lewis acid sites, mainly V^{5+}/V^{4+} ions, in different oxidation states and/or coordination environments

(e.g., tetrahedral, octahedral, polyoxo species, dimers, etc.). Owing to the different crystal structures of VCoAPO and VPP, a different nature of the vanadium ions is expected; in fact, this is observed in the IR spectra (Figure 10). The band at $\bar{\nu}$ = 1684 cm^{-1} is the most prominent signal in the spectrum of the VPP sample, whereas in the spectrum of the VCoAPO sample, two bands at $\bar{\nu}$ = 1680 and 1665 cm^{-1} are observed. From the structural characterization data, VCoAPO and VPP samples are characterized by the presence of V ions respectively in a tetrahedral and a square based bipyramidal coordination environment, and both of them show a mixed oxidation state of V (V^{5+}/V^{4+}). According to the lower coordination number of the V ions, their acid strength is expected to be lower, which would lead to a lower C=O stretching frequency shift after adsorption of acrolein, as clearly evidenced from the IR spectra. The band at $\bar{\nu}$ = 1730 cm^{-1} observed in the spectrum of the VO_x-WO_x sample is due to a ketone intermediate species formed on the catalyst surface by a secondary surface reaction[50,51] (Figure 10). Given that the reactivity of the surface oxygen species and their interaction with adsorbed acrolein are key in the reaction mechanism, another in situ FTIR spectroscopy study was performed placing both acrolein and O_2 in contact on the different catalysts surface at room temperature. The evolution of the surface species and molecules desorbed in the gas phase was studied as a function of the catalyst temperature, which was progressively increased (see the Experimental Section).

On the WV catalyst, the adsorption of acrolein at room temperature leads to hydrogen-bonded acrolein ($\bar{\nu}$ = 1695 cm^{-1}) and coordinatively bonded acrolein on Lewis surface sites ($\bar{\nu}$ = 1666 and 1650 cm^{-1}) (Figure 11-A). Given that the hydrogen-bonded complex is easily removed from the surface by evacuation, it can be assumed that it does not play an important role in the catalysis of acrolein oxidation. Upon increasing the temperature to 80°C, a new band appears at $\bar{\nu}$ = 1723 cm^{-1} at the expense of the bands at $\bar{\nu}$ = 1666 and 1650 cm^{-1}. The band at $\bar{\nu}$ = 1723 cm^{-1} is ascribed to carbonyl-bonded acrolein, referred to as surface complex III by Andrushkevich and Popova.[49] In complex III, the C=O moiety of acrolein is bound with an O atom that belongs to the oxide framework of the catalyst; this is believed to be the key intermediate for the selective oxidation of acrolein to acrylic acid on mixed-oxide catalysts. At room temperature and before

evacuation (see above), the band at approximately $\bar{\nu}$ = 1695 cm^{-1} is assigned to hydrogen-bonded acrolein; however, as this species quickly desorbs under vacuum, at this temperature (80°C) it must be assigned to another species bearing the C=O moiety and formed from the interaction of acrolein, oxygen, and the catalyst surface.

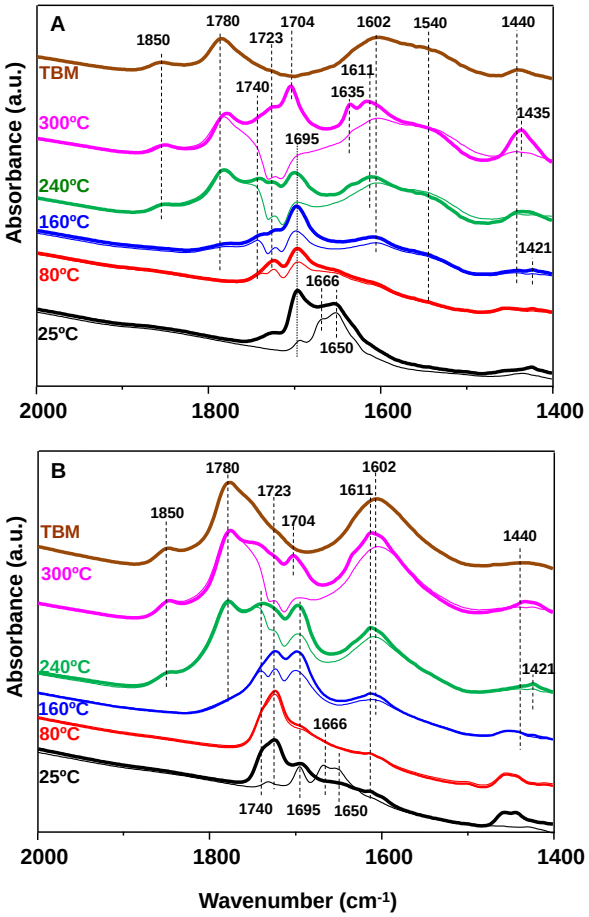

Figure 11. Mechanistic studies performed by co-adsorption of acrolein and oxygen at increasing temperatures, on samples WV (A), VO-WOx (B). Thin lines correspond to the sample at the given temperature while straight line corresponds to the sample at a given temperature but after cooling down the pellet to 25°C. TBM= spectrum achieved at 300°C but using a turbo molecular pump.

Considering the relatively low temperature (80°C) and bearing in mind the products observed in the reactivity tests, it is possible to assign this new band to acetaldehyde, formed by oxidative cleavage of the C=C bond of acrolein. At 80°C, a less intense IR band at $\bar{\nu}$ = 1740 cm^{-1} can also be observed, and it is assigned to a C=O bond corresponding to

a ketone functional group[52] produced as a byproduct of consecutive reactions occurring on the catalyst surface. Upon increasing the temperature to 160°C, the previous band at $\bar{\nu}$ = 1723 cm^{-1} is no longer detected on the catalyst surface, but it is detected in the gas phase. This band, together with a very weak band at $\bar{\nu}$ = 1421 cm^{-1}, also present in the re-adsorption spectra, is associated to acrylic acid. On the other hand, the IR bands ascribed to acetaldehyde ($\bar{\nu}$ = 1695 cm^{-1}) together with a new weak band at $\bar{\nu}$ = 1370 cm^{-1}, grow in intensity; acetaldehyde is also partially desorbed into the gas phase. Moreover, a complex set of IR bands at $\bar{\nu}$ = 1780, 1740, 1602, 1540, and 1440 cm^{-1} is detected on the catalyst surface. Given that these bands remain stable in the cool-down IR spectra, they should be ascribed to surface-adsorbed species. The band at $\bar{\nu}$ = 1740 cm^{-1} (already detected at 80°C and associated to C=O vibration of adsorbed ketones) has also been reported as the intermediate species toward the formation of adsorbed cyclic anhydride. Indeed, the IR band at $\bar{\nu}$ = 1780 cm^{-1} is characteristic of cyclic anhydride species.[52] The other bands at $\bar{\nu}$ = 1540 and 1440 cm^{-1} are due to acetate species, whereas the band at $\bar{\nu}$ = 1602 cm^{-1} is characteristic of a C-O-C bond of a lactone-type compound. All these species are formed because of overoxidation of the initially adsorbed intermediate complexes. Upon increasing the temperature to 240°C, the formation of acrylic acid and acetaldehyde is favored, both as adsorbed surface species and desorbed in the gas phase. At 300°C, acrylic acid formation ($\bar{\nu}$ = 1723, 1635, 1435 cm^{-1}) is strongly enhanced; an additional sharp band detected at $\bar{\nu}$ = 1704 cm^{-1} is symptomatic of acetic acid formation (bending vibration of the carboxylic OH group appears at $\bar{\nu} \approx$ 1440 $cm^{->1}$). Acetic acid may be formed by oxidation of acetaldehyde.[53]

To ascertain the influence of molecular oxygen and water vapor in the reaction mixture, the experiment just described was repeated by using the same catalyst, that is, WV, but under anaerobic conditions or in the presence of water (Figure 12). From the results it is clear that lattice oxygen species are the active species for the selective oxidation of acrolein to AA[54] and water helps its desorption[55] (i.e., it avoids consecutive reactions). However, owing to poorly resolved IR spectra (broadness) in the presence of water, our discussion will focus on the IR spectra of acrolein and O_2 co-adsorption in the absence of water.

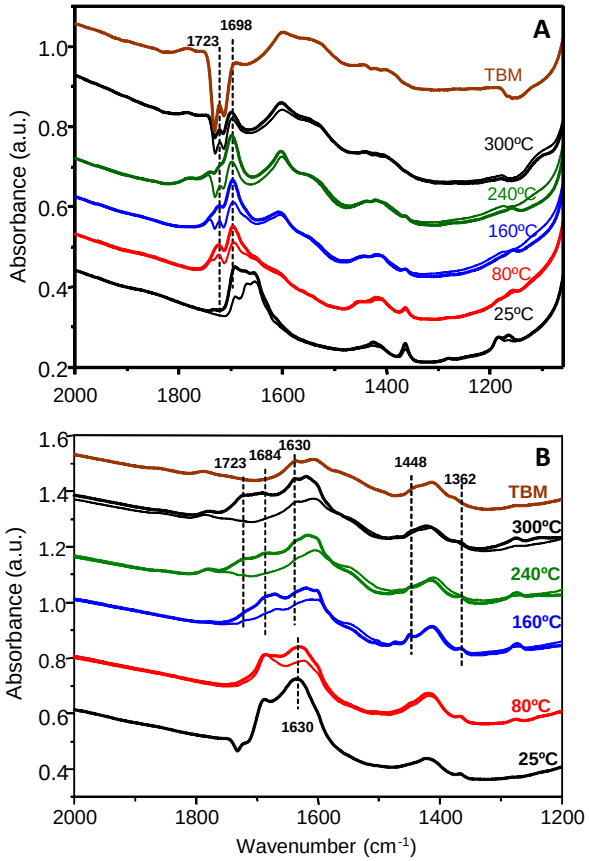

Figure 12. In situ FTIR study of the acrolein adsorption on WV. A) Under anaerobic condition, B) in presence of oxygen and water (acrolein/O_2/H_2O feed composition equal to 1/7/20 mol%).

Acrolein and oxygen were made to react on the VO-WO_x sample (Figure 11-B). Relative to WV and contrary to that observed in the catalytic tests (Figure 9-A), the exchanged V ions (extra-framework) seem to increase the reactivity of the surface oxygen species, as the carbonyl-bonded acrolein surface complex and ketone intermediate species ($\bar{\nu}$ = 1723 and 1740 cm^{-1}, respectively) are readily formed if the sample is kept at room temperature for some time (≈ 20 min). Upon increasing the temperature to 80°C, both bands increase in intensity. A further increase in the temperature to 160°C favors the gas-phase desorption of acrylic acid ($\bar{\nu}$ = 1723, 1611, and 1421 cm^{-1}) and acetaldehyde ($\bar{\nu}$ = 1695 cm^{-1}); surface species are also formed ($\bar{\nu}$ = 1780, 1740, 1602, and 1440 cm^{-1}). However, opposite to WV, a further increase in the temperature to 240°C-300°C slows down the gas-phase formation of acrylic acid and acetaldehyde, whereas the IR bands

associated to strongly adsorbed surface species increases. Acetic acid (gas-phase formation 1704 cm^{-1}) is also detected at 300°C. VO-WO_x presents an important proportion of strong acid sites (see Figure 3) and the highest acid density (as $\mu mol_{NH3}\ m^{-2}$) among all the V-containing catalysts reported herein; therefore, the acid sites seem to bind the product intermediates strongly, which hampers their desorption. This hypothesis is supported by the IR spectroscopy study, which highlights hindered desorption of the intermediate carbonyl complexes; this lowers the formation of acrylic acid and increases the formation of heavy compounds and CO_x. Interestingly, the absence of the IR band at $\bar{\nu}$ = 1540 cm^{-1} (associated to a COO^- moiety of an acetate species) can be related to the desorption of those adsorbed species as CO_x, as observed in the catalytic tests.

On VCoAPO and VPP, the in situ IR spectra of coadsorbed acrolein and O_2 (Figure 13,A-B) show behavior that is completely different to that of the HTB-like materials; this is not surprising taking into account the different nature of the surface V species.[24,35] As a general note, despite the fact that the just-mentioned differences in surface V species leads to slight shifts in the IR bands associated to some adsorbed molecular species, for easier comparison to the previous spectra and to avoid redundancy in the explanation of IR bands, the same IR bands will be used in the following portion of the text (and in the respective figures) to comment on the in situ IR studies. The discrepancies can be easily understood looking at the related figures.

On VCoAPO (Figure 13-A), the V ions in the tetrahedral environment clearly show a lower oxygen insertion capability for the partial oxidation of acrolein, which agrees with the absence of acrylic acid in the gas-phase IR spectrum and the absence of the IR band at $\bar{\nu}$ = 1723 cm^{-1} associated to the carbonyl surface complex. A similar observation was reported for another reaction, namely, the oxidative dehydrogenation of alkanes.[55] Instead, acetaldehyde ($\bar{\nu} \approx$ 1695 cm^{-1}) partially desorbs into the gas phase. Other species characterized by IR bands are shown at approximately $\bar{\nu}$ = 1670-1620 cm^{-1}, which correspond to ketone- or C=C-containing species. These results agree with the catalytic data, which indicate that a higher temperature is needed for the formation of acrylic acid because of the lower reactivity of the tetrahedral V ions. Moreover, opposite to V-

containing tungsten bronzes (in which V is in octahedral coordination), higher partial pressures of the reactants in the feed do not improve the formation of acrylic acid in the catalytic tests.

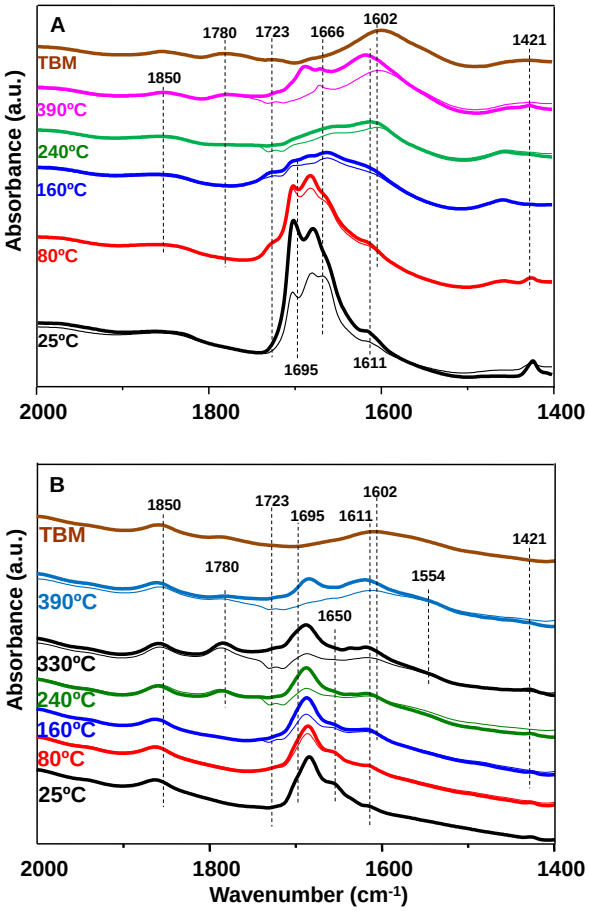

Figure 13. Mechanistic studies performed by co-adsorption of acrolein and oxygen at increasing temperatures, on samples VCoAPO (A) and VPP (B). Conditions as in Figure 11.

VPP behaves similarly to VCoAPO, that is, it shows low oxygen insertion ability without the formation of the carbonyl-bonded acrolein complex (Figure 13-B). Acetaldehyde (IR band at $\bar{\nu} \approx 1695$ cm^{-1}) is mainly desorbed in the gas phase, which starts at 80°C. At 240°C, cyclic anhydride like species form on the catalyst surface ($\bar{\nu}$ = 1780 cm^{-1}), and only at 330°C are small amounts of acrylic acid formed ($\bar{\nu}$ = 1723 cm^{-1}), but acetaldehyde (1695 cm^{-1}) remains the main species present in the gas phase. Interestingly, at 390°C the cyclic compounds ($\bar{\nu}$ = 1780 cm^{-1}) decrease, whereas a new broad band appears at $\bar{\nu}$ = 1554

cm^{-1}, which is associated to asymmetric COO^- stretching. The coordination of vanadium in VPP catalysts, that is, bipyramidal V^{4+} sites,[24] can result in oxygen insertion ability that lies in between that of VCoAPO (with V sites presenting tetrahedral coordination) and that of WV bronzes (with V sites presenting octahedral coordination), but high temperatures are required to perform the oxidation of acrolein. Besides, the reason why VPP needs lower concentrations of glycerol to obtain good selectivity to AA (see catalytic tests) can also be attributed to the relatively limited availability of the redox active sites on the surface, a peculiar feature of this catalyst also reported for other reactions.[56] To have a good fraction of V^{5+} sites available for oxidation (see XPS results, Table 1), it is necessary to keep the partial pressure of the reactants low and the partial pressure of O_2 (relatively) high.

1.3.4 Structure-reactivity correlations

A molecule of glycerol approaching the catalyst surface from the gas phase predominantly reacts with Brønsted acid sites to perform double dehydration into acrolein (Scheme 2, step 1). Acrolein that is produced must quickly desorb or selectively be oxidized; otherwise, the surface acid sites catalyze the formation of several byproducts, such as ketones, cyclic anhydrides, and lactone-type compounds. Acrolein that is desorbed in the gas phase can re-adsorb on the catalyst surface to react further (Scheme 2, step 2). However, it is likely that acrolein that remains adsorbed (without intermediate desorption) is preferentially oxidized over the former, which requires the close proximity of both acid and redox sites.

This is particularly true in the presence of glycerol, which is known to adsorb strongly on the catalyst surface and compete with acrolein adsorption.[17] Once acrolein is formed, Lewis acid sites are mainly responsible to coordinate the interaction of the aldehyde with the nucleophilic oxygen species (i.e., O^{2-}) present on the catalyst surface and generated by the presence of V ions.[57] In this way, an intermediate surface complex, that is, a carbonyl-bonded acrolein, is formed (Scheme 2, step 3). This is the key intermediate for the selective oxidation of acrolein into acrylic acid. In this reaction step, the coordination environment of V and its oxidation state play vital roles; specifically, a higher

coordination number of the vanadium-ions favors the oxidation of acrolein into AA.[44] In addition, the presence of V^{5+} can speed up the oxidation step, which can be of special importance to avoid consecutive reactions if working with very reactive species such as acrolein. The presence of in-framework or extra-framework species does not seem to be determinant, provided that the proximity of acid and redox sites is guaranteed.

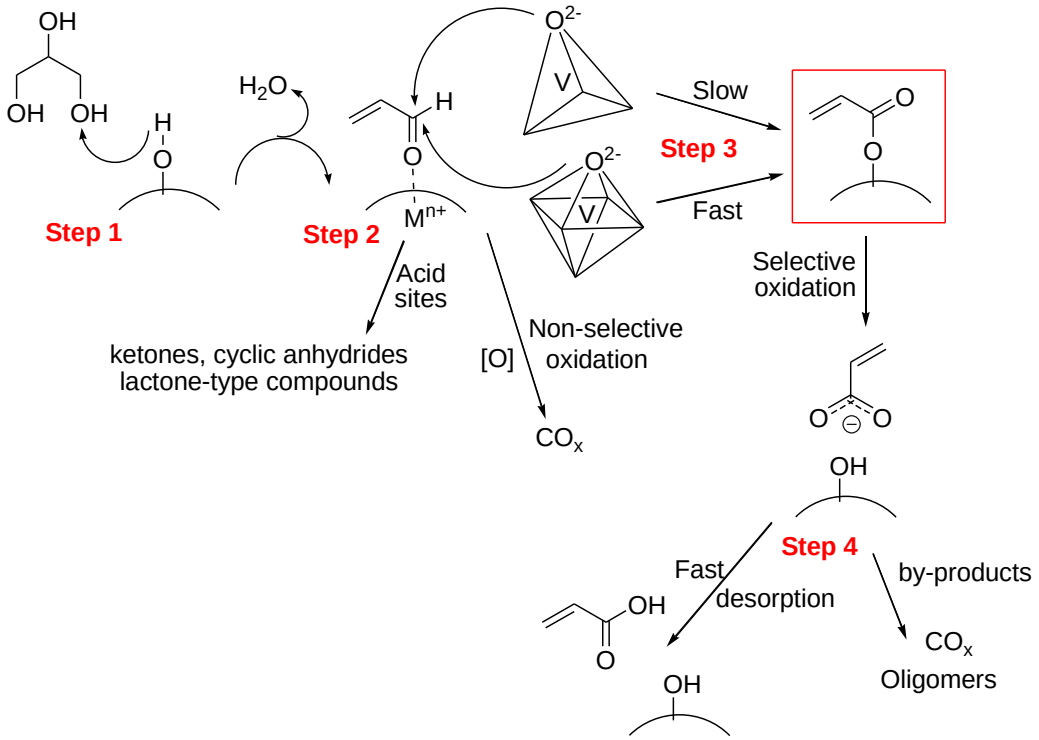

Scheme 2. Reaction mechanism for the glycerol oxidehydration reaction on acid catalysts with vanadium as the active redox element.

Although acid sites are not normally involved in the oxidation of acrolein into acrylic acid, they actually control the desorption step of the latter (Scheme 2, step 4). Owing to the strong nucleophilicity of the COO^- moiety, if the acidity of the catalyst surface is too strong and the acid density (as acid sites per m^2 of surface area) too high, the desorption step is impeded. In the last case, consecutive reactions on acid and/or redox sites lead to oligomerization and total oxidation. This observation is remarkable, as it points out that the one-pot oxidehydration of glycerol can be efficiently performed only by using catalysts that possess acid sites of sufficient strength and density to perform the

dehydration step, but not too strong and in too close proximity to impede the desorption of acrylic acid in the gas phase.

1.4 Conclusions

Several bifunctional catalysts were studied with the aim of finding molecular-level relations that link their structures to the respective catalytic behavior for the oxidehydration of glycerol into acrylic acid. Indeed, despite the fact that all catalysts presented acid properties to efficiently dehydrate glycerol into acrolein with vanadium as the only redox element, their catalytic performance as a function of temperature and partial pressures of reactants was remarkably different. A tangled scheme emerged, in which several physicochemical properties of the catalysts (derived from their different structures) were found to govern the three main elementary steps responsible for the catalytic phenomenon: adsorption, surface reactions, and desorption. Remarkably, the same surface features played different roles in the multiple steps required to produce acrylic acid from glycerol, that is, its dehydration into acrolein and the partial oxidation of the latter into the acid monomer. This work is the first example of a systematic study that aimed to find structure-reactivity correlations for a broad variety of vanadium-containing catalysts for the one-pot oxidehydration of glycerol into acrylic acid. It revealed the role played by the different physicochemical features of the catalysts and their influence on the overall catalytic performance, and it suggested several key features to pursue for the development of new catalysts.

2. A new synthetic route for the production of methacrylic acid starting from bio-propylene glycol

Methacrylic acid (MA) and its ester derivatives are widely used as monomers for the production of a wide range of polymers. In particular, poly(methyl methacrylate) (PMMA), commonly known as acrylic glass, is the primary polymer of this category and it provides strong, clear and lightweight plastics, usually employed in sheet form in glazing, signboards and lighting equipment[58]. Nowadays, the global market of PMMA is on boom and it is expected to keep growing in the near future, the latter trend mainly driven by the needs of the economics of the Asia-Pacific region. Consequently, the global market of its monomer, MMA, is estimated to exceed 4,8 million metric tons by 2020[108]. Most of the MMA production is still based on the acetone cyanohydrine route (ACH process), that was the first method industrially employed for manufacturing MMA in 1933, and the only process worldwide adopted until 1982[58,59]. Main drawbacks of the latter process are linked to the employment of toxic hydrogen cyanide (HCN) and the production of large quantities of ammonium bisulfate waste, opening serious safety and environmental sustainability issues. Hence, many efforts have been done in the last decades to develop valid alternatives for replacing the ACH process. In particular, only a few new processes have been commercialized until now, that utilize ethylene (C2-route, developed by BASF) and isobutene (C4-route, developed by Nippon Shokubai and Mitsubishi Rayon) as carbon sources. Even if economic considerations for the various processes also depend upon regional raw material costs and supplies, none of the alternative processes so far developed is clearly economically superior to the ACH route to warrant its replacement[58]. Another route has been examined for a long time, that is propionic acid (PA) or methyl propionate (MP) condensation with formaldehyde (or its derivatives). Notably, the latter method appears to be particularly appealing thanks to its limited number of steps[59].

In the latter scenario, here we propose a new synthetic route for the production of MA and/or MMA using propylene glycol (PG) as starting material. Moreover, our proposal

would provide the opportunity to produce MA/MMA from biomass resources, representing an interesting alternative to the classic petroleum-based route. Indeed, PG can be readily produced from bio-glycerol by means of a hydrogenolysis reaction, and this process has already been commercialized on industrial scale in 2010 [60].

The overall process formally consists in three reaction steps, oultined in Scheme 3: i) PG dehydration to propanal (PAL); ii) PAL oxidation to propionic acid (PA); iii) PA condensation with formaldehyde generated in-situ from methanol (MeOH). In particular, referring to reactions i) and ii), the research activity focussed on the possibility to perform the single-step gas phase transformation of PG into PA, by means of multifunctional catalysis (as previously done for glycerol oxydehydration to acrylic acid). This solution is particularly interestingly since it would allow to reduce the number of the steps of the overall process. Therefore, this chapter has been subdivided into two sections: the first one regards the direct transformation of PG into PA, while the second one concerns the production of MA from PA and MeOH.

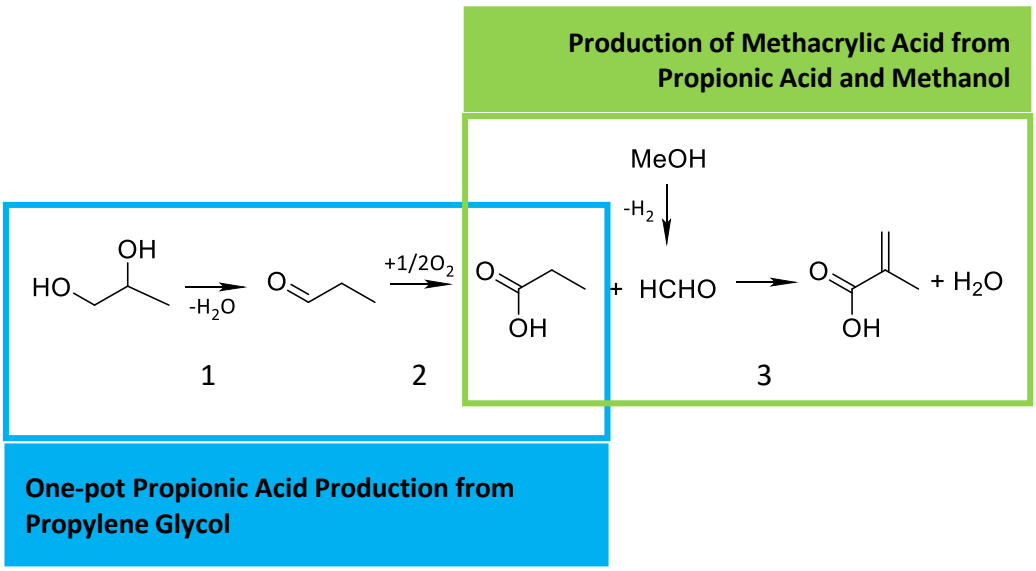

Scheme 3. Synthetic route for the production of methacrylic acid starting from bio-propylene glycol.

2.1 Gas-phase Propionic Acid Production from Propylene Glycol

2.1.1 Introduction

In this section, we report about a new route for propionic acid (PA) synthesis starting from propylene glycol (PG), as a first step in the synthesis of bio-based methacrylic acid. Moreover, PA is an important chemical used directly as bactericidal or as intermediate for the production of cellulose esters, plastic dispersions, herbicides, pharmaceuticals, fragrances and flavors.[61] PA is currently synthesized mainly through the Reppe synthesis where ethylene is made react with carbon monoxide and water in the presence of nickel tetracarbonyl. If on one hand the Reppe process is very efficient in terms of both conversion and selectivity, on the other hand it requires pressures as high as 100-300 bar, therefore being very energy-consuming; moreover, the non-renewable character of the raw materials used and toxicity concerns attributed to $Ni(CO)_4$, open obvious remarks about safety and sustainability of the process. In order to overcome these issues, an alternative route for producing propionic acid would be highly desirable. In this context, our proposal would provide the opportunity to produce propionic acid from biomass resources, representing an interesting alternative to the classic petroleum-based route. Indeed, as already mentioned, PG can be readily produced from bio-glycerol by means of a hydrogenolysis reaction, and this process has already been commercialized on industrial scale in 2010 [60].

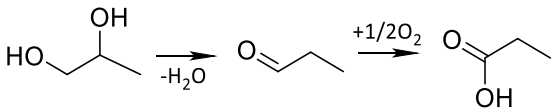

Scheme 4. The two reaction steps required for the transformation of propylene glycol into propionic acid.

As outlined in Scheme 4, the overall transformation from PG to PA includes two reaction steps: i) PG dehydration to propanal (PAL), promoted by acid catalysis, and ii) PAL oxidation to the corresponding acid, that needs redox catalysis. As previously discussed for the analogous transformation of glycerol into acrylic acid, different process

configurations can be taken into account, that are, the two-step process, with two reactors and two different catalytic beds, and the one-step process. Since PAL is industrially mainly employed as a chemical intermediate, and propionic acid is one of the main compounds produced from PAL[62], the one-step transformation would represent the ideal option. Indeed, it would allow to eliminate the intermediate step for the purification of the aldehyde, hence simplifying the reactor design. The one-step approach can be realized through two technical solutions: i) by structuring two different catalytic layers in a single reactor, an acid one and an oxidative one, respectively for the dehydration and the oxidation steps, and ii) by employing a multifunctional catalyst (acid and redox) which combines the two steps of the process into a single catalyzed transformation. If, on one hand, multifunctional catalysis approach is very demanding from the catalyst point of view, on the other hand, for the two in-series beds approach serious limitations can derive from being forced to use the same reaction conditions for both catalytic beds. Differently, the use of technologies useful to overcome this problem (e.g., interstage heat exchange) could severely affect the economic feasibility of the process.

In the latter scenario, PG conversion was investigated over different multifunctional acid and redox catalysts, that were previously proved to be effective for the analogous one-pot transformation of glycerol into acrylic acid: one, hexagonal tungsten bronzes (HTBs) with in-framework vanadium and molybdenum species[15,17]; two, a zeotype material, that is, modified-$AlPO_4$-5 catalysts with in-framework vanadium species[29]; three, a commercial vanadyl pyrophosphate (VPP) catalyst[27]. Moreover, the catalytic activity of a Mo-V-W-O mixed oxide with Mo_5O_{14} type phase[18] was finally investigated.

This work is divided in two sections: in the first part, the one-pot conversion of PG with HTB oxides (containing V and Mo as redox elements) is discussed, particularly focusing on the description of the overall reaction network; in the second part, the catalytic performances of different multifunctional acid and redox materials (still containing V and Mo as redox elements) are described. In both the sections, a comparison with the one-pot transformation of glycerol to acrylic acid is also realized. Overall, this study allowed us to shed light on the complex reaction network and understand which are the main

critical points of the PG-to-PA one-pot process, finally suggesting several key features to follow for the development of new catalysts.

2.1.2 Experimental Section

2.1.2.1 Catalyst preparation

Hydrothermal synthesis of HTBs

W-V-O (WV), W-Nb-O (WNb) and W-Mo-V-O (WMoV) oxides with hexagonal tungsten bronze type phase were prepared through the hydrothermal method, following a previously reported procedure.[15,17] The initial solutions were prepared from the salts of selected metals, i.e. ammonium metatungstate hydrate (≥ 85 wt% WO_3 basis, Sigma-Aldrich), vanadium (IV) oxide sulfate hydrate (≥ 99.99%, Sigma-Aldrich), niobium oxalate (mono-oxalate adduct, ABCR), and ammonium heptamolybdate tetrahydrate (guaranteed reagent (GR) for analysis, Merck). Ammonium metatungstate was dissolved in water and oxalic acid was used as the reducing agent. Vanadium sulfate, niobium oxalate and ammonium heptamolybdate were then added to the clear solution of tungsten. The solution was transferred to a teflon-lined stainless steel autoclave, fitted with two valves that allow purging the autoclave with a flow of nitrogen, so as to create an inert atmosphere. An over pressure of nitrogen (1 bar) was finally set. The autoclaves were heated at 175°C for 48 h. The solid obtained was filtered off with distilled water and dried at 100°C for 16 h. Finally, the solid (precursor) was heat-treated at 600°C during 2 h under N_2.

Hydrothermal synthesis of modified AlPO4-5

Modified $AlPO_4$-5 sample (VCoAPO) was synthesized by hydrothermal method using triethylamine as a template.[29] Cobalt was introduced during the synthesis to improve the acid properties of $AlPO_4$-5 catalyst. Vanadium was added during the synthesis, so as to obtain in-framework vanadium species Aluminum hydroxide (Catapal A, Sasol) was added to an 85% solution of phosphoric acid (Aldrich) in water, and the mixture was stirred until a homogeneous solution was obtained. Triethylamine was added to this mixture under continuous stirring. Then an aqueous solution of cobalt (II) acetate was incorporated along with a V_2O_5/triethylamine solution. The final reaction mixture was

stirred until achieving a homogeneous gel. The gel was introduced in Teflon-lined stainless steel autoclaves and heated at 200°C for 16 hours. After crystallization, the sample was centrifuged at 10,000 rpm, washed with distilled water and dried overnight at 100°C.

Commercial VPP catalyst

The commercial VPP catalyst used for this study was the industrial catalyst used by DuPont to produce maleic anhydride from *n*-butane; this catalyst was studied in depth by various authors.[27] Particularly, we used its calcined form.

Synthesis of MoVW catalysts with Mo5O14 type structure

The Mo–V–W-O catalyst, with a Mo_5O_{14} type structure (MoVW), was prepared from an aqueous solution of ammonium heptamolybdate (GR for analysis, MERCK), vanadium (IV) oxide sulfate hydrate and ammonium metatungstate (with a Mo/V/W molar ratio of 0.68/0.23/0.09), by evaporation in a rotavapor (at 50°C). The solid was dried at 100°C overnight and then calcined in air at 350°C. Lastly, the solid was heat-treated in N_2 at 500◦C for 2 h.

2.1.2.2 Catalyst characterization and gas-phase catalytic tests

For details about the analysis carried out for the catalysts characterization and the experimental of catalytic tests, see sections 1.2.2 and 1.2.3. Residence time was calculated as W/F, by the ratio between catalyst weight (g) and total gas flow (mL/min), the latter being measured at room temperature.

2.1.3 Results and Discussion

2.1.3.1 Physicochemical properties of the oxides

Characterization data of WV, VCoAPO and VPP catalysts are reported in section 1.3.1, whereas WMoV oxide with HTB structure and MoVW with Mo_5O_{14} were previously characterized, data reported in ref. [10,7].

Table 3 summarizes the main physicochemical properties of the catalysts.

Table 3. Phisicochemical properties of the catalysts. *Ps-C = pseudo crystalline.

Sample	Phase	SSA (BET) ($m^2 g^{-1}$)	NH_3-TPD ($\mu mol_{NH3} g^{-1}$)	NH_3-TPD ($\mu mol_{NH3} m^{-2}$)
WV	HTB	21	76	3,7
WMoV	Ps-C*	38	129	3,4
VCoAPO	$AlPO_4$-5 (AFI)	263	241	0,9
VPP	$(VO)_2P_2O_7$	41	90	2,2
MoVW	Mo_5O_{14}	6	21	3,5

2.1.3.2 Catalytic tests

PG conversion with HTB oxides

W-Nb-O oxide with HTB structure

First, PG conversion was investigated on a purely acidic W-Nb-O mixed oxide (WNb) with HTB structure (WNb) with the aim of focussing on the dehydration step only of the oxydehydration process, and to check whether this class of materials are able to perform the selective dehydration of PG into PAL. Indeed, it is well-know that on acidic catalysts, in addition to PAL, PG can also convert into acetone and allylic alcohol, depending on which hydroxyl group is involved into the dehydration process[63–65]. Referring to literature, it is interesting to highlight the fact that PAL generally is the main dehydration product with most of the acid materials so far studied for PG dehydration. The latter behavior was explained by Zhang et al.[65] on the basis of the mechanism reported in Scheme 5. In particular, 1,2-diols are known to undergo the pinacol rearrangement to give the corresponding aldehyde[66], hence the authors proposed that protonation of either of the hydroxyl groups and rearrangement can generate three reactive carbenium intermediates which yield acetone, PAL and allyl alcohol. The secondary carbenium ion, leading to PAL, is more stable than the primary one, thus it is expected to have the higher concentration. Despite this fact, acid/base features of the catalysts might considerably influence PG conversion[64] and HTB oxides appear to possess the proper acid properties

to perform the selective dehydration of PG to PAL, both in terms of acid strength and type of acid sites, where the preponderance of Brønsted sites was proved to be beneficial for the reaction[64]. In particular, the introduction of Nb into WO_x with HTB structure was previously proved to improve the acid properties of WO_x HTB oxide[67,68], in terms of both total acidity, strength and Brønsted-to-Lewis ratio of the acid sites, as well as its thermal stability.

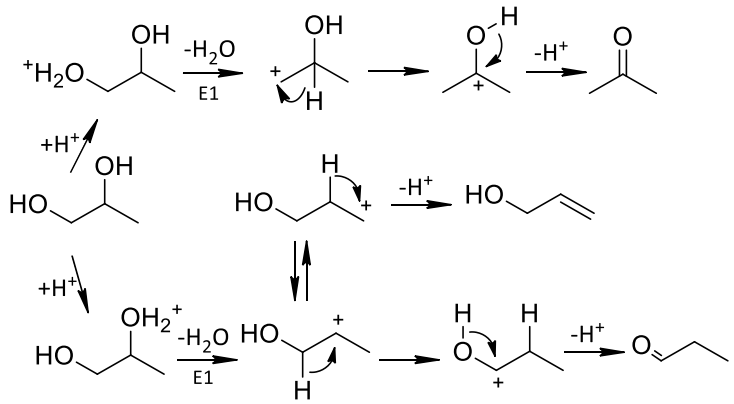

Scheme 5. PG dehydration over solid acid catalysts.

In Figure 14., PG conversion on WNb sample is reported as a function of temperature. The experiments were carried out in the same reaction conditions, in terms of feed composition and residence time, employed for the oxidehydration reaction, with oxygen and water in the inlet feed (feed composition mol% $PG/O_2/H_2O/N_2$ = 2/4/40/54). It can be immediately noticed that this catalyst performs rather well for PG selective dehydration into PAL. Indeed in the range of temperature between 240-260°C, yields up to 86% were obtained, whereas acetone and allylic alcohol yields were always lower than 2%. The glycol conversion was always high in the whole range of temperature investigated, being complete for values of temperature higher than 240°C. For lower temperatures, the formation of heterocyclic acetals was observed, reported as "dioxolanes" in the graph. These molecules derive from a reversible bimolecular reaction between unconverted PG and an aldehyde, this reaction being promoted by acid catalysis as well. In particular, three different species of dioxolanes were detected: 2-ethyl-4-methyl-1,3-dioxolane, 2,4-methyl-1,3-dioxolane and 4-methyl-1,3-dioxolane,

supposedly deriving from the condensation reactions between the glycol and PAL, acetaldehyde and formaldehyde respectively (Scheme 6).

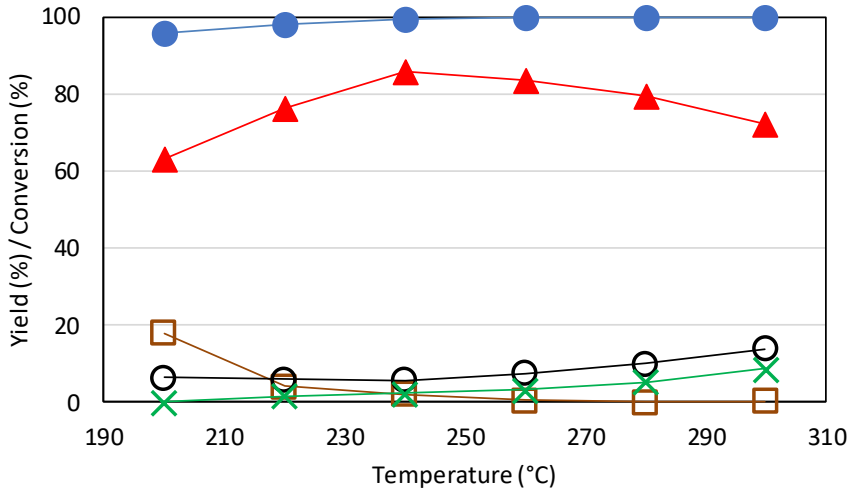

Figure 14. PG conversion on WNb sample as a function of temperature. Symbols: PG conversion (●), PAL (▲), dioxolanes (□), others (○), CO_x (X). "Others" includes: acetaldehyde, acetone, acrolein, methacrolein, allylic alcohol, 1-PrOH, acetic acid, propionic acid, 2-methyl-2-pentenal and unknown compounds. Carbon loss is always minor than 7%. Reaction conditions: feed composition (mol%): $PG/O_2/H_2O/N_2$ = 2/4/40/54; W/F (time factor) = 0,01 g*min/mL.

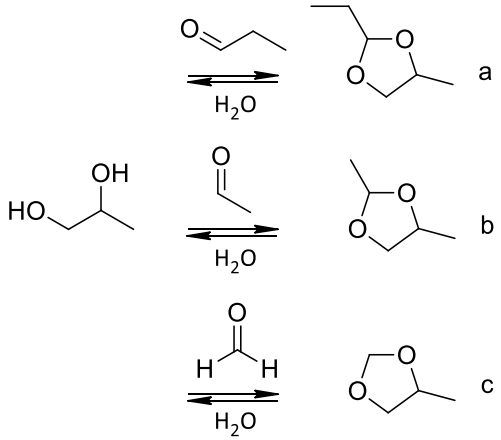

Scheme 6. Formation of cyclic acetals from condensation between PG and PAL, acetaldehyde and formaldehyde: a) 2-ethyl-4-methyl-1,3-dioxolane; b) 2,4-methyl-1,3-dioxolane; c) 4-methyl-1,3-dioxolane.

Anyway, with this catalyst, high yields into 2-ethyl-4-methyl-1,3-dioxolane (the acetal deriving from PAL) were obtained, whereas 2,4-methyl-1,3-dioxolane and 4-methyl-1,3-

dioxolane only formed in minor amount. Dioxolanes formed in considerable amount at lower reaction temperatures and incomplete PG conversion, as already observed for other catalytic systems[63,65,69], and rapidly decreased while increasing temperature, mainly in favor of the corresponding aldehydes, with PAL yield increasing from 63% at 200°C to 86% at 240°C. Above this temperature, PAL slowly decreased reaching a 72% yield at 300°C, mainly in favor of the formation of carbon oxides, acetaldehyde, acetic acid, propionic acid and acrolein (reported as "others" in figure), all of them arguably deriving from oxidation reactions. Hence, the loss of selectivity into PAL for temperatures higher than 240°C could depend on the presence of oxygen in the inlet feed. Therefore, an experiment was performed feeding PG on WNb sample without oxygen in the feed, at the temperature of 240°C.

Table 4. PG conversion with WNb: the effect of O_2 in the inlet feed. Reaction conditions: temperature = 240°C, W/F = 0,01 g*min/mL, feed composition (mol%) $PG/O_2/H_2O/N_2$ = 2/4/40/54, reaction time = 1h with O_2 and 2h without O_2. *Others = acetaldehyde, acetone, acrolein, methacrolein, allylic alcohol, 1-propanol, acetic acid, propionic acid and unknown compounds.

Feed composition $PG/O_2/H_2O$ mol%	**2/4/40**	**2/-/40 (no O_2)**
PG Conversion (%)	99,3	99,5
Yield (%)		
PAL	85,8	87,3
Dioxolanes	2,1	0,9
2-methyl-2-pentenal	0,5	2,9
CO_x	2,4	-
Others*	5,3	3,9
Carbon Loss	3,2	4,5

In Table 4, the results obtained in the second hour of reaction are reported. Indeed, during the first hour a higher carbon loss was observed, fact that was not observed while co-feeding oxygen and that could reasonably be attributed to an initial adsorption of some unidentified species on the catalyst surface. After two hours reaction, a yield of

87% to PAL was obtained, comparable to the result of the experiment carried out with co-feeding oxygen. Overall, the selectivity to PAL does not significantly increase when performing the reaction without oxygen in the feed. Indeed, on one hand the amount of by-products deriving from oxidation reactions (carbon oxides, acetaldehyde, acetic acid, propionic acid and acrolein), as well as the amount of dioxolanes, was reduced; on the other hand, the formation of 2-methyl-2-pentenal, deriving from the self-condensation of PAL, slightly increased. The addition of oxygen to the inlet feed could be beneficial to limit the deactivation phenomena that typically occur for gas phase dehydration reactions on acid catalysts. Therefore, even if no significant differences of PAL yield were observed after two hours reaction time, the presence of oxygen could arguably affect catalyst lifetime. Hence, time-on-stream experiments should be performed in order to study the deactivation phenomena of WNb catalyst and the effect of oxygen in the feed for PG dehydration reaction.

W-(Mo)-V-O oxides with HTB structure

First, the influence of temperature on PG conversion was investigated on W-V-O oxide (WV) (Figure 15), in the range of temperature between 200 and 340°C. The experiments were carried out in the same reaction conditions, in terms of feed composition and residence time, previously employed for the glycerol oxidehydration process[17] (feed composition (mol%) $PG/O_2/H_2O/N_2$ = 2/4/40/54; W/F = 0,01 g*min/mL), whereas the lower temperature investigated is smaller (200°C vs 290°C) because of the lower vaporization temperature of the glycol (188°C) compared to glycerol (290°C).

The main reaction products were PAL, dioxolanes, acetaldehyde, acetic acid, propionic acid and carbon oxides. Minor compounds, reported as “others” in the graph, and showing a maximum 6% total yield, were allylic alcohol, acetone, 1-propanol, acrolein, methacrolein and acrylic acid. Referring to the dehydration step of the process, as already shown by WNb, WV catalyst was also able to selectively dehydrate PG into the desired product PAL, showing very low yields to acetone and allylic alcohol. Despite this fact, the maximum yield to PAL obtained with this sample was about 30% at 220°C. For temperatures lower than 240°C and incomplete PG conversion, dioxolanes formed in

considerable amount, as already observed with WNb. However, with WV dioxolanes deriving from the acetalization of acetaldehyde and formaldehyde also formed in considerable amount, together with the dioxolane deriving from PAL. Increasing the temperature, dioxolanes yield rapidly decreased mainly in favor of PAL and acetaldehyde. Then, a further increase of temperature made PAL progressively decrease, with acetic acid and carbon oxides rapidly increasing and becoming the main reaction products for temperatures higher than 280°C whereas, interestingly, propionic acid, that is our desired product, formed in minor amounts only with a maximum yield of 11% at 260°C.

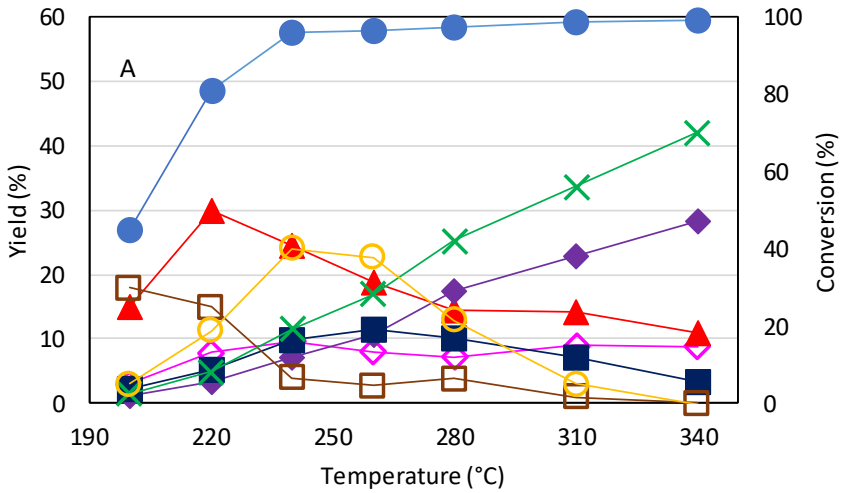

Figure 15. PG conversion as a function of temperature with WV. Symbols: PG conversion (●), PAL (▲), dioxolanes (□), acetaldehyde (◊), acetic acid (◆), propionic acid (■) and carbon loss (○), CO_x (X). Reaction conditions: feed composition (mol%) $PG/O_2/H_2O/N_2$ = 2/4/40/54; W/F (time factor) = 0,01 g*min/mL.

Arguably, acetic acid may generate from the oxidation of acetaldehyde while the latter might originate directly from PG, by means of a C-C oxidative cleavage, but also from the intermediate PAL. Together with acetaldehyde, the C-C cleavage reaction might also generate a molecule of formaldehyde, which can be further oxidized to formic acid or CO/CO_2, as reported in reaction Scheme 7. Unfortunately, the analytical system associated to the plant was not able to detect both formaldehyde and formic acid, hence a quantification of the latter two compounds could not be performed. Anyway, as to

ascertain their presence, an injection into HPLC-RID of a reaction sample was also made, and their formation was confirmed. Finally, a contribution to C_1 and C_2 compounds deriving from the final product, propionic acid, could not have been discharged as well.

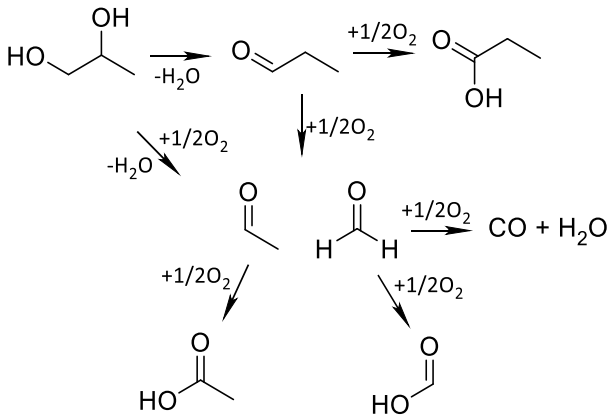

Scheme 7. Possible reaction network for PG conversion on WV oxide.

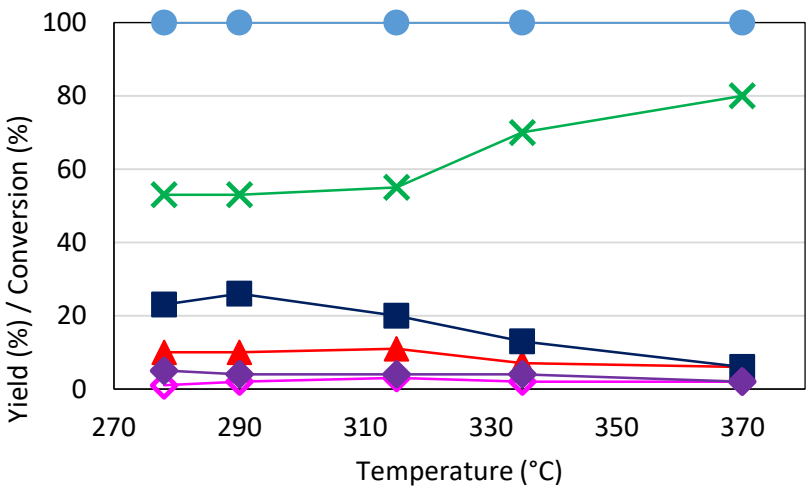

Figure 16. GLY conversion as a function of temperature with WV. Symbols: GLY conversion (●), acrolein (▲), acetaldehyde (◊), acetic acid (◆), acrylic acid (■) and CO_x (X). Reaction conditions: feed composition (mol%) $GLY/O_2/H_2O/N_2$ = 2/4/40/54; W/F = 0,01 g*min/mL.

It was also interesting to compare reactivity results of PG conversion with those obtained by feeding glycerol. In Figure 16 catalytic results for glycerol conversion as a function of temperature performed with WV are reported. Experiments here shown were carried out using the same reaction conditions, in terms of feed composition and residence time,

as those used with PG. All in all, it is important to mention that with glycerol the transformation into the corresponding acid (acrylic acid) prevailed over the formation of acetaldehyde and acetic acid in a certain range of temperature, and the maximum yield of 26% into acrylic acid was obtained at 290°C. On the other hand, a greater amount of carbon oxides was formed in the whole range of temperature investigated.

At this point, PAL was fed on WV catalyst in order to check whether this material might be able to perform the selective oxidation of the intermediate aldehyde into propionic acid (results are reported in Figure 17). PAL converted into propionic acid, acetaldehyde, acetic acid, and carbon oxides. Moreover, the formation of a remarkable amount of heavy compounds, especially deposited on the internal surface of the reactor, was also observed. However, it was not possible to make an accurate assessment of these species, from both a qualitative and quantitative point of view. Hence, the carbon loss was introduced in Figure 17 and it was mainly attributed to the formation of heavy compounds.

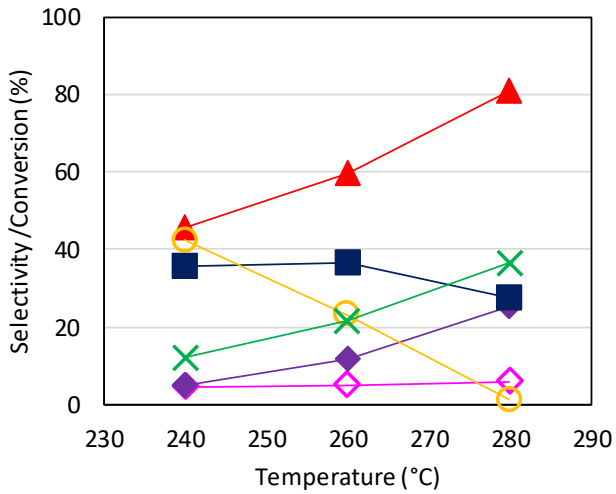

Figure 17. PAL conversion as a function of temperature with WV . Symbols: PAL conversion (▲), acetaldehyde (◊), acetic acid (◆), propionic acid (■), CO_x (X) and carbon loss (○). Reaction conditions: feed composition (mol%) $PAL/O_2/H_2O/N_2$ = 2/4/40/54; residence time = 0,01 g*min/mL.

The catalyst activity considerably increased with temperature, with PAL conversion raising from about 40% at 240°C up to 80% at 280°C. Propionic acid prevailed over the

other reaction products for lower reaction temperatures, showing the maximum selectivity of 37% at the temperature of 260°C. Nevertheless, this selectivity value was limited at lower temperatures by a high formation of heavy compounds, arguably deriving from condensation of the aldehyde itself, promoted by the acidity of the catalyst. The redox ability of the catalyst appeared to be largely affected by the reaction temperature and, presumably, at lower temperatures the rate of the oxidation might be slower and this fact could favor the condensation reactions promoted by the acid sites. The carbon loss substantially decreased while increasing the temperature; on the other hand, the formation of a considerable amount of C_1 and C_2 compounds, arguably deriving from the oxidative cleavage of PAL, was also observed.

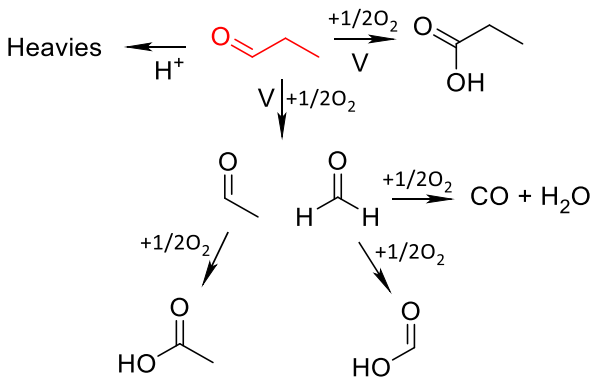

Scheme 8. Conversion of PAL on WV catalyst.

Overall, it is important to highlight the fact that the experiments carried out by feeding PAL on WV catalyst showed quite a good selectivity into propionic acid, suggesting that the family of hexagonal tungsten bronze materials might be effective catalysts to perform this reaction.

Then, it was decided to test another catalytic system belonging to the family of HTB oxides consisting in the tricomponent W-Mo-V-O system, labelled as WMoV (WMoV-3 in ref. [17]). The latter sample was chosen because of two main reasons. First, it was previously proved to be more effective than WV for both the glycerol oxidehydration, leading to the maximum acrylic acid yield of 50%, and the selective oxidation of acrolein

to acrylic acid. This behavior was attributed to its higher acid and redox properties that allow to dehydrate glycerol more efficiently and are responsible for a faster oxidation of the intermediately formed acrolein into acrylic acid and an easier desorption of the latter molecule from the catalyst surface[17]. Moreover, only a few papers regarding the gas phase oxidation of PAL to propionic acid are present in literature, and the most effective catalyst so far reported seems to be a system based on a Mo-V-O mixed oxide (hence containing both V and Mo as redox elements), which is typical catalyst for the gas phase oxidation of acrolein to acrylic acid[70].

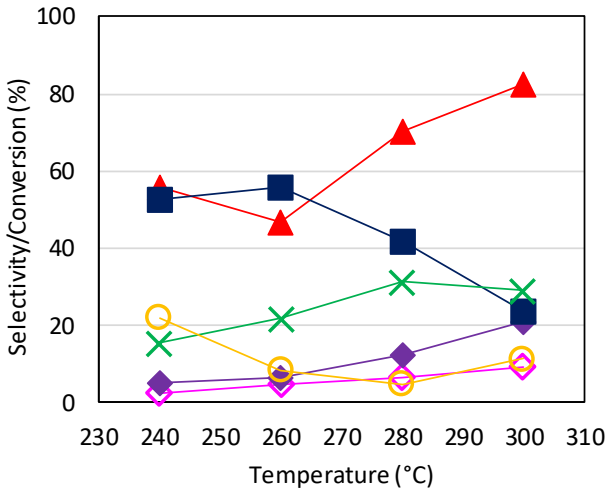

Figure 18. PAL conversion as a function of temperature with WMoV. Symbols: PAL conversion (▲), acetaldehyde (◊), acetic acid (◆), propionic acid (■), CO_x (X) and carbon loss (○). Reaction conditions: feed composition (mol%) $PAL/O_2/H_2O/N_2$ = 2/4/40/54; residence time = 0,01 g*min/mL.

First, PAL was fed over WMoV (Figure 18) and, compared to WV, a higher selectivity of 55% and a maximum yield of 29% were obtained at the temperature of 240°C, together with a lower amount of heavy compounds, acetaldehyde and acetic acid, in the range between 240 and 280°C. Then, a further increase of temperature up to 300°C led to an additional decrease of propionic acid selectivity, mainly in favor of acetic acid.

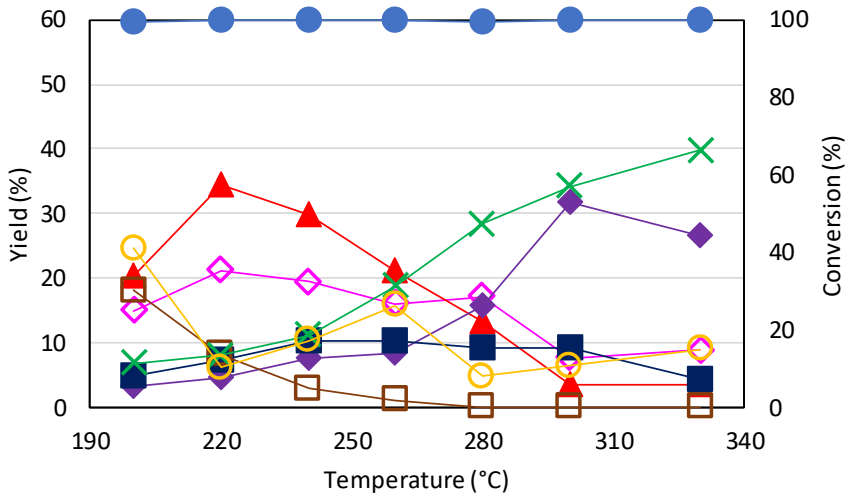

Figure 19. PG conversion as a function of temperature with WMoV. Symbols: PG conversion (●), PAL (▲), dioxolanes (□), acetaldehyde (◊), acetic acid (◆), propionic acid (■) and carbon loss (○), CO_x (X). Reaction conditions: feed composition (mol%) $PG/O_2/H_2O/N_2$ = 2/4/40/54; residence time = 0,01 g*min/mL.

At this point, we decided to perform the direct transformation of PG into propionic acid on the tricomponent oxide (Figure 19). Indeed, the higher acid properties of the WMoV HTB (Table 3) could be beneficial for the dehydration step of the whole process enhancing the formation rate of PAL from PG, as it happened when feeding glycerol[17]. However, despite the good premises, a very low yield into propionic acid was observed also in this case, still with a maximum value of 10% at the temperature of 240-260°C. In contrast with the WV sample, PG conversion was complete in the whole range of temperature investigated. However, apart from this, WMoV showed a catalytic behavior very similar to that one shown by WV. Dioxolanes formed in remarkable amounts at the lower temperatures, and readily decreased along with an increase of temperature mainly in favor of the aldehydes (PAL and acetaldehyde). Yield to aldehydes tended to decrease while increasing the temperature, whereas, on the other hand, acetic acid and carbon oxides increased, becoming the main reaction products for temperatures over 280°C. Conversely, propionic acid always was a minor reaction product in the whole range of temperature. Also in this case, it is interesting to highlight the fact that when glycerol was fed over WMoV in the same reaction conditions (feed composition

polyol/O_2/H_2O =2/4/40 and W/F = 0,01 g*min/mL), the yield to acrylic acid was 31% , with acetaldehyde and acetic acid always showing very low yields[17].

Overall, HTB systems appeared to be quite efficient to promote the selective oxidation of PAL into propionic acid for lower reaction temperatures (240-260°C), whereas increasing the temperature, the formation of acetaldehyde, acetic acid and carbon oxides increasingly prevailed over oxidation to propionic acid. Despite this fact, the whole oxidehydration reaction could not be efficiently performed in the range of temperatures 240-260°C, where PAL could be selectively converted into propionic acid. Therefore, reactivity experiments suggested that for HTB catalysts there might have been a loss of selectivity to propionic acid due to some undesired reaction occurring directly on PG, not only on the intermediate PAL. This loss of selectivity might have been ascribed in part to the formation of dioxolanes by condensation of PG and intermediate PAL (however, occurring only at lower temperatures), and in part to the formation of acetaldehyde, and hence acetic acid, deriving from the oxidative cleavage of PG itself.

Therefore, in order to confirm the complete reaction scheme for PG transformation on HTB oxides, a mechanistic study was performed with WMoV, investigating its catalytic behavior as a function of contact time, under isothermal conditions (240°C). The results are shown in Figure 20. PAL, dioxolanes and acetaldehyde appear to be kinetically primary products, since their selectivities were higher than zero when extrapolated at nil residence time. PAL and dioxolanes also are intermediate compounds, in fact for both of them selectivity declined upon increasing residence time. In particular, PAL selectivity first increased, reaching a maximum for W/F 0,002 g*min/mL, and then it started to decrease mainly in favor of oxidation products. PAL initial increase could reasonably be related to dioxolanes selectivity decrease: supposedly, for low PG conversion, PAL could rapidly react with unconverted PG by means of reversible condensation to form the cyclic acetal. Then, increasing the residence time, consecutive reactions involving the intermediate PAL (and also PG itself) could shift the equilibrium towards the reagents (PAL and PG) leading to a decrease of dioxolanes selectivity. Acetaldehyde selectivity kept increasing with residence time and this behavior could have been explained by taking in consideration two contributions: acetaldehyde deriving from 2,4-methyl-

dioxolane (generated by the condensation of unconverted PG and acetaldehyde itself, the latter deriving from PG oxidative cleavage) and, in minor amount, from the oxidative cleavage of intermediate PAL. Propionic acid, acetic acid and carbon oxides appear to be secondary and final products, since their selectivities were higher than zero when extrapolated at nil residence time and then kept increasing with residence time. In theory, acetaldehyde might also derive from propionic acid C-C scission, even if the latter experiment does not support this hypothesis. In order to verify that there is no significant contribution of propionic acid cleavage, an experiment feeding PAL on WMoV was also performed. Results are reported in Figure 21 and are consistent with the kinetic study performed by feeding PG. Indeed propionic acid selectivity did not decrease in favor of other products.

Overall, these kinetic studies confirmed that acetaldehyde may generate directly from PG, supposedly by means of an oxidative cleavage reaction, promoted by the V redox sites of the catalyst. The latter reaction thus competes with PG dehydration into PAL, catalysed by the acid sites of the oxide, and is responsible for the loss of selectivity into propionic acid in the oxydehydration process.

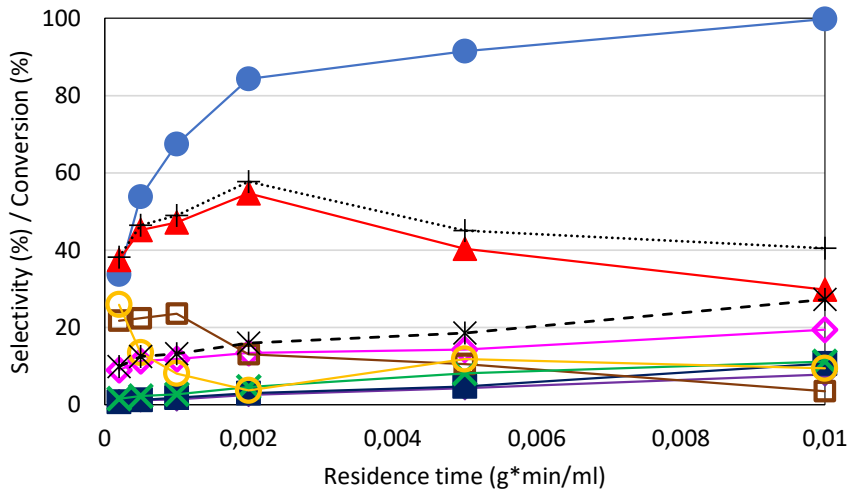

Figure 20. PG conversion as a function of W/F on WMoV sample at the temperature of 240°C and feed composition (mol%) = PG/O_2/H_2O/N_2 = 2/4/40/54. Symbols: PG conversion (●), PAL (▲), dioxolanes (□), acetaldehyde (◊), acetic acid (◆), propionic acid (■), CO_x (X), carbon loss (○), PAL + propionic acid (+) and acetaldehyde + acetic acid (*).

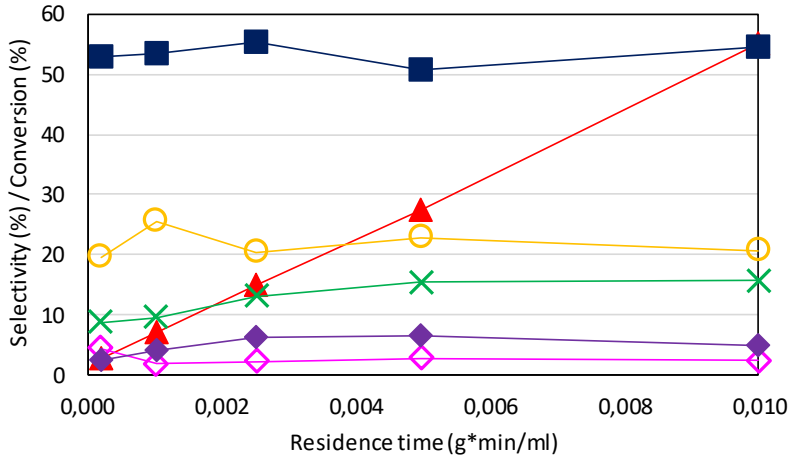

Figure 21. PAL conversion as a function of W/F with WMoV. Symbols: PAL conversion (▲), acetaldehyde (◊), acetic acid (◆), propionic acid (■), CO_x (X) and heavy compounds (○). Reaction conditions: feed composition (mol%) PAL/O_2/H_2O/N_2 = 2/4/40/54, temperature = 240°C.

In order to investigate more in detail the reactions that can be promoted by the redox functionalities of our multifunctional catalyst, PG was also fed on a catalyst containing V as redox element, that is a vanadium oxide supported on silica (VO_x/SiO_2), synthesized by the procedure reported in ref. [71]. Indeed, the latter sample should not possess the proper acid features necessary to promote PG dehydration[72]. Indeed, when PG was fed on VO_x/SiO_2 without adding oxygen in the inlet feed, a low conversion of about 17% and a yield to PAL of 5% were observed (Table 5). PAL was the main reaction product, but also acetone was formed with a yield of about 3% (selectivity 20%), that is the dehydration product deriving from the elimination of the primary hydroxyl group of PG. All in all, this sample was not active in PG dehydration, and neither was selective to PAL. Interestingly, another reaction product observed, with a 2% yield and 14% selectivity, was hydroxyacetone, while the latter never formed when PG was made react on HTB oxides; this compound might derive from the dehydrogenation of the secondary hydroxyl group of PG.

Table 5. PG conversion with VO_x/SiO_2: the effect of O_2 in the inlet feed. Reaction conditions: temperature = 325°C, Residence time = 0,01 g*min/mL, feed composition (mol%) $PG/O_2/H_2O/N_2$ = 2/4/40/54, reaction time = 1h with O_2 and 2h without O_2.

Feed composition $PG/O_2/H_2O$ mol%	**2/4/40**		**2/-/40 (no oxygen in the feed)**	
PG Conversion (%)	82,2		17	
	Yield (%)	Selectivity (%)	Yield (%)	Selectivity* (%)
Acetaldehyde	22,8	27,8	1,0	6,6
PAL	11,0	13,4	5,3	33,2
Acetone	0,9	1,1	3,3	20,5
Acetic Acid	12,0	14,6	0,6	4,1
Propionic Acid	0,2	0,2	0,7	4,4
Dioxolanes	0,5	0,6	1,2	7,7
Hydroxyacetone	0,4	0,5	2,3	14,3
Others*	3,9	4,7	1,4	9,1
CO_x	5,6	6,9	-	-
Total yields/selectivities	56,0	69,8	15,8	-
Carbon Loss	26,2	30,2	-	-

*Others = acrolein, methacrolein, allylic alcohol, 1-propanol and unknown compounds.

Then, PG was fed with oxygen and its conversion was first studied as a function of temperature, in the same reaction conditions previously employed for HTB oxides (Figure 22).

This catalyst is much less active that HTB oxides, indeed total conversion was reached at the temperature of 400°C. The most abundant reaction product observed in the whole range of temperature investigated was acetaldehyde, followed by acetic acid and, for higher temperatures, by carbon oxides.

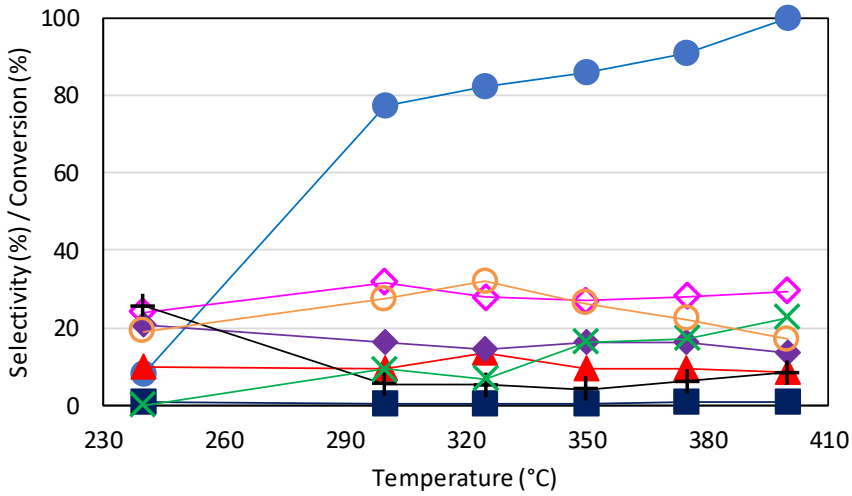

Figure 22. PG conversion as a function of temperature with VO_x/SiO_2. Symbols: PG conversion (●), PAL (▲), acetaldehyde (◊), acetic acid (◆), propionic acid (■), others (+), CO_x (X) and carbon loss (○). Reaction conditions: feed composition (mol%) $PG/O_2/H_2O/N_2$ = 2/4/40/54; residence time = 0,01 g*min/mL. Others = acrolein, methacrolein, allylic alcohol, 1-propanol and unknown compounds.

Propionic acid was always detected as a residual product, with also about 10% of selectivity to PAL. The selectivities to acetaldehyde, acetic acid and PAL remained approximately constant in the whole range of temperature investigated. On the other hand, carbon oxides yield increased with temperature, mainly to the detriment of the carbon loss for temperatures higher than 325°C. It is important to highlight the fact that the carbon loss was always very high with this catalyst. In principle, carbon loss might derive from different phenomena, such as the formation of compounds with high molecular weight, that cannot be eluted by gas-cromatography or that deposit on the reactor walls; carbonaceous deposits on the catalyst surface; formaldehyde and/or formic acid, that cannot be detected by the analytical system associated with the laboratory plant. In order to find an explanation for the origin of the carbon loss, a thermogravimetric analysis with stream of air was performed on the spent catalyst up to the temperature of 600°C, and no significant weight decrease was detected. The formation of heavy compounds deposited on the walls of the reactor was neither observed. Then, the solution collected during the experiment performed at the temperature of 325°C was also analysed by means of HPLC, equipped with a RID

detector. The latter analysis allowed us to realise about the formation of formaldehyde and formic acid in remarkable amounts, even if a quantitative analysis could not be performed. Moreover, the presence of additional species with high molecular weight, that could have been not detected by means of GC-FID, was not observed. Overall, combining all these information, the carbon loss observed with VO_x/SiO_2 sample could reasonably be associated to the formation of formaldehyde and formic acid. Formaldehyde may derive from the oxidative cleavage of PG, PAL, and propionic acid. Formic acid arguably generated from the selective oxidation of formaldehyde.

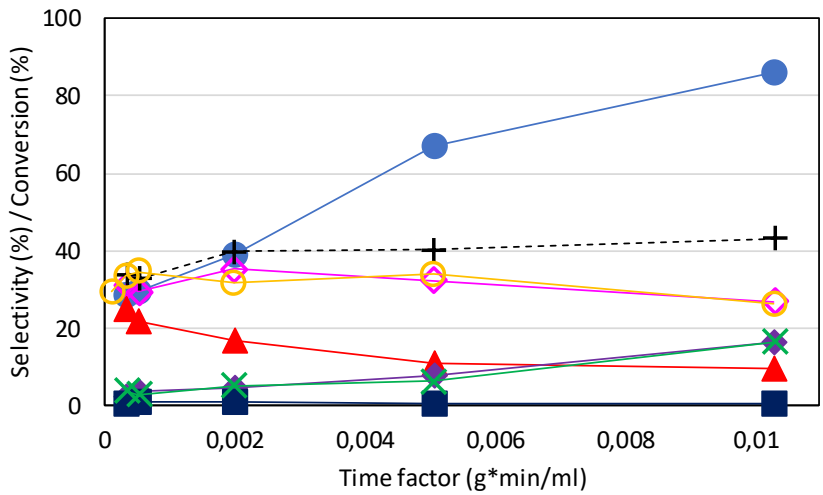

Figure 23. PG conversion as a function of W/F with VO_x/SiO_2. Symbols: PG conversion (●), PAL (▲), acetaldehyde (◊), acetic acid (◆), propionic acid (■), CO_x (X), carbon loss (○) and acetaldehyde + acetic acid (+). Reaction conditions: feed composition (mol%) $PG/O_2/H_2O/N_2$ = 2/4/40/54, temperature = 350°C

In order to better evaluate the kinetic relationships between the products and the reagent, an experiment was also performed with VO_x/SiO_2 feeding PG and oxygen at the temperature of 350°C while varying the W/F (time factor); results are reported in Figure 23. Both acetaldehyde and PAL appeared to be primary products, being their selectivity higher than zero when extrapolated at nil residence time. PAL selectivity kept decreasing while increasing residence time, indicating that the aldehyde also is an intermediate product. Despite this fact, PAL seemed to convert into acetaldehyde (and hence acetic acid) and carbon oxides rather than to propionic acid, since the selectivity to the latter

compounds was always extremely low. On the other hand, acetaldehyde slightly increased with residence time before starting to decrease, mainly in favour of acetic acid. However, when considering acetaldehyde and acetic acid together, the total selectivity kept increasing while PAL decreasing. Acetic acid and carbon oxides appeared to be secondary and final products, since their selectivities tended to zero when extrapolated at nil residence time and then continually kept increasing. Eventually, the carbon loss was also higher than zero when extrapolated at nil residence time, and slightly decreased while increasing the residence time. It is also interesting to note that, when feeding oxygen, acetone always was a minor product, its selectivity being always lower than 2%, in contrast to experiments carried out without oxygen in the feed (Table 5). Acetone was never detected in remarkable amount, neither for low residence time values.

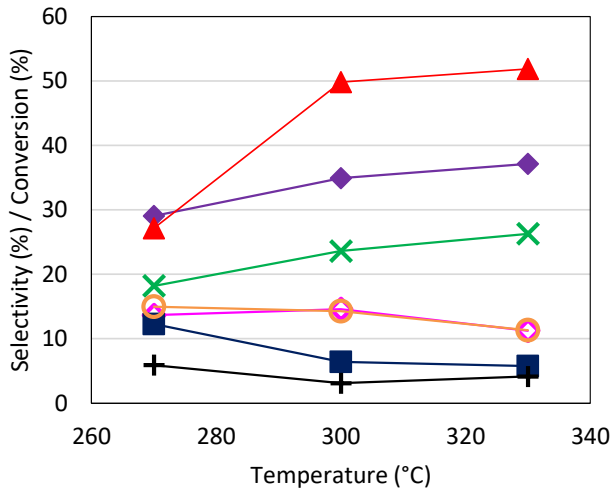

Figure 24. PAL conversion as a function of temperature with VO_x/SiO_2. Symbols: PAL conversion (▲), acetaldehyde (◊), acetic acid (◆), propionic acid (■), CO_x (X), others (+) and carbon loss (○). Reaction conditions: feed composition (mol%) $PAL/O_2/H_2O/N_2$ = 2/4/40/54; W/F = 0,01 g*min/mL.

Moreover, PAL was also fed on VO_x/SiO_2 catalyst, and results are reported in Figure 24. The experiments confirmed that this material is not able to selectively oxidize PAL into propionic acid, since the selectivity into the acid was rather low in the whole range of temperature investigated, and the formation of acetic acid, carbon oxides and acetaldehyde always prevailed. All in all, PAL also appeared to easily undergo an

oxidative cleavage reaction on VO_x/SiO_2 catalyst, and the carbon loss could be attributed, also in this case, to the formation of formaldehyde and formic acid. Similar results were also obtained by Suprun et al with a catalyst based on VO_x supported on TiO_2. Indeed, the yield to propionic acid was always significantly lower than that one to C_1 and C_2 carboxylic acids (formic and acetic acid), hence also in that case the C-C cleavage of PAL was more preferred than its selective oxidation to propionic acid[73].

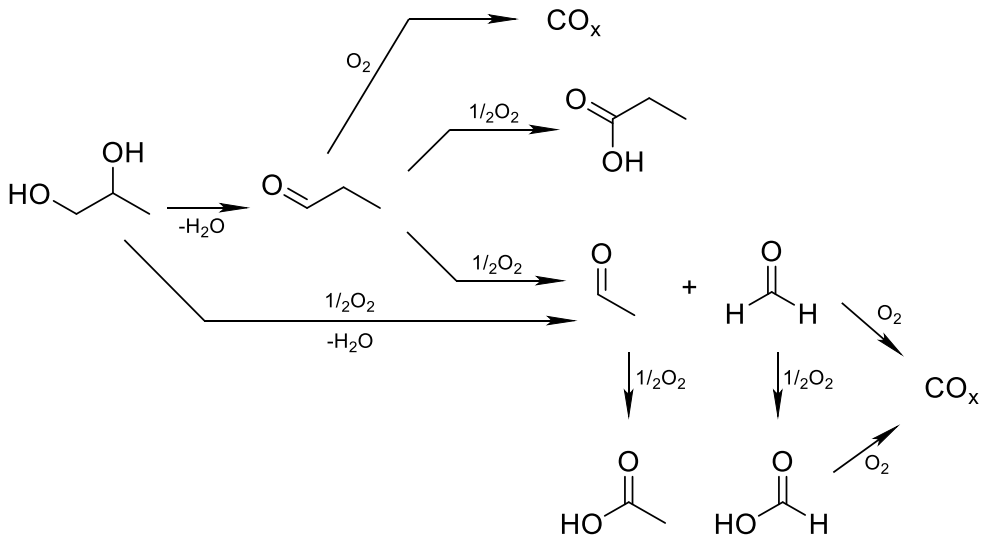

Scheme 9. Overall reaction network for PG conversion with VO_x/SiO_2 catalyst.

On the basis of the considerations above reported , the results of the experiments are overall consistent with the reaction network reported in Scheme 9 for PG conversion on VO_x/SiO_2 catalyst. PG can easily undergo a C-C cleavage leading to the formation of acetaldehyde and formaldehyde. Both aldehydes can further be oxidized to the corresponding C_1 and C_2 carboxylic acids. The formation of carbon oxides appears to derive from the consecutive decomposition of formaldehyde and/or formic acid, however an additional contribution deriving from PAL unselective oxidation cannot be discharged. Despite its low acid properties, VO_x/SiO_2 catalyst was able to convert PG into PAL with a relatively high selectivity. Anyway, it was not able to transform selectively the aldehyde into propionic acid, since the C-C cleavage of the aldehyde prevailed over the selective oxidation to the corresponding acid.

Referring to PG conversion on HTB oxides, still remained unclear how PG oxidative cleavage is influenced by temperature. Hence, another experiment was performed with WMoV at the higher temperature of 300°C (Figure 25), with the aim of examining on how PG oxidative cleavage reaction is affected by temperature. Indeed, in contrast to PAL oxidation that can be easily investigated by feeding directly the aldehyde, PG oxidative cleavage reaction is more difficult to study because of the complex reaction network occurring when the glycol and oxygen are co-fed on multifunctional catalysts. In particular, it was proved that, also with HTB oxides, acetaldehyde does not only derive from PG but also from the cleavage of the intermediate PAL, and the contribution of the latter reaction remarkably increases with temperature (Figure 21). Hence, especially at higher temperatures, it is difficult to distinguish the contribution of the two reactions leading to the formation of acetaldehyde when performing PG oxidehydration. Therefore, a measure of the influence of temperature on PG oxidative cleavage might be obtained by performing kinetic experiments in function of residence time at different reaction temperatures and extrapolating acetaldehyde selectivity at nil residence time, where the formation of the latter could be attributed to PG cleavage only.

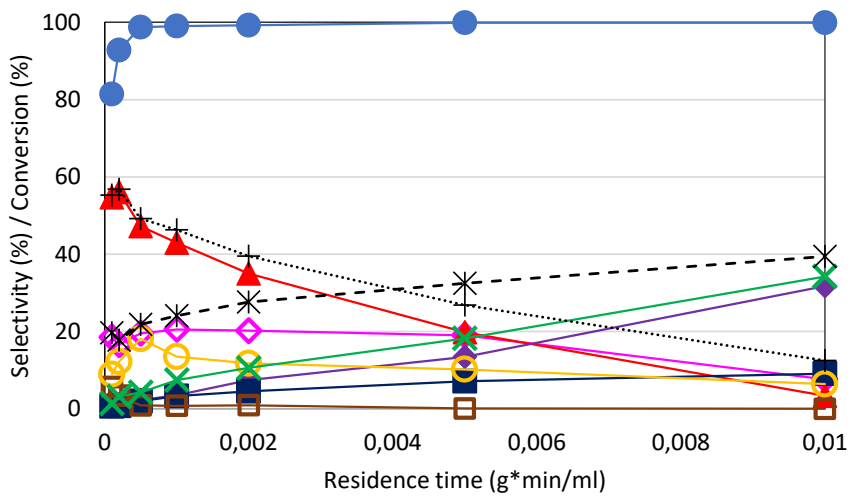

Figure 25. PG conversion as a function of W/F with WMoV at the temperature of 300°C and feed composition (mol%) = $PG/O_2/H_2O/N_2$ = 2/4/40/54. Symbols: PG conversion (●), PAL (▲), dioxolanes (□), acetaldehyde (◊), acetic acid (◆), propionic acid (■), CO_x (X), carbon loss (○), PAL + propionic acid (+) and acetaldehyde + acetic acid (*).

Accordingly, by extrapolating the acetaldehyde selectivity at nil residence time for the two experiments, the selectivity at 300°C (Figure 25) appeared to be higher than that obtained at 240°C (Figure 21) (about 20% vs 10%). However, it must be considered that at 240°C the formation of 2,4-methyl-1,3-dioxolane, deriving from the acetalization of unconverted PG with acetaldehyde formed by PG oxidative cleavage, was also observed for lower residence times, whereas at 300°C it did not form. Therefore, taking into account the amount of acetaldehyde transformed into 2,4-methyl-1,3-dioxolane, acetaldehyde selectivity turned out to be just about 5% smaller at the lower temperature investigated. The latter result suggest that PG oxidative cleavage on HTB oxides might be influenced by temperature to a lesser extent compared to PAL. Indeed, when the conversion of PAL was studied in function of temperature (Figure 18), the selectivity to acetaldehyde + acetic acid was found to increase from 7% at 240°C to 30% at 300°. From experiments performed at 300°C, the kinetic relationship between acetic acid and acetaldehyde also became clear, with acetic acid being a secondary product deriving from acetaldehyde oxidation. Indeed, acetic acid selectivity was null when extrapolated at nil residence time and then it kept increasing with residence time, while acetaldehyde progressively decreased for W/F values higher than 0,005g*min/mL.

Concluding, the experiments carried out on multifunctional HTB oxides are consistent with the overall reaction network reported in Scheme 10. The direct transformation of PG into propionic acid turned out to be a very challenging process, since both the reactant PG and the intermediate PAL may undergo a number of different reactions that finally decrease selectivity to the desired product.

In particular, HTB oxides were found to be quite efficient in the selective oxidation of PAL into propionic acid in the range of temperature between 240-260 °C whereas, increasing the temperature, both the C-C cleavage of the aldehyde and the formation of carbon oxides prevailed over the oxidation to propionic acid. On the other hand, the lower was the reaction temperature, the higher was the formation of heavy compounds deriving from condensation reactions promoted by the acid sites of the catalysts.

Referring to the first step of the process, the selectivity into PAL was limited by two competitive reactions: i) the formation of 2-ethyl-4-methyl-1,3-dioxolane, deriving from the acetalization of the aldehyde with unconverted PG, promoted by the acid sites of the catalysts; ii) the C-C oxidative cleavage of the glycol, that led to the formation of C_1 and C_2 compounds, such as acetaldehyde, formaldehyde, acetic acid, formic acid and carbon oxides. PG cleavage did not appear to be much sensitive to reaction temperature, whereas the formation of 2-ethyl-4-methyl-1,3-dioxolane could be definitely reduced by increasing temperature and hence PG conversion. However, as already mentioned before, increasing the temperature, PAL cleavage and unselective oxidation started to prevail over the formation of propionic acid.

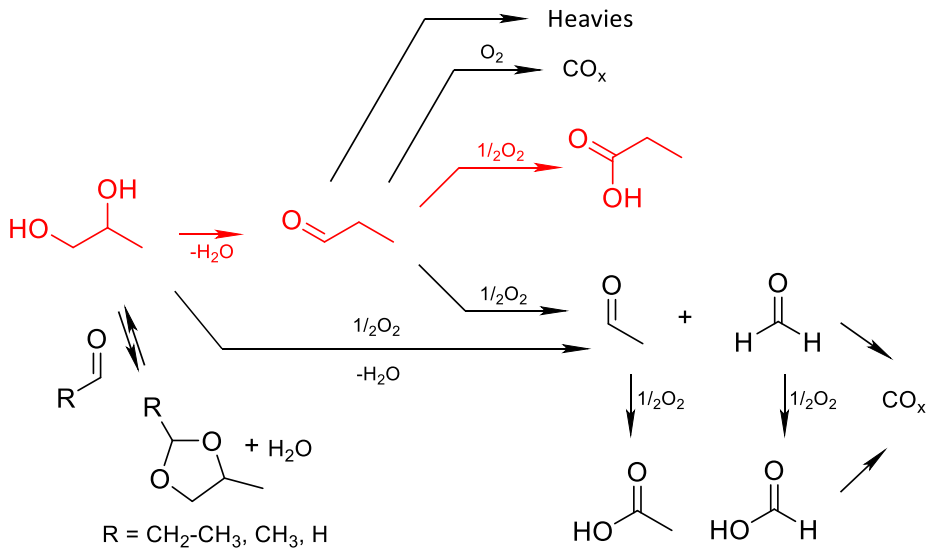

Scheme 10. Overall reaction network for PG conversion on multifunctional HTB oxides. In red, the desired reaction pathway.

About the mechanism responsible for the formation of acetaldehyde on HTB oxides

Looking at the overall reaction network outlined after the reactivity experiments performed on HTB oxides, the mechanism responsible for the formation of acetaldehyde (and hence acetic acid) from both PG and glycerol, still remains unclear.

A few hypothesis can be formulated to explain the formation of acetaldehyde. First, we took into considerations the possibility of formation of acetone or, most likely, of an

acetone-like species adsorbed on the catalysts surface by PG dehydration (Scheme 11). As previously shown, in the presence of an acid catalyst, acetone may generate from the elimination of the secondary hydroxyl group in PG. Similar considerations can be made for glycerol oxidehydration process: the formation of acetaldehyde might derive from hydroxyacetone, or an hydroxyacetone-like species, as depicted in Scheme 12, since the latter molecule is the dehydration product generated by elimination of the secondary hydroxyl group of glycerol.

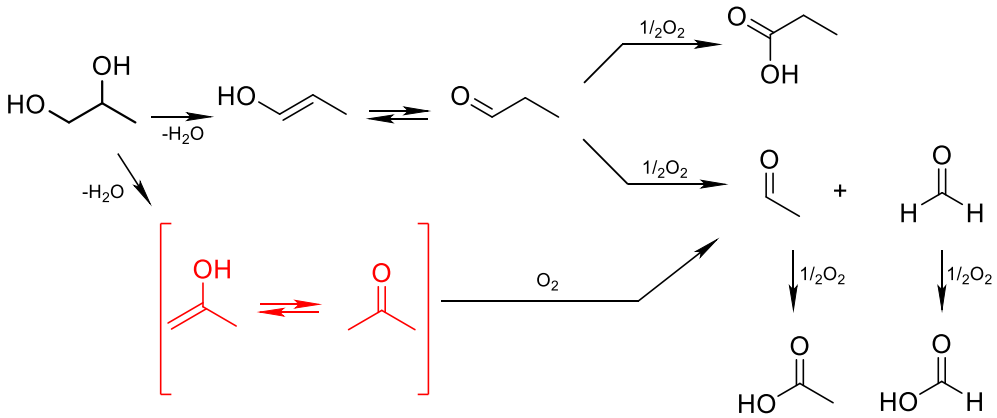

Scheme 11. Acetone or acetone-like specie as intermediate for the formation of acetaldehyde from PG.

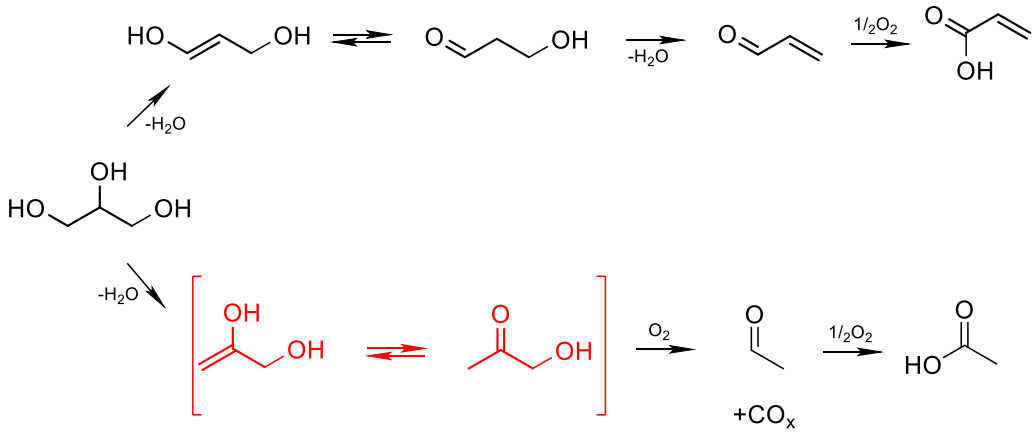

Scheme 12. Hydroxycetone or hydroxyacetone-like specie as intermediates for the formation of acetaldehyde from glycerol.

Therefore, a few reactivity experiments were carried out by feeding directly acetone (Table 6) and hydroxyacetone (Table 7) with WV and WMoV HTB catalysts. Theoretically,

if these two molecules are the reaction intermediates in the mechanism leading to PG and glycerol cleavage, respectively, they shoud be converted to the same products as those obtained during transformation of the latter compounds.

Table 6. Acetone conversion with WV and WMoV. Reaction conditions: W/F = 0,01 g*min/mL, feed composition (mol%) Acetone/O_2/H_2O/N_2 = 2/4/40/54, temperature = 280°C. *Others = PAL, acrolein, propionic acid, acrylic acid and unknown compounds.

	WV	WMoV
Conversion (%)	35,3	49,6
Selectivity (%)		
Acetaldehyde	0,8	6,1
Acetic Acid	37,9	31,2
COx	45,1	46,6
Others*	0,0	1,6
Carbon Loss	16,3	14,4

Table 7. Hydroxyacetone conversion with WV and WMoV. Reaction conditions: W/F = 0,01 g*min/mL, feed composition (mol%) HA/O_2/H_2O/N_2 = 2/4/40/54, temperature = 280°C. *Others = acetone, acrolein, propionic acid and acrylic acid.

	WV	WMoV
Conversion (%)	96,3	99,9
Selectivity (%)		
Acetaldehyde	7,5	12,5
Acetic Acid	35,8	32,5
COx	47,7	50,0
Others*	0,9	2,7
Carbon loss	8,1	2,3

First, it is important to highlight the fact that a rather low conversion of acetone was observed on both HTB oxides. Carbon oxides and acetic acid were the main reaction products whereas low selectivity to acetaldehyde was obtained. These results suggest that acetone on HTB oxides might convert directly to acetic acid rather than to acetaldehyde, as already reported by Conceptiòn et al. for propane and propylene

oxidation on V and Mo-V based catalysts[71]. In conclusion, PG oxidative cleavage does not appear to go through the generation of an acetone-like species as the main intermediate.

On the other hand, when hydroxyacetone was fed on HTB oxides, an almost complete conversion was observed, together with a higher selectivity to acetaldehyde. Therefore, the formation of acetaldehyde, and hence acetic acid, from glycerol on HTB oxides, might derive from the conversion of hydroxyacetone formed by glycerol dehydration.

Referring to PG conversion on redox oxides, it should be also taken into account the possibility of formation of hydroxyacetone (or a hydroxyacetone-like species adsorbed on catalyst surface) by oxidation of PG secondary hydroxyl group. Hence, PG and glycerol might share the same intermediate for the generation of acetaldehyde, and hence acetic acid, on HTB oxides, even if this species likely derives from different reaction pathways (dehydration from glycerol and oxidation from PG).

Finally, piruvaldehyde was also considered as a possible reaction intermediate, since the latter molecule might generate from the oxidation of both hydroxyl groups of PG. Results of reactivity experiment feeding piruvaldehyde are reported in Table 8.

Table 8. Piruvaldehyde conversion on WMoV sample. Reaction conditions: W/F = 0,01 g*min/mL, feed composition (mol%) Pir/O_2/H_2O/N_2 = 2/4/40/54, temperature = 280°C. *Others = acetone, acrolein, propionic acid and acrylic acid.

	Hydroxyacetone	Piruvaldehyde
Conversion (%)	99,9	99,9
Selectivity (%)		
Acetaldehyde	12,5	20,8
Acetic Acid	32,5	40,5
COx	50,0	30,5
Others*	2,7	0,6
Carbon loss	2,3	7,5

Interestingly, similarly to hydroxyacetone, piruvaldehyde conversion was almost complete and the formation of remarkable amounts of acetaldehyde, acetic acid and carbon oxides was also observed. Moreover, compared to hydroxyacetone

piruvaldehyde showed a lower yield to carbon oxides together with the formation of a higher amount of acetaldehyde. Overall, it appears that both hydroxyacetone and piruvaldehyde can potentially act as intermediate compounds for the generation of acetaldehyde, and acetic acid, from PG (but also from glycerol) on HTB oxides. Arguably, the preferential formation of either of the intermediates might depend on the way PG is adsorbed and binds to the catalysts surface, namely by either one or both oxygen atoms of the two hydroxyl groups, as illustrated in Figure 26.

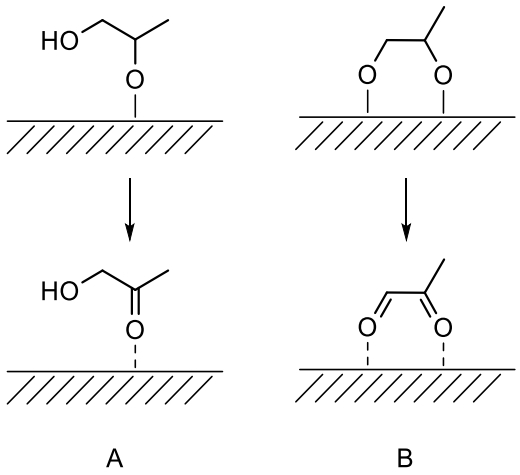

Figure 26. Models for PG adsorption on the catalysts surface.

PG conversion with different V-containing catalysts

In addition to HTB oxides, PG conversion was also studied with different catalysts containing vanadium as redox element, that are, a modified-$AlPO_4$-5 catalysts with in-framework vanadium species[29] (VCoAPO), and a commercial vanadyl pyrophosphate (VPP) catalyst[27]. Like HTB oxides, both of them were previously employed for the direct transformation of glycerol into acrylic acid, results reported in the first chapter of the thesis. VCoAPO and VPP catalytic performances for direct PG transformation to PA were also compared to that of WV catalyst.

First, the influence of temperature on PG conversion was investigated for the three catalysts, WV, VPP and VCoAPO (Figure 27, Figure 28 and Figure 29, respectively). The

experiments were carried out under the same reaction conditions, in terms of feed composition and residence time, previously employed for glycerol oxidehydration with the same catalysts, whereas the range of temperature was modified because of the different boiling point of the two polyols. Therefore, with PG it was possible to explore reaction temperatures even lower than 290°C.

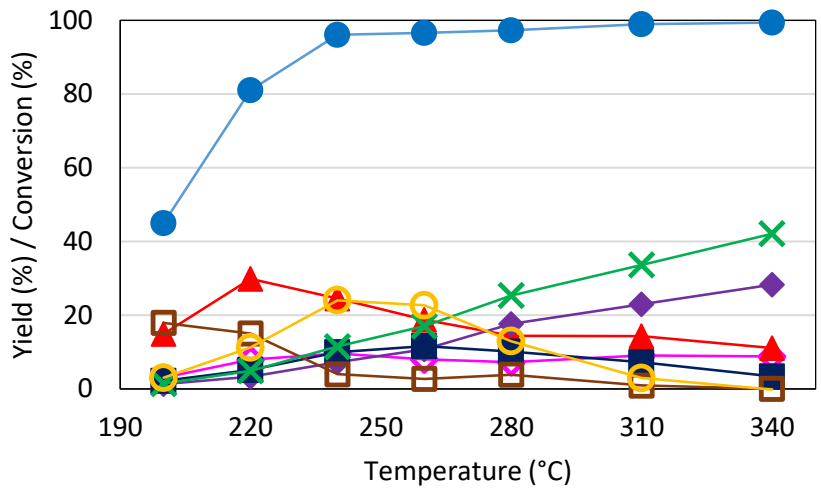

Figure 27. PG conversion as a function of temperature with WV. Symbols: PG conversion (●), PAL (▲), dioxolanes (□), acetaldehyde (◊), acetic acid (◆), propionic acid (■) and carbon loss (○), CO_x (X). Reaction conditions: feed composition (mol%) $PG/O_2/H_2O/N_2$ = 2/4/40/54; W/F = 0,01 g*min/mL.

In all cases main reaction products were PAL, dioxolanes, acetaldehyde, acetic acid, and carbon oxides. Minor compounds, reported as "others" in the graphs, and showing a maximum 6% total yield, were allylic alcohol, acetone, 1-propanol, acrolein, methacrolein, acrylic acid, ethanol, methanol and ethylene. Referring to the dehydration step of the process, it is worth mentioning that the three systems were able to selectively dehydrate PG into PAL. Indeed, as already mentioned in the previous section, besides PAL, on acidic catalysts PG can also convert into acetone and allylic alcohol, depending on which hydroxyl group is involved into the dehydration process.[63–65] For the three catalysts, PAL was the main dehydration product, and very low yields to acetone and allylic alcohol were shown. This behavior can possibly be related to the predominant Brønsted-type acid character of these materials[64].

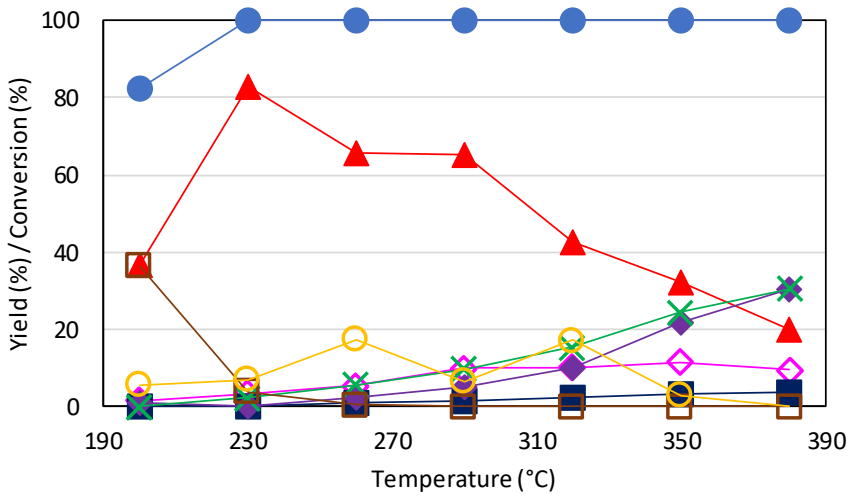

Figure 28. PG conversion as a function of temperature with VPP. Symbols: PG conversion (●), PAL (▲), acetaldehyde (◊), acetic acid (◆), propionic acid (■), dioxolanes (□), CO_x (X) and carbon loss (○). Reaction conditions: feed composition (mol%) $PG/O_2/H_2O/N_2$ = 2/4/40/54; W/F = 0,01 g*min/mL.

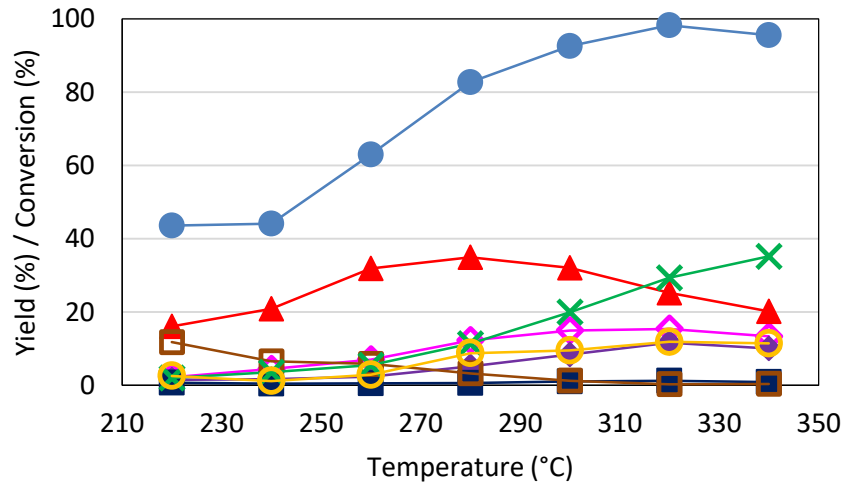

Figure 29. PG conversion as a function of temperature with VCoAPO. Symbols: PG conversion (●), PAL (▲), acetaldehyde (◊), acetic acid (◆), propionic acid (■), dioxolanes (□), CO_x (X) and carbon loss (○). Reaction conditions: feed composition (mol%) $PG/O_2/H_2O/N_2$ = 2/4/40/54; residence time = 0,01 g*min/mL.

At lower temperatures, the formation of heterocyclic acetals was observed, reported as "dioxolanes" in the graphs; these molecules formed by the bimolecular reaction between unconverted PG and an aldehyde (Scheme 6). In particular, three different

dioxolanes were detected: 2-ethyl-4-methyl-1,3-dioxolane, 2,4-methyl-1,3-dioxolane and 4-methyl-1,3-dioxolane, supposedly deriving from the condensation reactions between the glycol and PAL, acetaldehyde and formaldehyde, respectively. With all catalysts, dioxolanes formed in considerable amount at lower reaction temperatures and incomplete PG conversion, as already observed for other catalytic systems[63,65,69]. Conversely, the corresponding dioxolane deriving from the acetalization of glycerol with acrolein, was never detected, possibly due to the higher reaction temperature employed when feeding glycerol. Indeed, during PG conversion, dioxolanes yields rapidly decreased while increasing temperature in favor of the corresponding aldehydes, and for temperatures higher than 290°C, dioxolanes yields were practically null with the three catalysts. Then, a further increase of temperature made PAL progressively decrease mainly in favor of acetaldehyde, acetic acid and CO_x whereas, interestingly, with all three catalysts propionic acid formed in minor amounts only. Indeed, VCoAPO barely showed a yield of 1% at the temperatures of 300-320°C, and VPP a 4% maximum yield at temperatures as high as 350-380°C. WV showed the maximum yield of 11% obtained at the temperature of 260°C, this value being higher than that reported for VCoAPO and VPP catalysts, but still very low. Moreover, acetaldehyde and acetic acid were two of the main reaction products, especially for higher temperatures where acetic acid became the main product for WV and VPP catalysts, together with carbon oxides.

Despite the fact that the same reaction products were detected with the three catalysts, they displayed quite a different catalytic behavior in function of temperature, differences being particularly evident at the lower temperatures. Indeed, VPP appeared to be a very active catalyst, complete conversion being already observed at the temperature of 230°C, and highly selective for the production of PAL at lower temperatures. In particular, a remarkable yield to PAL as high as 82% (with complete conversion) was obtained at the temperature of 230°C. Conversely, WV showed a maximum yield to PAL of 30% only (with selectivity 37%) at the temperature of 220°C, whereas VCoAPO showed a 35% yield (with selectivity 42%) at the higher temperature of 280°C. The lower yield and selectivity to PAL, for the latter two catalysts compared to VPP, was due to the simultaneous formation of both acetalization products, dioxolanes,

and of products deriving from C-C bond scission and oxidation reactions, such as acetaldehyde, acetic acid, propionic acid and carbon oxides. The formation of the latter products suggests that WV and VCoAPO, unlike VPP, show a certain redox activity even at the lower temperatures.

Despite the different range of temperatures investigated, a similar catalytic behavior was also observed for glycerol transformation. However, when comparing PG and glycerol reactivity, it is worth mentioning that with the latter reactant the transformation into the corresponding acid (acrylic acid) prevailed over the formation of acetaldehyde and acetic acid, in a certain range of temperature. Conversely, as already mentioned, propionic acid always was a minor reaction product of PG oxidehydration. The different catalytic behavior as a function of temperature, can be ascribed to the different oxygen insertion ability of the materials, as previously reported in regard to acrolein oxidation (see section 1.3.3). Indeed, VPP showed a lower oxygen insertion ability compared to both WV and VCoAPO, and this feature can explain why the VPP catalyst needs a higher temperature in order to perform the oxidation reaction.

In the previous section, a complete study was performed with the aim to elucidate the overall reaction network for PG conversion on HTB oxides, reported in Scheme 10. In particular, it was proved that both PG and the intermediate PAL could undergo a C-C scission to generate acetaldehyde and formaldehyde/carbon oxides, and acetaldehyde could further be oxidized into acetic acid. Like WV, VPP and VCoAPO catalysts also displayed high yields to acetaldehyde and acetic acid, especially at higher temperatures. Therefore, PAL was first fed on VPP and VCoAPO catalysts in order to check whether they might be able to perform the selective oxidation of PAL to propionic acid (Figure 31 and Figure 32, respectively). As already discussed in the previous chapter, for WV the formation of propionic acid, acetaldehyde, acetic acid, carbon oxides and heavy compounds was observed, and propionic acid prevailed over the other reaction products in the range of temperature 240-260°C, showing the maximum selectivity of 37% at the temperature of 260°C (reported in Figure 30). On VPP and VCoAPO, PAL also converted into propionic acid, acetaldehyde, acetic acid, carbon oxides and heavy compounds.

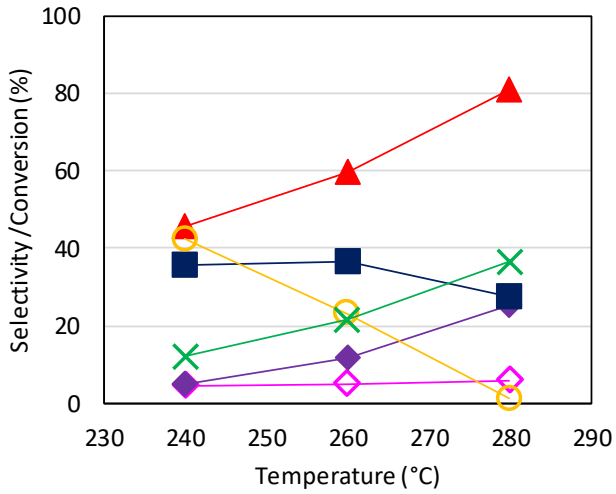

Figure 30. PAL conversion as a function of temperature with WV. Symbols: PAL conversion (▲), acetaldehyde (◊), acetic acid (◆), propionic acid (■), CO_x (X) and carbon loss (○). Reaction conditions: feed composition (mol%) PAL/O_2/H_2O/N_2 = 2/4/40/54; W/F = 0,01 g*min/mL.

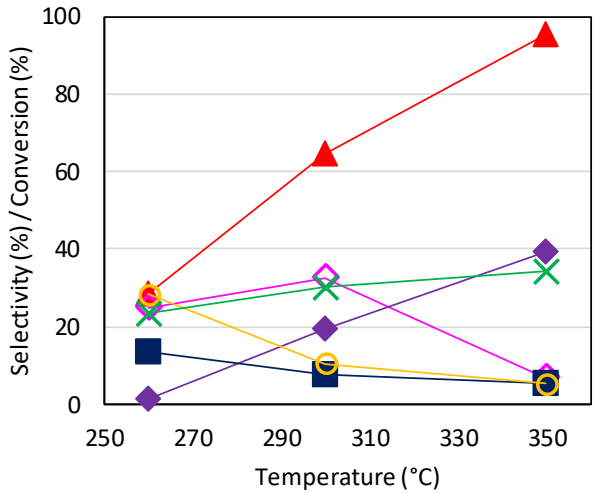

Figure 31. PAL conversion as a function of temperature with VPP. Symbols: PAL conversion (▲), acetaldehyde (◊), acetic acid (◆), propionic acid (■), CO_x (X) and carbon loss (○). Reaction conditions: feed composition (mol%) PAL/O_2/H_2O/N_2 = 2/4/40/54; W/F = 0,01 g*min/mL.

However, despite the formation of the same reaction products, the product distribution was remarkably different. Indeed, with VPP and VCoAPO, propionic acid was always a minor product in the whole range of temperature investigated. Common to all catalysts, PAL conversion increased with temperature, anyway VPP appeared to be less active than the other two materials. The formation of carbon oxides increased with temperature,

and so did acetic acid, while, for VPP and VCoAPO, acetaldehyde selectivity tended to decrease. A considerable amount of heavy compounds was generated at low temperatures, which however rapidly decreased when the temperature was increased.

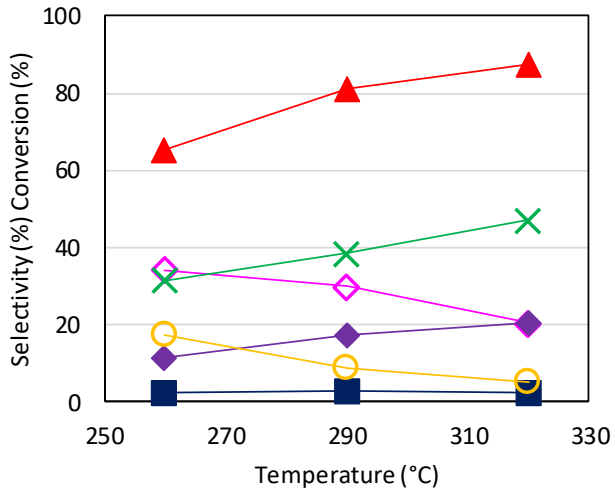

Figure 32. PAL conversion as a function of temperature with VCoAPO. Symbols: PAL conversion (▲), acetaldehyde (◊), acetic acid (◆), propionic acid (■), CO_x (X) and carbon loss (○). Reaction conditions: feed composition (mol%) PAL/O_2/H_2O/N_2 = 2/4/40/54; W/F = 0,01 g*min/mL.

Overall, results obtained with VPP and VCoAPO showed that these two systems are not able to perform the selective oxidation of PAL to propionic acid, probably because of the oxidative cleavage that leads to the formation of acetaldehyde, acetic acid and carbon oxides, as already demonstrated for HTB oxides. Moreover, it might also be possible that propionic acid, forming from selective oxidation of PAL, might be unstable on VPP and VCoAPO being rapidly converted into C_1 and C_2 compounds. In order to shed light on the formation of acetaldehyde and acetic acid, an experiment was performed by feeding PAL on VPP, in order to study the effect of residence time (Figure 33). Opposite to the experiments carried out with HTB (Figure 21), this experiment clearly showed that PAL preferentially converted into C_2 and C_1 products, by means of oxidative cleavage. Indeed, acetaldehyde, carbon oxides and propionic acid selectivities were higher than zero when extrapolated at nil conversion, which means that they all are kinetically primary products. Anyway, acetaldehyde and carbon oxides selectivites were much higher than

selectivity to propionic acid, the latter being extremely low even at the smallest residence time and remaining approximately constant while increasing the residence time. The kinetic relationship between acetaldehyde and acetic acid was also clearly outlined by this experiment, since the drop of acetaldehyde selectivity went at the same pace of acetic acid selectivity increase.

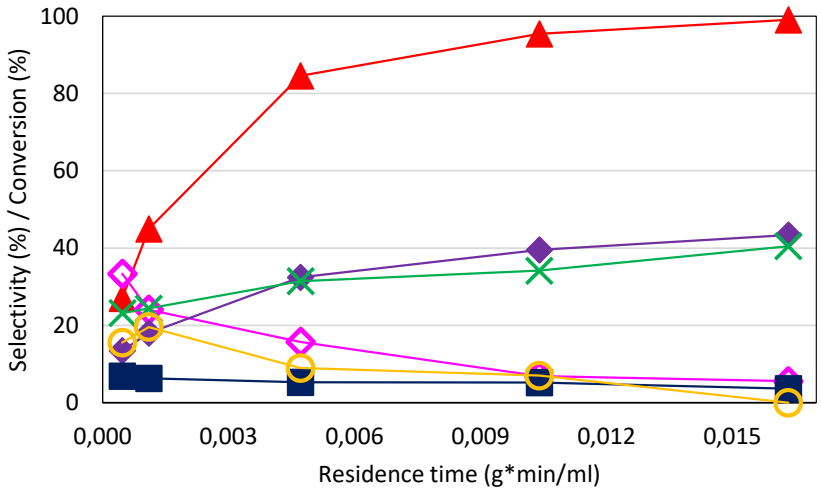

Figure 33. PAL conversion as a function of W/F with VPP. Symbols: PAL conversion (▲), acetaldehyde (◊), acetic acid (◆), propionic acid (■), CO_x (X) and carbon loss (○). Reaction conditions: feed composition (mol%) PAL/O_2/H_2O/N_2 = 2/4/40/54, temperature = 350°C.

Analyzing the results of the experiments reported so far for both PAL and PG conversion on the three catalysts, it emerges that the HTB appeared to be rather effective to promote the selective oxidation of PAL into propionic acid in a certain range of temperature, nevertheless the whole oxidehydration reaction (i.e., from PG to propionic acid) could not be efficiently performed. Therefore, reactivity experiments suggest that with HTB there was a loss of selectivity also deriving directly from PG, besides the loss due to the cleavage of the intermediate PAL, and this was then proved by means of kinetic experiments performed by feeding directly PG on HTB oxides (Figure 20). Opposite to HTBs, in the case of VPP and VCoAPO catalysts, experiments carried out by feeding PAL confirmed that the second step of the oxidehydration reaction could not be

performed. However, in this case an additional contribution to the selectivity loss deriving from PG cleavage, could not be excluded.

Finally, in order to confirm the complete reaction scheme for PG conversion on both VPP and VCoAPO catalysts, kinetic experiments were also performed by feeding the glycol while varying the residence time. The experiments were carried out at the temperature values where the maximum yield to propionic acid was obtained, at 350°C for VPP and 320°C for VCoAPO.

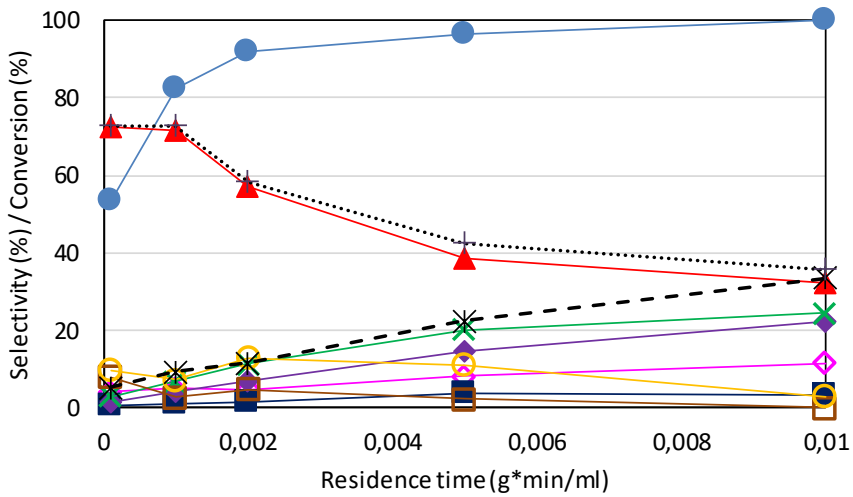

Figure 34. PG conversion as a function of W/F with VPP sample. Symbols: PG conversion (●), PAL (▲), acetaldehyde (◊), acetic acid (◆), propionic acid (■), CO_x (X), dioxolanes (□), carbon loss (○), PAL + propionic acid (*) and acetaldehyde + acetic acid (+). Reaction conditions: feed composition (mol%) $PG/O_2/H_2O/N_2$ = 2/4/40/54, temperature = 350°C.

Referring to VPP reactivity (Figure 34), PAL appeared to be both a kinetically primary product and an intermediate compound, since its selectivity was higher than zero when extrapolated at nil residence time and then progressively decreased while increasing the residence time. The same considerations could be made for dioxolanes, even if their selectivities were here rather low even for extremely low values of residence time, probably because of the high reaction temperature. Acetaldehyde also appeared to be a kinetically primary product, since its selectivity was slightly higher than zero when extrapolated at nil conversion; however, opposite to PAL and dioxolanes, acetaldehyde

selectivity increased with residence time, meaning that it also generated from an intermediate compound, mainly PAL, and not only from the glycol. On the other hand, propionic acid, acetic acid and carbon oxides selectivity values tended to zero when extrapolated to nil residence time, and then they kept increasing with residence time, behaving like kinetically secondary products. Overall, this kinetic experiment indicates that VPP is able to selectively transform PG into the intermediate PAL, while the oxidative cleavage reaction of PG to C_1 and C_2 compounds only contributes to a small extent. Hence, opposite to HTB oxides, for VPP the major loss of selectivity for the whole oxidehydration process originates from PAL oxidative cleavage and not from the glycol itself.

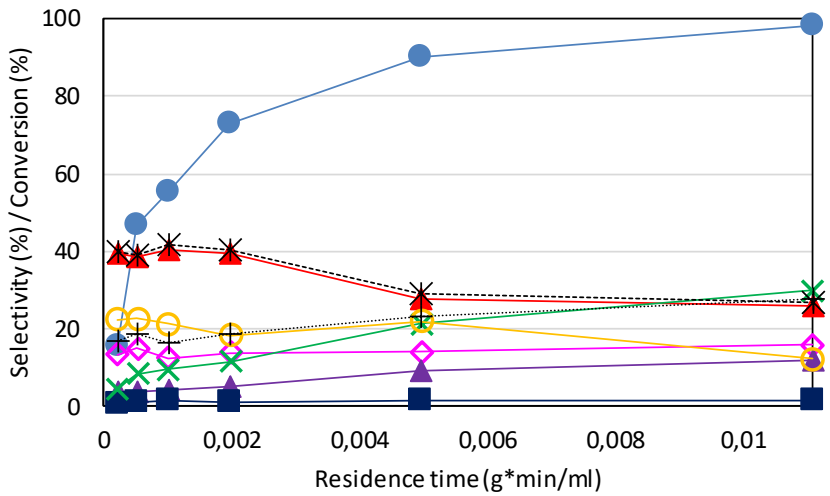

Figure 35. PG conversion as a function of W/F with VCoAPO. Symbols: PG conversion (●), PAL (▲), acetaldehyde (◊), acetic acid (◆), propionic acid (■), CO_x (X), carbon loss (○), PAL + propionic acid (*) and acetaldehyde + acetic acid (+). Reaction conditions: feed composition (mol%) $PG/O_2/H_2O/N_2$ = 2/4/40/54, temperature = 320°C.

Similar considerations can be made for the experiment performed with VCoAPO. Also with this catalyst, PAL behaved like a kinetically primary product and an intermediate compound, since its selectivity was higher than zero when extrapolated at nil residence time and then progressively decreased while increasing the residence time. In this case, dioxolanes only formed in traces also for extremely low residence time values. Acetaldehyde also appeared to be a kinetically primary product, being its selectivity

higher than zero when extrapolated at nil residence time. In particular, as it happened with HTB oxides, PG could easily undergo the oxidative cleavage reaction with VCoAPO, since acetaldehyde selectivity extrapolated at nil residence time approached the value of 20%. Unlike for VPP, where acetaldehyde selectivity kept increasing with residence time, with VCoAPO acetaldehyde remained approximately constant. This behavior could derive from the combination of two different contributions: on one hand, acetaldehyde might have been progressively consumed, by its oxidation to acetic acid and, on the other hand, it might have generated from the scission of intermediate PAL. Acetic acid and carbon oxides selectivities tended to zero when extrapolated to nil residence time, and then they kept increasing with residence time, acting like kinetically secondary products. A similar behavior was shown by propionic acid, even if its selectivity remained always extremely low.

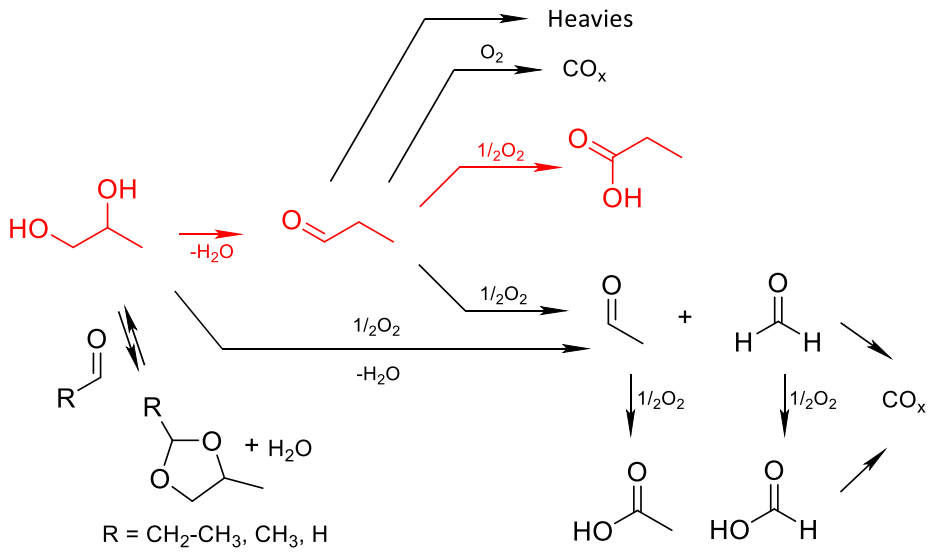

Scheme 13. Overall reaction network for PG conversion on multifunctional HTB oxides. In red, the desired reaction pathway.

On the whole, it can be confirmed that the overall reaction network reported in Scheme 10, already discussed in the previous chapter, is valid for all of the three catalysts investigated. Nonetheless, it is evident that the peculiar acid and redox features of each material influence in a different way the various stages of the whole process, even if

none of the materials investigated so far possess all the characteristics necessary to favour the desired pathway.

Eventually, the following remarks can be outlined from reactivity experiments:

- Referring to the second step of the process, that is PAL oxidation, VPP and VCoAPO were proved to be poorly efficient in promoting the selective oxidation of the intermediate aldehyde into propionic acid. In particular, they both favoured a C-C cleavage reaction that led to the predominant formation of acetaldehyde, acetic acid and carbon oxides. On the other hand, HTB oxides displayed quite good selectivities to propionic acid, even if this was limited to the range of temperature between 240 and 260°C. Indeed, increasing the temperature the selectivity into the acid rapidly decreased in favour of acetaldehyde, acetic acid and carbon oxides.
- Referring to the first step of the whole process, it was demonstrated that all of the three catalysts were selective in PG dehydration into PAL, being acetone and allylic acid yields always extremely low. However, WV and VCoAPO displayed a low activity at lower reaction temperatures, and the unconverted glycol remained available to react with PAL through an acetalization reaction, promoted by the acid sites of the samples as well. For HTB oxides, the formation of dioxolanes, that occured in the range of temperature where the catalyst also worked better for PAL oxidation, could decrease the selectivity to PAL, and hence the selectivity into the consecutive product, propionic acid. On the other hand, VPP remarkably turned out to be highly active and selective in PG dehydration into PAL. Indeed, VPP displayed complete conversion already at 230°C, together with a residual formation of dioxolanes and a yield to PAL as high as 82%.

  Besides the formation of dioxolanes, also PG oxidative cleavage, promoted by the redox sites of the bifunctional catalysts, could compete with PG dehydration. It is worth mentioning that VPP is the only catalyst where PG dehydration definitely prevailed over PG oxidative cleavage, even at higher temperatures, as elucidated by kinetic experiments performed at 350°C. This behaviour might be attributed to the high acid features of VPP catalyst that are able to enhance the rate of the dehydration over the oxidation.

Table 9. Comparison of PAL and acrolein conversion on VPP catalyst. Reaction conditions: feed composition (mol%) PAL/O_2/H_2O/N_2 = 2/4/40/54, temperature = 350°C, residence time = 0,01 g*min/mL.

	PAL			Acrolein	
Conversion (%)	95			48	
	Yield (%)	**Selectivity (%)**		**Yield (%)**	**Selectivity (%)**
Propionic Acid	5	5	**Acrylic Acid**	36	75
Acetaldehyde	7	7	**Acetaldehyde**	1	2
Acetic Acid	38	40	**Acetic Acid**	2	4
CO_x	33	35	**CO_x**	8	17
Carbon loss	-	13	**Carbon loss**	-	2

Table 10. Comparison of PAL and acrolein conversion on VCoAPO catalyst. Reaction conditions: feed composition (mol%) PAL/O_2/H_2O/N_2 = 2/4/40/54, residence time = 0,01 g*min/mL, temperature = 320°C (PAL) and 350°C (acrolein).

	PAL			Acrolein	
Conversion (%)	87			56	
	Yield (%)	**Selectivity (%)**		**Yield (%)**	**Selectivity (%)**
Propionic Acid	2	2	**Acrylic Acid**	9	16
Acetaldehyde	18	21	**Acetaldehyde**	3	5
Acetic Acid	18	21	**Acetic Acid**	3	5
CO_x	41	47	**CO_x**	26	46
Carbon loss	-	9	**Carbon loss**	-	28

Finally, acrolein was also fed on VPP and VCoAPO catalysts in order to appreciate the different behavior of the two aldehydes for oxidation to the corresponding acid (Table 9). In both cases, PAL conversion was much higher than that of acrolein, and acetaldehyde, acetic acid and carbon oxides were the main by-products. However, the products distribution was remarkably different, particularly in the case of VPP, where a 75% selectivity into acrylic acid was obtained from acrolein, against the 5% only into propionic acid from PAL. With VCoAPO, the formation of acetaldehyde and acetic acid

was much lower from acrolein than from PAL. Anyway the selectivity into acrylic acid was not very high, mainly due to an abundant formation of both carbon oxides and heavy compounds.

Overall, the differences between PAL and acrolein reactivity might be attributable to the presence of the C-C insaturation in the latter compound, that might stabilize the aldehyde and facilitate oxygen insertion on the carbon atom of carbonyl functionality.

PG conversion with Mo-V-W-O oxide with Mo_5O_{14} structure

Finally, the catalytic behavior of a mixed Mo-V-W-O oxide with Mo_5O_{14} (MoVW) structure was investigated. Mo-V oxides are typical catalysts for acrolein oxidation to acrylic acid[74]. From the few papers available in the literature about PAL selective oxidation, propionic acid selectivity reached values as high as 55-60%[70], the latter being achieved on a molybdenum-vanadium mixed oxide catalyst. It is known that MoVW oxide with Mo_5O_{14} structure owns poor acid properties, hence it wouldn't be the ideal candidate to perform dehydration reactions. Indeed, when glycerol was fed on this system to perform oxidehydration into acrylic acid, a very low yield into acrolein was observed, together with a severe formation of heavy compounds and no acrylic acid[68]. However, referring to literature, PG dehydration appears to occur more easily compared to glycerol dehydration on the same type of acid catalysts[64]. Consequently, PG was fed over MoVW without oxygen in the inlet feed, in order to study the dehydration step only, and a reasonable selectivity of 54% at 71% PG conversion was obtained at the temperature of 280°C (results reported in Table 11). The same experiment, without oxygen in the feed, was also carried out on WMoV oxide with HTB structure. The latter sample showed an almost total complete conversion and a higher selectivity into PAL, behavior that can be reasonably attributed to its higher acid properties.

PAL was then fed on MoVW oxide in the same reaction conditions employed for the other catalysts, and catalytic results as a function of temperature are reported in Figure 36. This catalytic system turned out to be more efficient than HTB for PAL oxidation into propionic acid, leading to the maximum yield of 45% at the temperature of 280°C and a

selectivity of 70%, maintained in the whole range of temperature investigated (vs the maximum selectivity of 55% for WMoV with HTB structure).

Table 11. PG conversion on MoVW oxide with Mo_5O_{14} structure and WMoV-HTB samples without oxygen in the inlet feed. Reaction conditions: feed composition (mol%) $PAL/O_2/H_2O/N_2$ = 2/-/40/58, residence time = 0,01 g*min/mL, temperature = 280°C.

	MoVW Mo_5O_{14}		WMoV HTB
PG Conversion (%)	71		97,9
	Yield (%)	**Selectivity (%)**	**Selectivity (%)**
Acetaldehyde	5,9	8,3	2,6
PAL	38,1	53,6	69,7
Acetone	3,5	4,9	2,0
Others	5,1	7,2	4,4
Carbon Loss	-	26	21,3

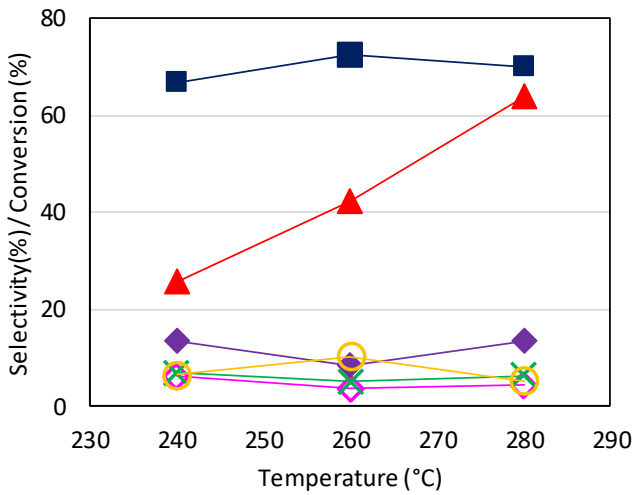

Figure 36. PAL conversion as a function of temperature on MoVW with Mo_5O_{14} structure. Symbols: PAL conversion (▲), acetaldehyde (◊), acetic acid (◆), propionic acid (■), CO_x (X) and carbon loss (○). Reaction conditions: feed composition (mol%) $PAL/O_2/H_2O/N_2$ = 2/4/40/54; residence time = 0,01 g*min/mL.

Eventually, PG was fed with oxygen on MoVW to perform the oxydehydration reaction; catalytic performance as a function of temperature is summarised in Figure 37. Also with

this catalyst, the formation of dioxolanes was observed for lower temperatures, gradually decreasing while increasing temperature and conversion. Interestingly, this catalyst displayed very low yields into carbon oxides in the whole range of temperature, slightly increasing while raising the temperature. Selectivity of both acetic and propionic acid, respectively deriving from acetaldehyde and PAL selective oxidation, progressively increased with temperature, while, on the other hand, selectivity to both the aldehydes tended to decrease.

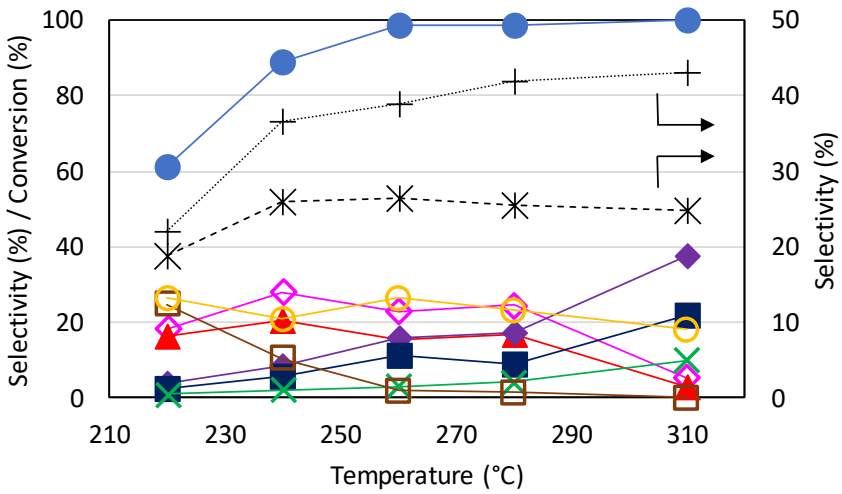

Figure 37. PG conversion as a function of temperature on MoVW with Mo_5O_{14} structure. Symbols: PG conversion (●), PAL (▲), acetaldehyde (◊), acetic acid (◆), propionic acid (■), dioxolanes (□), CO_x (X), carbon loss (○), PAL + propionic acid (*) and acetaldehyde + acetic acid (+). Reaction conditions: feed composition (mol%) $PG/O_2/H_2O/N_2$ = 2/4/40/54; residence time = 0,01 g*min/mL.

Despite MoVW showed a good performance in the selective oxidation of PAL into propionic acid, in oxidehydration the latter molecule always was a minor reaction product only. At the temperature of 310°C, when oxidation products definitely prevailed over the other products, this catalyst displayed the higher yield, and selectivity as well, of 22% into propionic acid so far obtained in PG oxidehydration. At the same time, the selectivity into PAL finally dropped, hence the latter result could be clearly related to the ability of the catalyst to efficiently convert PAL into propionic acid. Despite this fact, in PG oxydehydration, propionic acid selectivity still was very low, with acetaldehyde and

acetic acid being the principal reaction products. Since it was previously proved that the formation of the latter two compounds from the intermediate PAL gave a minor contribution, the main loss of selectivity for PG conversion into propionic acid, arguably derived from the first step of the overall process.

All in all, catalytic results strongly suggest that also with MoVW PG easily undergoes C-C cleavage, and this behavior can reasonably be explained taking into account the acid properties of the material, that are not high enough to promote PG dehydration instead of C-C cleavage.

2.1.4 Conclusions

The direct transformation of PG into PA by means multifunctional catalysis, turned out to be a very challenging process, since both the reactant PG and the intermediate PAL may undergo a number of different reactions that finally decrease selectivity to the desired product. The catalytic activity of different acid and redox catalysts was investigated, and the peculiar features of each material were proved to influence in a different way the various stages of the whole process, even if none of them possesses all the characteristics necessary to favour the desired pathway. Overall, this study was useful to understand which are the main critical points of the one-pot process, finally suggesting several key features to follow for the development of new catalysts.

Notably, VPP and WNb catalysts were proved to be very active and selective towards PG dehydration, showing yields into PAL respectively of 82 and 87%, at total conversion. On the other hand, MoVW oxide with Mo_5O_{14} type phase displayed good performances for PAL selective oxidation, showing a selectivity into PA of 70% -under non-optimized conditions-, that is the best result so far reported for the gas-phase oxidation of PAL to PA. Hence, further studies will be performed in order to optimize the latter process, as well.

2.2 Production of Methacrylic Acid from Propionic Acid and Methanol

2.2.1 Introduction

In this section, the final step of the overall process for the production of methacrylic acid starting from glycerol (Scheme 3), will be taken into account. This step consists into the gas-phase aldol condensation between propionic acid and formaldehyde, using methanol as the source of the aldehyde, as reported in Scheme 14.

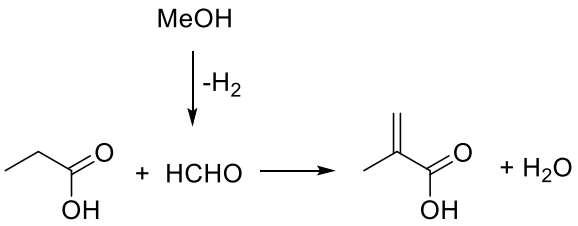

Scheme 14. Methacrylic acid synthesis from propionic acid and methanol.

To begin, a few considerations have to be done, about both the nature of the C_3 compound and the source of formaldehyde usually employed for this process. In particular, both propionic acid (PA)[75–83] and its methyl ester (MP)[84–89] have been used as C_3 reactants to perform the condensation reaction with formaldehyde (HCHO) for the production of, respectively, methacrylic acid (MA) and methyl methacrylate (MMA). Both Lucite International and BASF recently invested on the process for the production of MMA from MP, using respectively formalin and methylal as HCHO sources. Conversely, Eastman, that is a commercial producer of propionic acid, focused on the production methacrylic acid by the condensation of PA with HCHO[109].

From the catalysis point of view, for both PA and MP processes, either acid-base catalysts and materials with a predominant acid character, were proved to be active for the condensation reaction. Indeed, the formation of MA/MMA is expected to derive from a first condensation step, leading to the formation of an intermediate aldol adduct, followed by the dehydration of the aldol to the corresponding C_4 compound, as outlined

in Scheme 15. The aldol reaction is known to undergo by both acid and basic catalysis, whereas the dehydration step is typically acid- catalyzed.

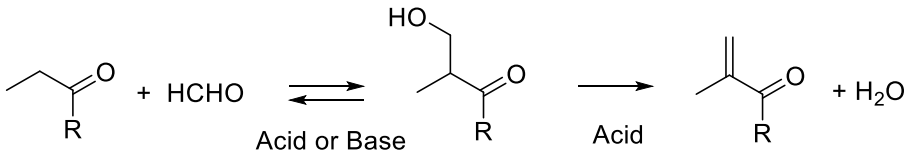

Scheme 15. Reaction pathway generally accepted for the formation of MA/MMA from PA/MP and HCHO, passing through the generation of an intermediate aldol compound. R = -OH or -OMe.

Typical acid-base catalysts consist of alkali or alkaline earth metal oxides supported on acidic materials, such as silica or zeolites[80,83–85,87,89–91]. In particular, the best performances are generally obtained when using Cs as basic element. The catalysts with predominant acid character are usually metal oxides, as Nb_2O_5, WO_3, Ta_2O_3 and phosphorous oxides, the latter commonly combined with oxides of other elements, e.g. V, Si, Sn, B and W[76–79,81,82,86,92,93].

A few remarks about the source of HCHO are reported as well. The following compounds are commonly used: i) formalin, that is a saturated water solution of HCHO, containing also MeOH as stabilizer; ii) trioxane, the cyclic trimer of HCHO; iii) hemiformal, obtained dissolving solid paraformaldehyde in MeOH. Generally, the use of formalin is not preferred as the source of HCHO, because both the reaction rate and the selectivity into MA and MMA are proved to be decreased by the presence of water in the reaction feed. Trioxane can be dissolved into PA or MP and then it can easily depolymerize by heating, just before feeding the solution in the reactor. Moreover, it does not contain neither water nor MeOH. For all these reasons, trioxane is commonly employed when performing the reaction of PA with HCHO, since the presence of MeOH in the feed, in some cases, was proved to limit the activity of the catalysts. On the other hand, the reaction of MP with HCHO is generally performed in the presence of a large amount of MeOH in the feed, in order to avoid the hydrolysis of MMA and MP, hence the use of hemiformal is preferred.

It is important to mention that HCHO is a volatile, toxic and human carcinogenic molecule, hence the safety issues consist into one of the main drawbacks when using HCHO and its derivatives are reagents. In this context, MeOH would represent a valid alternative source of HCHO, since it is easier and safer to handle than the compounds mentioned above, and HCHO would be only generated in-situ, by means of a dehydrogenation reaction (Scheme 14). Therefore, when using MeOH as source of HCHO, the catalyst must also possess dehydrogenating features together with the proper acid/base characteristics necessary to promote the aldol condensation. A few attempts to obtain combined catalysts have already been performed, adding to typical acid/base condensing materials dehydrogenating elements like Ag[85,90], Cu, Zn, Te and Se[94].

Moreover, when MeOH was employed as source of HCHO (much less frequent than the others), MP was always used as reagent to perform the condensation reaction[85,90,94]. Even if the authors do not specifically justify the choice to feed MP and not PA together with MeOH, it can reasonably be attributed to the will of avoiding the possible esterification of PA. Indeed, it was previously proved that the rate of PA esterification (and also the reverse MP hydrolysis) is higher than the rate of the condensation reaction. As outlined in Scheme 14, the main drawback of this reaction could be the concomitant formation of water, that might decrease the selectivity into MMA and MA. On the other hand, referring to the overall proposal for the production of MA/MMA starting from glycerol (Scheme 3), feeding directly PA, the additional step for the esterification of PA into MP before performing the condensation reaction would be avoided. Moreover, the process is expected to need medium-high reaction temperatures, because of the dehydrogenation step of MeOH into HCHO. Supposing that the formation of MA evolves by the mechanism depicted in Scheme 15, hence passing through the generation of an aldol intermediate, the higher temperatures might then favor the last dehydration step of the aldol adduct, finally shifting the equilibrium towards MA. Consequently, it was decided to perform the reaction of PA with MeOH as a first attempt. Since the condensation reaction was proved to be promoted by acid catalysis as well, we decided to investigate the catalytic behavior of phosphate-based materials, starting from

aluminium phosphate (AlPO). The catalytic activity of AlPO material was fully investigated as a function of reaction parameters, such as feed composition, temperature and residence time. This study allowed us to define the reactions that might occur when feeding PA and MeOH on pure acid catalysts.

2.2.2 Experimental

2.2.2.1 Synthesis of Aluminium Phosphate catalyst

Aluminium phosphate (AlPO) catalyst was prepared using a method adapted from the literature[95], that consists in the precipitation of metal phosphates from an aqueous solution. A solution of the metal cation was prepared by dissolving about 40g of the precursor $AlCl_3$ (Sigma Aldrich, > 99%) into 300 mL of distilled water. Then, 300 mL of 1M phosphoric acid solution was added to the cation solution under continuous stirring and the pH was brought from acid values up to 7 with 28% aqueous NH_3, in order to promote the precipitation of the metal phosphate (nominal Al/P ratio about 1). A neutral pH was necessary to both quantitatively precipitate the phosphate and to limit hydroxide formation. The precipitate was further decanted for 4 hours, filtered and then washed with 2L of distilled water. Finally, the white solid was dried at 120°C for one night, and calcined at 550°C for 3 hours. It was then pressed into tablets and crushed to obtain particles with size between 30 and 60 mesh.

2.2.2.2 Characterization of Aluminium Phosphate catalyst

Characterization of the catalyst was performed by means of IR, XRD, SEM-EDX, BET surface area, and NH_3-TPD analysis. X-ray diffraction (XRD) patterns were acquired with a Philips PW 1050/81 apparatus controlled by a PW1710 unit (λ = 0.15418 nm (Cu), 40 kV, 40 mA), in the range of $5° < 2\theta < 80°$. The scanning rate was $0.05° \ 2\theta \ s^{-1}$ and the step time 1s. The specific surface area was measured using a Carlo Erba Sorpty 1700, and applying the single-point BET method. Around 0.5 g of the sample were placed inside the sample holder and then heated at 150 °C under vacuum in order to release water, or other molecules adsorbed. Attenuated total reflectance spectra of the materials were recorded at room temperature with an ALPHA-FTIR instrument at a resolution of 2 cm-

1. SEM-EDX images were collected with a Zeiss EP EVO 50, equipped with an EDX probe Oxford Instruments INCA ENERGY 350. General conditions of the microscope were: EHT 20 KeV, high vacuum (10^{-6} Pa) or variable vacuum between 60 – 100 Pa. The EDX probe used a Mn K_α radiation with 133 eV of resolution. The acidity of the catalyst was measured by means of ammonia temperature programmed desorption analysis (NH_3-TPD) and experiments were performed with a TPD/TPR/TPO Micromeritics instrument. The sample (about 0,3g) was first pre-treated in He flow (20mL/min) at the temperature of 400°C for 30 minutes (ramp 10°C/min). After cooling down to 80 °C, NH_3 was adsorbed by flowing the catalysts under a 30% NH_3–He gas mixture (30 mL/min) for 30 minutes, with subsequent He treatment at 80°C for 15 minutes, to remove physisorbed ammonia. Catalysts were then heated under a He flow of 20 mL/min, at a heating rate of 10 °C/min up to 500°C, and kept at this temperature for 40 minutes. Between the sample holder and the TCD, a trap containing zeolites able to adsorb water was placed, in order to suppress signals due to water desorption.

2.2.2.3 Gas-phase catalytic tests

Gas-phase reactivity experiments were performed by using the same continuous flow reactor previously employed for glycerol and propylene glycol oxydehydration processes, operating at atmospheric pressure. For each condition, all the reaction parameters are listed in each figure. A catalyst amount ranging from 1 to 4g was loaded in pellet form (30-60 mesh). Residence time is calculated as the ratio between catalyst amount (g) and total gas flow (mL/min), the latter being measured at room temperature. The residence time was varied by keeping constant the total gas flow and changing the catalyst amount. Inlet feed composition was also changed according to the desired compositions. The catalytic results were obtained after a reaction time of 60 min. The effluent stream was bubbled through three in-series abatement devices filled with acetonitrile, and put into a cool bath at the temperature of 0-2°C. After the abatement step, where the condensable organic molecules were collected, the gaseous stream still containing CO_2 and, in some conditions light olefins, was fed into an automatic sampling system for on-line gas chromatography (GC-TCD) analysis. The aqueous solution was

analyzed off-line by GC-FID analysis, using a reference standard (valeric acid). Both the gas chromatographic analyses were performed with a Hewlett–Packard 5890 instrument, equipped with either FI and TC detectors. A semi-capillary ZB-FFAP (nitroterephthalic acid modified polyethylene glycol) column was used for the separation of condensed compounds, whereas for the separation of non-condensable products, a Silica Plot was used. Compounds were identified by means of both GC–MS analysis and the injection of pure reference standards for the comparison of retention times in the GC associated to the plant. The conversion of the reagents was calculated with the formula: $X_{Rj} = [(\text{mol } R_j^{in} - \text{mol } R_j^{out})/\text{mol } R_j^{in}]*100$, where mol R_j^{in} and mol R_j^{out} represent the moles of the reagent R_j (propionic acid or methanol). The yield and selectivity of each product was calculated on both propionic acid and methanol basis, by the formulas: $Y_{Pi} = [(\text{mol } P_i^{out} * \nu_{Rj})/ (\text{mol } R_j^{in} * \nu_{Pi})]*100$, $S_{Pi} = (Y_{Pi}/ X_{Rj})*100$. In particular, mol P_i^{out} represent the moles of the *i*th reaction product P and, ν_{Pi} and ν_{RJ} are the stechiometric coefficients respectively of the *i*th product and the jth reagent. The mass balance was calculated on carbon basis, hence considering the total moles of carbon atom in the inlet feed and those measures at the end of the reaction. It was calculated by the formula: carbon balance = $(\text{mol } C_{TOT}^{out}/ \text{mol } C_{TOT}^{in})*100$. Total selectivities, both in respect to PA and MeOH, were also calculated on carbon basis.

2.2.3 Results and discussion

2.2.3.1 Physicochemical properties of Aluminium Phosphate catalyst

Characterization of the catalyst was performed by means of FT-IR, XRD, SEM-EDX, BET surface area, and NH_3-TPD analysis.

FT-IR analysis was used to confirm the formation of the desired phosphate, and spectra of the catalyst before and after calcination are shown in Figure 38 . Both spectra display adsorption bands between 1045 and 1080 cm^{-1} related to P-O stretching[96] in tetrahedral PO_4^{3-}. Slight differences in the position of the P-O band vibration between calcined and non-calcined samples can be due to different hydration degrees. Bands in the range 800-400 cm^{-1} are related to O-P-O and Al-O-P vibration modes[96]. Bands centred at 1628-1634 cm^{-1} and falling in the range 3500-2900 cm^{-1} indicate the presence of water,

probably adsorbed on the catalyst surface. Band centred at about 1434 cm^{-1} and bands in the region 3000-2800 cm^{-1} in spectra of non-calcined samples are related to N-H vibrations, arguably due to the presence of some residual ammonium ion deriving from the synthesis. It also reveals the presence of acid sites able to bind ammonia. Anyway, the ammonium ion was decomposed and released into the gas phase as ammonia during calcination, since its corresponding band disappeared in calcined sample.

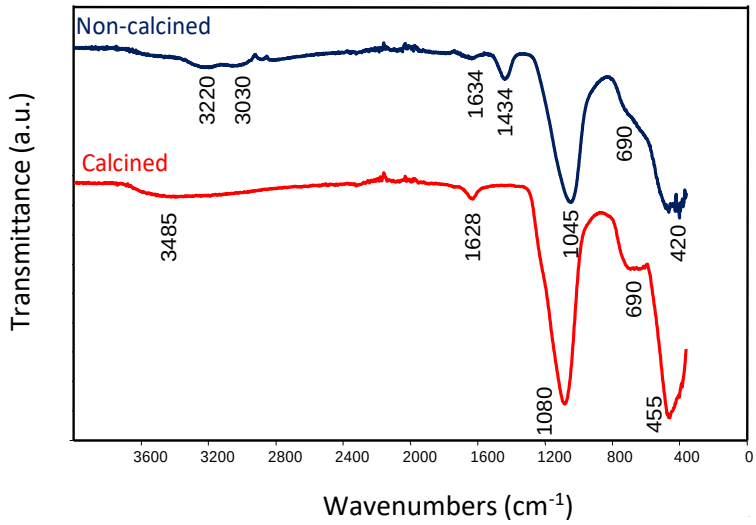

Figure 38. FT-IR spectra of AlPO catalyst. Blue line refers to the catalyst before calcination, red line to calcined catalyst.

EDX analysis also confirmed the development of the $AlPO_4$ catalyst, without impurities of alumina or other compounds, as already observed by means of FT-IR. Indeed, the analysis was carried out on different spots of the SEM image (Figure 39), and an Al/P/O ratio always close to 1/1/4 was measured.

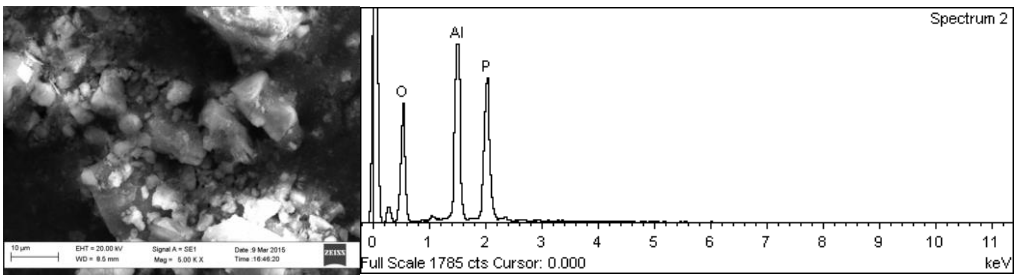

Figure 39. SEM image of AlPO catalyst and corresponding EDX spectra.

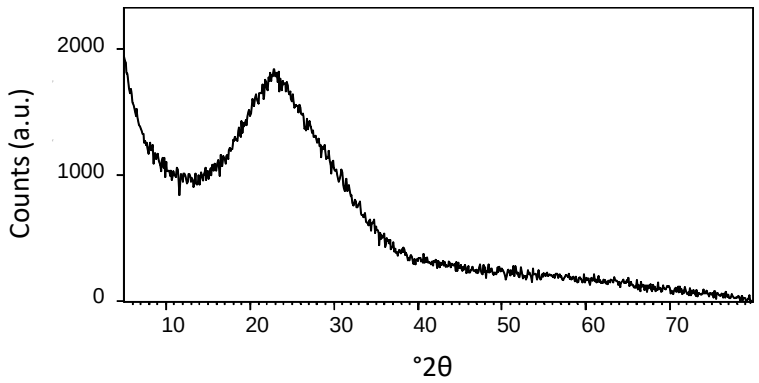

Figure 40. XRD pattern of AlPO catalyst.

XRD analysis of the calcined sample, reported in Figure 40, enabled us to determine the structure of the phosphate material. As evident from XRD pattern, AlPO catalyst appear to be amorphous, without any crystalline domain, since it only shows a broad reflection centred at low 2θ around 25.

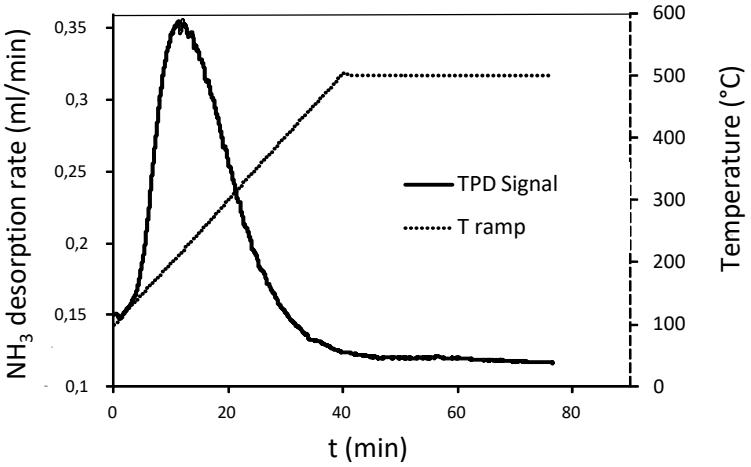

Figure 41. NH_3-TPD desorption profile as a function of time.

AlPO specific surface area was determined by means of the BET technique, and turned out to be 150 m^2/g. Moreover, the phosphate acidity was evaluated by means of ammonia temperature programmed desorption analysis (NH_3-TPD). This analysis can provide information on the strength and the number of acid sites. The strength is measured from NH_3 desorption temperature: in particular, the higher is the temperature, the stronger are the sites. The total amount of acid sites is obtained from

the quantification of the amount of desorbed ammonia by the integration of TPD signals. Hence, the total acidity of the material is expressed in terms of NH_3 μmoles desorbed per unit surface area or unit catalyst weight; values are reported in Table 12.

Ammonia desorption profile as a function of temperature is shown in Figure 41 and it displays one single peak with a maximum around 200°C, indicating the presence of medium-strength acid sites.

Table 12. Summary of chemical and physical features of AlPO catalyst.

AlPO chemical and physical features	
Phase	Amorphous
Al/P/O atomic ratio	1/1/4
SSA BET (m^2/g)	150
Amount of acid sites	5.8 μmol/m^2 865 μmol/g

A complete summary of chemical and physical features of AlPO catalyst is reported in Table 12. Overall, characterization analysis allowed us to confirm that an amorphous $AlPO_4$ catalyst was obtained, without impurities of other compounds. Moreover, this material shows a considerable specific surface area and acid properties.

2.2.3.2 Catalytic tests

Catalytic activity of AlPO material was fully investigated as a function of reaction parameters, such as feed composition, temperature and residence time. Generally speaking, main reaction products consist of: methyl propionate (MP) and dimethyl ether (DME), respectively deriving from the esterification of PA with MeOH (Scheme 16) and MeOH condensation (Scheme 17). The development of the latter two products could have reasonably been expected, since it is well known that both of the two reactions are promoted by acid catalysis[96–99].

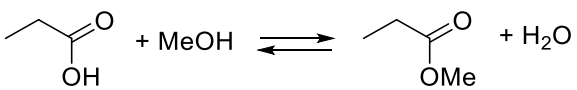

Scheme 16. Esterification of propionic acid with MeOH.

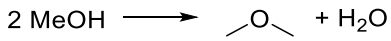

Scheme 17. MeOH condensation to DME.

Another molecule was formed in significant amount, that is 3-pentanone, arguably deriving from the ketonisation reaction of PA[100]. The latter reaction converts two molecules of a carboxylic acid into a ketone, CO_2 and water, as depicted in Scheme 18.

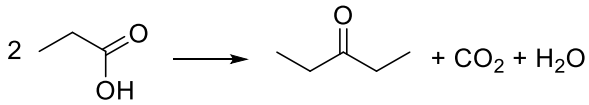

Scheme 18. Ketonisation of propionic acid.

Other products, detected as minor compounds, were: methacrylic acid, methyl methacrylate, C_3-C_7 olefins, 3-pentanone-2-methyl, 2-pentanone-3-methyl and methyl isobutyrrate. Moreover, the formation of a great amount of aromatic compounds was also observed, but only for the higher temperature and residence time values,. The identification of reaction products in both the vapor phase collected at the exit of the reactor, and the aqueous solution accumulated in the refrigerated condensers was carried out by means of GC-MS. It is important to mention that formaldehyde, supposedly deriving from MeOH dehydrogenation, was never detected. However, its formation, although in minor amount, cannot be completely excluded because of two reasons: with the GC-MS analysis, formaldehyde peak overlaps with those of other products, whereas with the GC-FID analysis performed with the on-line system downstream to the plant, formaldehyde cannot be detected. Moreover, it was not possible to quantify DME, even if its formation was definitely confirmed by GC-MS analysis. Indeed, the latter compound was only partially retained by the solvent contained into the refrigerated condenser.

Catalytic experiments were first aimed at studying the influence of feed composition while keeping constant the molar fraction of propionic acid (6%), and varying MeOH molar fraction from 3 to 12%, in order to obtain PA/MeOH molar ratios ratios equal to 2, 1 and 0,5 (Figure 42). The molar fraction of PA equal to 6% was chosen on the basis of the most common reaction conditions reported so far in literature for propionic acid

condensation with formaldehyde. The latter experiments were performed at the temperature of 300°C and residence time of 1g*min/mL; the values of selectivity calculated with respect to propionic are displayed in the figure. Incresing MeOH content, PA conversion increased from 50% to almost 90%, whereas MeOH conversion slightly decreased from 93% to 82%. MP was the main reaction product, obtained with a remarkable selectivity of 90% for the lower MeOH molar content in feed. Its selectivity then decreased while increasing MeOH, reaching the minimum of 74% for a MeOH molar content equal to 12%. Even if DME could not be quantified, the reduction of MP selectivity can be reasonably related to the increase of ether selectivity (this was confirmed by means of GC-MS analysis). Since MP and DME were the most abundant products deriving from MeOH, it is possible to calculate a rough estimate of DME formation by taking into account the sum of selectivities to compounds deriving from MeOH.

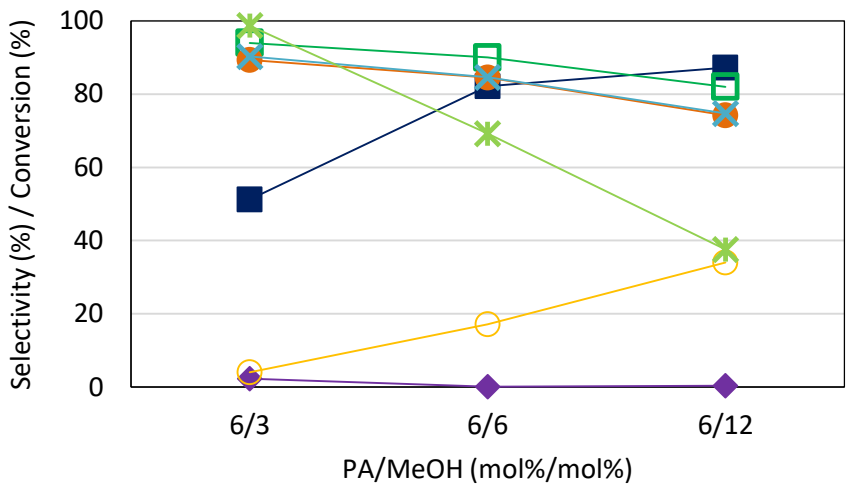

Figure 42. Reactivity experiments as a function of feed composition. PA molar fraction was kept constant and equal to 6%, while MeOH molar fraction is varied from 3% to 12%. Other reaction conditions: temperature = 300°C, *W/F* = 1g*min/*mL*. Symbols: (■) PA conversion, (□) MeOH conversion, (●) MP selectivity, (◆) 3P selectivity, (X) total selectivities calculated on PA basis, (*) total selectivities calculated on MeOH basis, (○) carbon loss.

Finally, under the conditions employed for this experiment, we did not observe the formation of compounds deriving from condensation reactions. Only a very small

amount of 3-pentanone was detected when the reaction was carried out with the minimum MeOH content in the feed. Overall, AlPO catalayst appeared to be rather efficient in the gas phase esterification of PA to MP. For the synthesis of MMA/MA, this fact may not be negative, since by the condensation of MP with MeOH, we could directly obtain MMA. On the other hand, increasing the content of MeOH in the feed, the dehydration of the alcohol to DME also occurred and it seemed to compete with the esterification, since the selectivity into MP was slightly reduced.

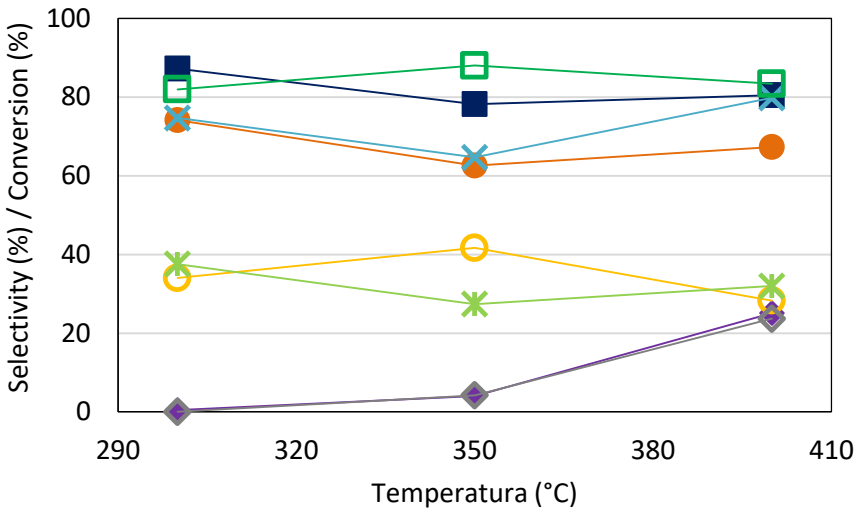

Figure 43. Reactivity experiments as a function of temperature. Other reaction conditions: feed composition PA/MeOH/N_2 = 6/12/82 mol%, *W/F* = 1g*min/*mL*. Symbols: (■) PA conversion, (□) MeOH conversion, (●) MP selectivity, (◆) 3P selectivity, (◊) CO_2 selectivity, (X) total selectivities calculated on PA basis, (*) total selectivities calculated on MeOH basis, (○) carbon loss.

Afterwards, catalytic performances were investigated in function of temperature, from 300°C to 400°C (Figure 43). W/F was equal to 1g*min/mL, and it was decided to work with a PA/MeOH molar ratio equal to 0,5 (PA/MeOH/N_2 = 6/12/82 mol%). Since the rate of PA esterification reaction appeared to be higher than the rate of condensation between PA and MeOH, we decided to work with the highest MeOH molar content previously investigated, in order to ensure that part of the MeOH fed was available to react with PA or/and MP to produce MA or/and MMA, respectively. The temperature appeared to have a considerable influence on the condensation processes, as outlined by the increase of PA ketonisation products, 3-pentanone and CO_2. Despite this fact, MA

was obtained in a barely detectable amount, and still no MMA was observed. On one hand, this fact can arguably be explained by taking in consideration that AlPO catalyst might not be able to dehydrogenate MeOH to formaldehyde, or to activate MeOH in order to promote its condensation with MA or MMA. On the other hand, the condensation is consecutive to the formation of formaldehyde from MeOH, hence it might have been necessary to increase the residence time.

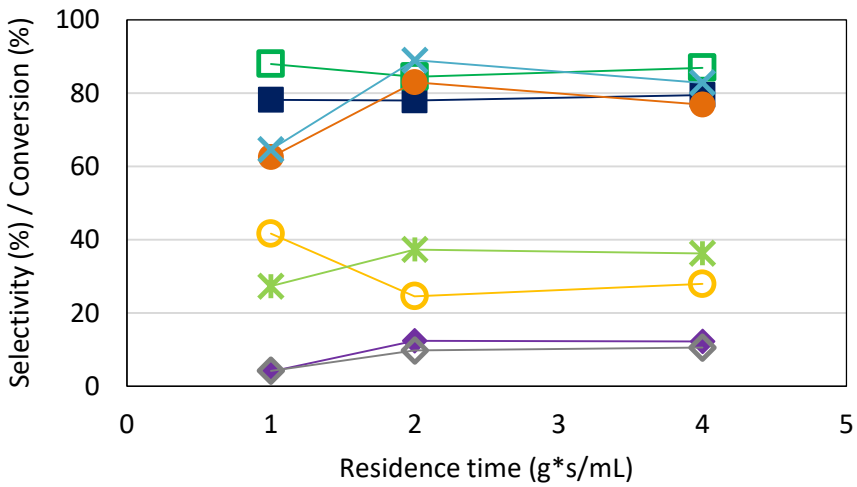

Figure 44. Reactivity experiments as a function of residence time *(W/F)*. Other reaction conditions: feed composition PA/MeOH/N_2 = 6/12/82 mol%, temperature = 350°C. Symbols: (■) PA conversion, (□) MeOH conversion, (●) MP selectivity, (◆) 3P selectivity, (◊) CO_2 selectivity, (X) total selectivities calculated on PA basis, (*) total selectivities calculated on MeOH basis, (○) carbon loss.

Therefore, the residence time was then increased from 1 to 4g*min/mL and these experiments were performed at both the temperatures of 350°C (Figure 44) and 400°C (Figure 45). At 350°C, still the formation of both MA and MMA was not observed, whereas at 400°C the overall selectivity to MA + MMA was equal to 7%, obtained for the higher residence time of 4g*min/mL. The latter result suggests that the desired reaction needs high temperature and residence time to occur; however, MA and MMA were minor reaction products. Indeed, these reaction conditions also favored the formation of very high amounts of aromatic compounds and carbon deposits on the catalysts surface, possibly due to the acid properties of the AlPO catalyst. The latter compounds

might derive from consecutive reactions occurring on both MP and 3-pentanone, since their selectivity decreased while increasing residence time, this trend being particularly pronounced for MP, whose selectivity steeply dropped from 67 down to 22%. Theoretically, it cannot be excluded that the formation of these heavy compounds might also come from DME or MeOH conversion.

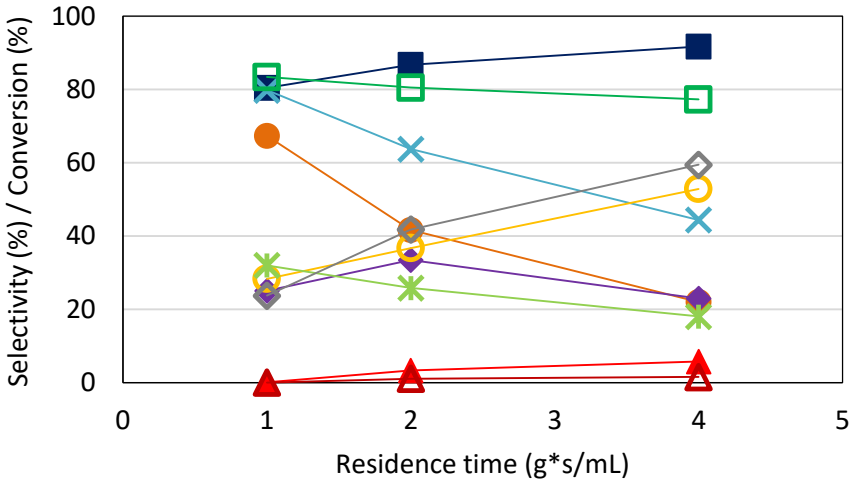

Figure 45. Reactivity experiments as a function of residence time *(W/F)*. Other reaction conditions: feed composition PA/MeOH/N_2 = 6/12/82 mol%, temperature = 400°C. Symbols: (■) PA conversion, (□) MeOH conversion, (●) MP selectivity, (◆) 3P selectivity, (◊) CO_2 selectivity, (▲) MA selectivity, (Δ) MMA selectivity, (X) total selectivities calculated on PA basis, (*) total selectivities calculated on MeOH basis, (○) carbon loss.

2.2.4 Conclusions

Considering the main reaction products of the process, finally the overall reaction network depicted in Scheme 19, can be outlined.

On the whole, it can be stated that the AlPO catalyst is not able to efficiently perform the coupling between PA (or its methyl ester) and MeOH, to give MA (or MMA). Indeed, MA was only obtained with the maximum selectivity of 7%, together with MMA, at the higher temperature and residence time investigated (400°C, 4g*min/mL). The selectivity of the process was limited by both the formation of DME, that may compete with MeOH dehydrogenation to generate formaldehyde, and the formation of heavy compounds and aromatics, arguably promoted by the acidity of the AlPO catalyst as well.

On the other hand, this material was proved to be remarkably efficient to perform the gas phase esterification of PA into the corresponding methyl ester, achieving the maximum selectivity of 90% into MP at the temperature of 300°C.

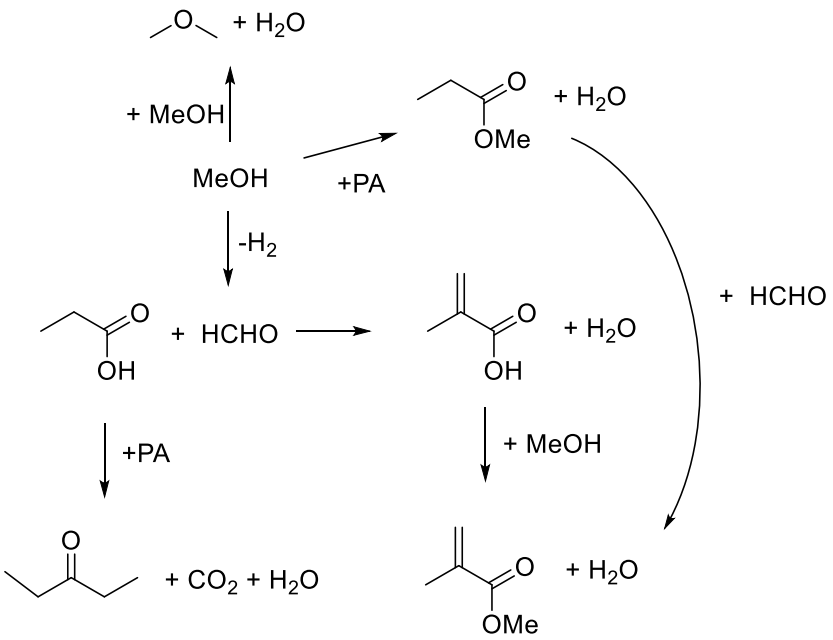

Scheme 19. Overall reaction network for PA and MeOH conversion with AlPO catalyst.

Finally, it is worth mentioning that AlPO appears to be able to perform the ketonization of propionic acid to 3-pentanone. This result is particularly interesting since phosphate-based catalysts have not been so far reported in literature as efficient catalysts for the ketonization process.

This reaction, that found its first application on industrial scale in the XIX century for acetone production from acetic acid, is recently regaining interest in the scientific community, especially for its application in the upgrading of biomass-derived oxygenates, such as bio-oils and chemicals deriving from pyrolysis and dehydration processes performed on biomasses[100–102]. Indeed, the ketonization process might remove the highly reactive carboxylic functional groups while increasing the size of the carbon chain. This reaction is commonly performed over metal oxides, both acid, basic and amphoteric[101–107]. In literature, it is widely accepted that the combination of acid and basic functionalities is beneficial for the ketonization reaction. Indeed, amphoteric

oxides, such as TiO_2, ZrO_2 and CeO_2, turned out to be the most active catalysts. Recently, also the catalytic activity of acid zeolites has been investigated, these materials showing relatively good performances as well[100,106]. Accordingly, referring to literature, AlPO catalyst might also possess the proper features to efficiently catalyze the ketonization reaction, hence further studies by feeding propionic acid will soon be performed.

References

[1] T. Ohara, T. Sato, N. Shimizu, G. Prescher, H. Schwind, O. Weiberg, K. Marten, H. Greim, *Ullmann's Encycl. Ind. Chem.* **2011**, *60*, DOI 10.1002/14356007.a01_161.pub3.

[2] R. Beerthuis, G. Rothenberg, N. R. Shiju, *Green Chem.* **2015**, *17*, 1341–1361.

[3] J. J. H. B. Sattler, J. Ruiz-Martinez, E. Santillan-Jimenez, B. M. Weckhuysen, *Chem. Rev.* **2014**, *114*, 10613–10653.

[4] P. Lanzafame, G. Centi, S. Perathoner, *Catal. Today* **2014**, *234*, 2–12.

[5] B. Katryniok, S. Paul, F. Dumeignil, *ACS Catal.* **2013**, *3*, 1819–1834.

[6] H. S. Chu, J. H. Ahn, J. Yun, I. S. Choi, T. W. Nam, K. M. Cho, *Metab. Eng.* **2015**, *32*, 23–29.

[7] J. Zhang, Y. Zhao, M. Pan, X. Feng, W. Ji, C. T. Au, *ACS Catal.* **2011**, *1*, 32–41.

[8] R. A. Sheldon, *Green Chem.* **2014**, *16*, 950–963.

[9] C. H. Zhou, H. Zhao, D. S. Tong, L. M. Wu, W. H. Yu, *Catal. Rev. - Sci. Eng.* **2013**, *55*, 369–453.

[10] A. Talebian-Kiakalaieh, N. A. S. Amin, H. Hezaveh, *Renew. Sustain. Energy Rev.* **2014**, *40*, 28–59.

[11] J. L. Dubois, *WO Patent, 2007/090991, assigned to Arkema Fr.* **n.d.**

[12] J. L. Dubois, *WO Patent, 2008/007002, assigned to Arkema Fr.* **n.d.**

[13] F. Wang, J. Xu, J.-L. Dubois, W. Ueda, *ChemSusChem* **2010**, *3*, 1383–1389.

[14] K. Omata, K. Matsumoto, T. Murayama, W. Ueda, *Catal. Today* **2016**, *259*, *Part*, 205–212.

[15] M. D. Soriano, P. Concepción, J. M. L. Nieto, F. Cavani, S. Guidetti, C. Trevisanut, *Green Chem.* **2011**, *13*, 2954–2962.

[16] J. Deleplanque, J. L. Dubois, J. F. Devaux, W. Ueda, *Catal. Today* **2010**, *157*, 351–358.

[17] A. Chieregato, M. D. Soriano, E. García González, G. Puglia, F. Basile, P. Concepción, C. Bandinelli, J. M. López Nieto, F. Cavani, *ChemSusChem* **2015**, *8*, 398–406.

[18] A. Chieregato, M. D. Soriano, F. Basile, G. Liosi, S. Zamora, P. Concepción, F. Cavani, J. M. López Nieto, *Appl. Catal. B Environ.* **2014**, *150–151*, 37–46.

[19] A. Chieregato, F. Basile, P. Concepción, S. Guidetti, G. Liosi, M. D. Soriano, C. Trevisanut, F. Cavani, J. M. L. Nieto, *Catal. Today* **2012**, *197*, 58–65.

[20] L. G. Possato, W. H. Cassinelli, T. Garetto, S. H. Pulcinelli, C. V Santilli, L. Martins, *Appl. Catal. A Gen.* **2015**, *492*, 243–251.

[21] C. F. M. Pestana, A. C. O. Guerra, G. B. Ferreira, C. C. Turci, C. J. A. Mota, *J. Braz. Chem.*

Soc. **2013**, *24*, 100–105.

[22] X. Feng, Y. Yao, Q. Su, L. Zhao, W. Jiang, W. Ji, C.-T. Au, *Appl. Catal. B Environ.* **2015**, *164*, 31–39.

[23] F. Wang, J.-L. Dubois, W. Ueda, *J. Catal.* **2009**, *268*, 260–267.

[24] A. Chieregato, J. M. López Nieto, F. Cavani, *Coord. Chem. Rev.* **2015**, *301–302*, 3–23.

[25] Y. S. Yun, K. R. Lee, H. Park, T. Y. Kim, D. Yun, J. W. Han, J. Yi, *ACS Catal.* **2015**, *5*, 82–94.

[26] H. O. Pastore, S. Coluccia, L. Marchese, *Annu. Rev. Mater. Res.* **2005**, *35*, 351–395.

[27] N. F. Dummer, W. Weng, C. Kiely, A. F. Carley, J. K. Bartley, C. J. Kiely, G. J. Hutchings, *Appl. Catal. A Gen.* **2010**, *376*, 47–55.

[28] C. S. Griffith, V. Luca, *Chem. Mater.* **2004**, *16*, 4992–4999.

[29] P. Concepción, J. M. López Nieto, *Catal. Commun.* **2001**, *2*, 363–367.

[30] M. D. Soriano, A. Chieregato, S. Zamora, F. Basile, F. Cavani, J. M. López Nieto, *Top. Catal.* **2015**, 1–8.

[31] E. Garcia-Gonzalez, M. D. Soriano, E. Urones-Garrote, J. M. Lopez Nieto, *Dalt. Trans.* **2014**, *43*, 14644–14652.

[32] P. Concepción, T. Blasco, J. M. López Nieto, A. Vidal-Moya, A. Martínez-Arias, *Microporous Mesoporous Mater.* **2004**, *67*, 215–227.

[33] E. I. Ross-Medgaarden, I. E. Wachs, *J. Phys. Chem. C* **2007**, *111*, 15089–15099.

[34] I. E. Wachs, G. Deo, B. M. Weckhuysen, A. Andreini, M. A. Vuurman, M. de Boer, M. D. Amiridis, *J. Catal.* **1996**, *161*, 211–221.

[35] M. D. Argyle, K. Chen, A. T. Bell, E. Iglesia, *J. Catal.* **2002**, *208*, 139–149.

[36] J. T. Grant, C. A. Carrero, A. M. Love, R. Verel, I. Hermans, *ACS Catal.* **2015**, *5*, 5787–5793.

[37] F. Cavani, S. Luciani, E. D. Esposti, C. Cortelli, R. Leanza, *Chem. – A Eur. J.* **2010**, *16*, 1646–1655.

[38] F. Cavani, D. De Santi, S. Luciani, A. Löfberg, E. Bordes-Richard, C. Cortelli, R. Leanza, *Appl. Catal. A Gen.* **2010**, *376*, 66–75.

[39] A. Caldarelli, M. A. Banares, C. Cortelli, S. Luciani, F. Cavani, *Catal. Sci. Technol.* **2014**, *4*, 419–427.

[40] J. P. Lourenço, M. I. Macedo, A. Fernandes, *Catal. Commun.* **2012**, *19*, 105–109.

[41] M. Massa, A. Andersson, E. Finocchio, G. Busca, F. Lenrick, L. R. Wallenberg, *J. Catal.* **2013**, *297*, 93–109.

[42] M. Massa, A. Andersson, E. Finocchio, G. Busca, *J. Catal.* **2013**, *307*, 170–184.

[43] H. Zhang, Z. Hu, L. Huang, H. Zhang, K. Song, L. Wang, Z. Shi, J. Ma, Y. Zhuang, W. Shen, et

al., *ACS Catal.* **2015**, *5*, 2548–2558.

[44] G. S. Foo, D. Wei, D. S. Sholl, C. Sievers, *ACS Catal.* **2014**, *4*, 3180–3192.

[45] P. Concepción, A. Corma, J. M. López Nieto, J. Pérez-Pariente, *Appl. Catal. A Gen.* **1996**, *143*, 17–28.

[46] Y. Kamiya, H. Nishiyama, M. Yashiro, A. Satsuma, T. Hattori, *Sekiyu Gakkaishi (Journal Japan Pet. Institute)* **2003**, *46*, 62–68.

[47] E. Yoda, A. Ootawa, *Appl. Catal. A Gen.* **2009**, *360*, 66–70.

[48] J. Tichý, *Appl. Catal. A Gen.* **1997**, *157*, 363–385.

[49] T. V Andrushkevich, G. Y. Popova, *Russ. Chem. Rev.* **1991**, *60*, 1023.

[50] J. M. L. Nieto, P. Concepcion, a Dejoz, H. Knozinger, F. Melo, M. I. Vazquez, *J. Catal.* **2000**, *189*, 147–157.

[51] T. J. ; A. A. Davydov, *Collect. Czech. Chem. Commun.* **1976**, *41*, 834–838.

[52] D. Shee, G. Deo, *J. Mol. Catal. A Chem.* **2009**, *308*, 46–55.

[53] K. Bhattacharyya, S. Varma, A. K. Tripathi, S. R. Bharadwaj, A. K. Tyagi, *J. Phys. Chem. B* **2009**, *113*, 5917–5928.

[54] G. Centi, F. Cavani, F. Trifirò, *Springer, New York* **2001**, *XIX*.

[55] T. Blasco, J. M. L. Nieto, *Appl. Catal. A Gen.* **1997**, *157*, 117–142.

[56] G. Pavarelli, J. Velasquez Ochoa, A. Caldarelli, F. Puzzo, F. Cavani, J. L. Dubois, *ChemSusChem* **2015**, *8*, 2250–2259.

[57] G. Centi, F. Cavani, F. Trifirò, in *Sel. Oxid. by Heterog. Catal.*, Springer US, Boston, MA, **2001**, pp. 203–283.

[58] W. J. Bauer, *Ullmann's Encycl. Ind. Chem.* **1934**, DOI 10.1002/14356007.a16_441.pub2.

[59] K. Nagai, *Appl. Catal. A Gen.* **2001**, *221*, 367–377.

[60] A. Martin, U. Armbruster, I. Gandarias, P. L. Arias, *Eur. J. Lipid Sci. Technol.* **2013**, *115*, 9–27.

[61] Z. W. Ulf-Rainer Samel, Walter Kohler, Armin Otto Gamer, Ullrich Keuser, Shang-Tian Yiang, Ying Jin, Meng Lin, *Ullmann's Encycl. Ind. Chem.* **2014**, DOI 10.1002/14356007.a22_223.pub3.

[62] A. J. Papa, *Ullmann's Encycl. Ind. Chem.* **2012**, DOI 10.1002/14356007.a22_157.pub2.

[63] K. Mori, Y. Yamada, S. Sato, *Appl. Catal. A Gen.* **2009**, *366*, 304–308.

[64] L. Z. Tao, S. H. Chai, H. P. Wang, B. Yan, Y. Liang, B. Q. Xu, *Catal. Today* **2014**, *234*, 237–244.

[65] D. Zhang, S. A. I. Barri, D. Chadwick, *Appl. Catal. A Gen.* **2011**, *400*, 148–155.

[66] B. Török, I. Bucsi, T. Beregszàszi, I. Kapocsi, A. Molnàr, *J. Mol. Catal. A Chem.* **1996**, *107*, 305–311.

[67] A. Chieregato, F. Basile, P. Concepción, S. Guidetti, G. Liosi, M. D. Soriano, C. Trevisanut, F. Cavani, J. M. L. Nieto, *Catal. Today* **2012**, *197*, 58–65.

[68] A. Chieregato, M. D. Soriano, F. Basile, G. Liosi, S. Zamora, P. Concepción, F. Cavani, J. M. López Nieto, *Appl. Catal. B Environ.* **2014**, *150–151*, 37–46.

[69] D. Sun, Y. Yamada, S. Sato, *Appl. Catal. A Gen.* **2014**, *487*, 234–241.

[70] J. Svachula, J. Machek, *Catal. Letters* **1989**, *3*, 257–262.

[71] P. Concepciòn, P. Botella, J. M. Lòpez Nieto, *Appl. Catal. A Gen.* **2004**, *278*, 45–56.

[72] L. Niinisto, A. Auroux, A. Gervasini, P. Carniti, J. Kera, *Catal. Today* **2004**, *96*, 187–194.

[73] W. Y. Suprun, D. Kießling, T. Machold, H. Papp, *Chem. Eng. Technol.* **2006**, 1376–1380.

[74] J. Tichý, *Appl. Catal.* **1997**, *157*, 363–385.

[75] M. Ai, *J. Catal.* **1990**, *296*, 9517.

[76] M. Ai, *Appl. Catal.* **1988**, *36*, 221–230.

[77] M. Ai, *Appl. Catal.* **1990**, *63*, 365–373.

[78] M. Ai, H. Fujihashi, S. Hosoi, A. Yoshida, *Appl. Catal. A Gen.* **2003**, *252*, 185–191.

[79] Ai. M, *Bull. Chem. Soc. Jpn* **1990**, *63*, 1217–1220.

[80] O. H. Bailey, R. A. Montag, J. S. Yoo, *Appl. Catal. A Gen.* **1992**, *88*, 163–177.

[81] P. Moggi, V. Massimo, D. Azeglio, *Appl. Catal.* **1983**, *6*, 293–306.

[82] R. Nebesnyi, O. Petelka, *Symp. "Chemistry Chem. Technol. 2013"* **2013**, 21–23.

[83] J. Tai, R. J. Davis, *Catal. Today* **2007**, *123*, 42–49.

[84] M. Ai, *Appl. Catal. A Gen.* **2005**, *288*, 211–215.

[85] M. Ai, *Catal. Today* **2006**, *111*, 398–402.

[86] Y. V Dmytruk, V. V Ivasiv, R. V Nebesnyi, S. V Maykova, **2015**, *6*, 4–7.

[87] B. Li, R. Yan, L. Wang, Y. Diao, *Catal. Letters* **2013**, 829–838.

[88] B. Li, R. Yan, L. Wang, Y. Diao, Z. Li, S. Zhang, *Ind. Eng. Chem. Res.* **2014**, *2*.

[89] Y. Wang, R. Yan, Z. Lv, H. Wang, L. Wang, *Catal. Letters* **2016**, *146*, 1808–1818.

[90] M. Ai, *Sci. bases Prep. Heterog. Catal.* **2006**, *162*, 457–464.

[91] J. Li, J. Tai, R. J. Davis, *Catal. Today* **2006**, *116*, 226–233.

[92] M. R. Gogate, J. J. Spivey, J. R. Zoeller, *Catal. Today* **1997**, *36*, 243–254.

[93] J. J. Spivey, M. R. Gogate, J. R. Zoeller, R. D. Colberg, *Ind. Eng. Chem. Res.* **1997**, *5885*, 4600–4608.

[94] Merger, *United States Patent*, **1982**, 228284.

[95] V. L. Sushkevich, V. V Ordomsky, I. I. Ivanova, *Appl. Catal. A Gen.* **2012**, *442*, 21–29.

[96] V. S. Kumar, A. H. Padmasri, C. V. V Satyanarayana, I. A. Kumar, *Catal. Commun.* **2006**, *7*, 745–751.

[97] M. Muller, U. Hubsch, *Ullmann's Encycl. Ind. Chem.* **2012**, DOI 10.1002/14356007.a08.

[98] W. Riemenschneider, H. M. Bolt, *Ullmann's Encycl. Ind. Chem.* **2012**, DOI 10.1002/14356007.a09_565.pub2.

[99] J. Sun, G. Yang, Y. Yoneyama, N. Tsubaki, *ACS Catal.* **2014**.

[100] T. N. Pham, T. Sooknoi, S. P. Crossley, D. E. Resasco, *ACS Catal.* **2013**, *3*, 2456–2473.

[101] C. A. Gärtner, J. C. Serrano-ruiz, D. J. Braden, J. A. Dumesic, *ChemSusChem* **2009**, 1121–1124.

[102] C. A. Gaertner, J. C. Serrano-ruiz, D. J. Braden, J. A. Dumesic, *J. Catal.* **2009**, *266*, 71–78.

[103] G. Zalewski, E. Burno, A. Jerzak, *Appl. Catal. A Gen.* **2014**, *470*, 278–284.

[104] R. Pestman, R. M. Koster, A. Van Duijne, J. A. Z. Pieterse, V. Ponec, *J. Catal.* **1997**, *272*, 265–272.

[105] O. Nagashima, S. Sato, R. Takahashi, T. Sodesawa, *J. Mol. Catal. A Chem.* **2005**, *227*, 231–239.

[106] H. Bayahia, E. Kozhevnikova, I. Kozhevnikov, *Chem. Commun.* **2013**, *3*, 3842–3844.

[107] C. A. Gaertner, J. C. Serrano-ruiz, D. J. Braden, J. A. Dumesic, *Ind. Eng. Chem. Res.* **2010**, 6027–6033.

[108] www.strategir.com/MarketResearch/Methyl_Methacrylate_MMA_Market_Trends

[109] http://database.thinking.nexant.com/about/cs/news/items/0004.cfm

Publications

Publications related to the topics of this PhD thesis:

- **Multielement crystalline and pseudocrystalline oxides as efficient catalysts for the direct transformation of glycerol into acrylic acid**, Chieregato A., Soriano M.D., Garcìa-Gonzàlez E., Puglia G., Basile F., Conceptiòn P., Bandinelli C., Lòpez Nieto J.M., Cavani F., (2015) **ChemSusChem**, 8 (2), 398-406;
- **Structure–Reactivity Correlations in Vanadium-Containing Catalysts for One-Pot Glycerol Oxidehydration to Acrylic Acid**, Chieregato A., Bandinelli C., Concepciòn P., Soriano M.D., Puzzo F., Basile F., Cavani F., Lòpez Nieto J.M., (2017) **ChemSusChem**, 10 (1), 234-244.

Publications related to other research projects:

- **On the chemistry of ethanol on basic oxides: revising mechanisms and intermediates in the Lebedev and Guerbet reactions**, Chieregato A., Ochoa J.V., Bandinelli C., Fornasari G., Cavani F., Mella M., (2015) **ChemSusChem**, 8 (2), 377-388;
- **An analysis of the chemical, physical and reactivity features of MgO-SiO_2 catalysts for butadiene synthesis with the Lebedev process**, Ochoa J.V., Bandinelli C., Vozniuk O., Chieregato A., Malmusi A., Recchi C., Cavani F., (2016) **Green Chem.**, 18, 1653-1663;
- **Adsorbent-Adsorbate Interactions in the Oxidation of HMF Catalyzed by Ni-Based MOFs: A DRIFT and FT-IR Insight**, Lucarelli C., Galli S., Maspero A., Cimino A., Bandinelli C., Lolli A., Ochoa, J.V., Vaccari A., Cavani, F., Albonetti S., (2016) **J. Phys. Chem. C***,* 120(28), 15310–15321.

Acknowledgements

I sincerely want to thank all the people that worked with me in the last three years, because these collaborations definitely were the best part of my PhD period.

I first want to thank my PhD supervisor Prof. Fabrizio Cavani for being my scientific guide and for his infectiuos enthusiasm, that really helped me to go on throughout the worst periods.

I also want to thank Prof. José Manuel López Nieto and his colleagues for the precious collaboration.

Then, a special thank goes to Alessandro Chieregato and Juliana Velasquez Ochoa. I realized that I lived something like an “imprinting phenomenon” with you… and someone would say that this is no good…

Thanks also to Carlo Lucarelli (it was really fun to work with you!), to all the guys, professors and researchers of the group, and to the students that worked with me very hard.

I finally thank Consorzio INSTM for my PhD grant.